Heat Flux at the Near-Surface and Atmosphere Boundary at Geothermal Areas: Development of Methods Used for Measurement and Quantification of the System

A Thesis

Presented in Partial Fulfillment of the Requirements for the

Degree of Master of Science

with a

Major in Geology

in the

College of Graduate Studies

University of Idaho

by

Gabriela Villegas

Major Professor: Jerry P. Fairley, Ph.D.

Committee Members: Peter B. Larson, Ph.D.; John C. Crepeau, Ph.D.

Administrator: Leslie Baker, Ph.D.

May, 2018

Authorization to Submit Thesis

This thesis of Gabriela Villegas, submitted for the degree of Master of Science with a Major in Geology and titled "Heat Flux at the Near-Surface and Atmosphere Boundary at Geothermal Areas: Development of Methods Used for Measurement and Quantification of the System," has been reviewed in final form. Permission, as indicated by the signatures and dates below, is now granted to submit final copies to the College of Graduate Studies for approval.

Major Professor

_____ Date _____

Jerry P. Fairley, Ph.D.

Committee Members

_____ Date _____

Peter B. Larson, Ph.D.

_____ Date _____

John C. Crepeau, Ph.D.

Administrator

_____ Date _____

Leslie Baker, Ph.D.

Abstract

Estimating the heat flux at the near-surface and atmospheric boundary in geothermal areas is a useful, yet difficult task. Through temperature measurements in the shallow subsurface, we can quantify the heat being transferred through soils, and many times the heat signature resulting from spatial measurements allows us to make suggestions about the system's flow and control paths. Despite the value in knowing this, through this study I have found that current methods used for measurement of soil temperatures may provide inaccurate readings if the tools used are made of a high thermal conductivity material, which in turn introduces error into the heat flux calculations. In this study, I use laboratory and field data to show that accurate shallow temperature gradients can be obtained using probes of low thermal conductivity material, these probes are described in detail. Additionally, I present a quantitative framework, which is currently lacking, for transient coupled land-air thermal interactions in geothermal systems.

Acknowledgements

First and foremost I would like to thank my advisor, Jerry Fairley, for taking me on as a graduate student, and teaching many valuable lessons. I thank him, not only for his teachings in the classroom about hydrogeology, geostatistics, mathematics, or heat transfer, but also for all the patience and time spent teaching me to become a better student and a more knowledgeable future worker through invaluable, and not often taught life lessons. I would also like to thank my Committee Members, Peter Larson, and John Crepeau, for their input, ideas, and their help throughout this year; all of these have made my thesis stronger.

I would also like to thank my research group, Cary Lindsey, Meg Aunan, and Adam Price for their willingness to help me in the lab and in the field, and their disposition to share ideas and advice me when I was feeling a bit lost. It would have been truly hard without them.

A special thanks to the faculty and staff in the Geological Sciences department at the University of Idaho, Moscow, and to the faculty and staff at the department of Earth Sciences at Montana State University, Bozeman, specially to my undergraduate advisor David Mogk. These people provided me with the tools and skills necessary for my success in graduate school. I must also thank the Geological Sciences Department for funding my studies through a teaching assistant position throughout the duration of my graduate work. I would also like to thank the Graduate and Professional Student Association for funding my travel to two different conferences at which I presented my research.

I must thank the owners of Burgdorf Hot springs for allowing us to work at their site on various occasions and for providing us with help a couple of times. Their kindness was also invaluable. I would also like to thank Matthew Lesiecki and Peter Robichaud from the USDA Forestry Service in Moscow for letting me use their equipment for a couple of weeks, for meeting with me several times, and for gathering the data collected and sending it my way. One last thanks to the University of Idaho machine shop facilities staff, specially to B. J. Schenck, who helped me with the creation of the ground temperature probes, much of this project could not have been done without them.

Dedication

I would like to specially thank my loving husband, Marshall, for helping me with the experimental set up, the math and programming portion of this thesis, and for being so supportive and kind in the hardest times. I could not have gotten through without him, as we struggled together through graduate school.

I have to thank my parents, Mario and Charito, and my sister, Laura, for encouraging me to get into graduate school, for always pushing me to be a better student, to strive for knowledge, and for being the amazing role models they are. Thanks for your encouragement and support, regardless of my attitude that week or month, and thanks for the great education you gave me while growing up at home.

Thanks to my puppy Kala, for keeping me warm through the hours of typing and for taking me out for walks when I was really stressed.

Lastly, I would like to thank God for showing me the way and guiding me with a helping hand at all times.

Table of Contents

List of Figures

List of Tables

List of Nomenclature

Dimensional Parameters

A	→ Area	m^2
T_∞	→ Atmospheric Temperature	$^\circ C, K$
z_c	→ Characteristic Depth	m
t_c	→ Characteristic Time	s
ρ	→ Density	$\frac{Kg}{m^3}$
z	→ Depth	m
E	→ Energy	J
c_p	→ Heat Capacity	$\frac{J}{KgK}$
q"	→ Heat Flux	$\frac{W}{m^2}$
h	→ Heat Transfer Coefficient	$\frac{W}{m^2K}$
T_o	→ Initial Temperature	$^\circ C, K$
x	→ Location	m
p	→ Period - t_c	s
T	→ Temperature	$^\circ C$, K
T_{Alp}	→ Temperatures Aluminum Plate	$^\circ C$
T_{cip}	→ Temperatures Cast Iron Pan	$^\circ C$
T_r	→ Temperatures Room	$^\circ C$
T_{ss}	→ Temperatures Soil Surface	$^\circ C$
K_T	→ Thermal Conductivity	$\frac{W}{mK}$
D	→ Thermal Diffusivity	$\frac{m^2}{s}$
t	→ Time	s

Non-Dimensional Parameters

β	→ Biot Number $\frac{h\sqrt{Dp}}{K_T}$
Γ_n	→ Conditional Variable
ξ	→ Nondimensional Depth
θ	→ Nondimensional Temperature
τ	→ Nondimensional Time

Non-Dimensional Parameters

ϵ $\rightarrow -\frac{q_z\sqrt{Dp}}{K_T T_o}$

κ $\rightarrow \pm\sqrt{2in\pi}$

χ $\rightarrow e^{\kappa\xi}$

Abbreviations

B_1 → Beaker 1000 mL

B_2 → Beaker 2000 mL

bs → Below Surface

brGDGTs → Branches glycerol dialkyl glycerol tetraethers

INL → Idaho National Laboratories

NIST → National Institute Standards and Technology

PPrb"X" → Plastic (Nylon) Probe # "X"

S → Sand

SSPrb"X" → Stainless Steel Probe # "X"

VS"X" → Vertical Sequence # "X"

W → Water

WFP"X" → Wildfire Probe # "X"

1 Chapter 1: Importance of Heat Flux Measurements

1.1 Introduction

Estimating the heat flux at the land surface can be a difficult task. This is partly because of the spatial variability of the thermal properties of the soil, but also, and perhaps more importantly, because of the time-varying atmospheric boundary condition. Such condition propagates a quasi-periodic signal into the subsurface, which causes the near surface heat flux to vary with time of day. The difference in heat flux observed in the shallow subsurface may be small enough to be neglected in most places, where the temperature variation will be low from soil to air (Manga and Kirchner, 2004). However, when we work in geothermal areas the temperatures of the fluids, and often times those of the soils, have a strong contrast with the ambient air temperatures, accounting for a larger portion of the heat budget (Price et al., 2017).

Under these conditions, an accurate way to estimate the annual average conductive heat flux is to install a vertical sequence of thermocouple sensors in the shallow subsurface, and collect enough temperature measurements to capture the full variability of the time varying signal. The vertical sequence often consists of a 50 cm to 1 m rod with two to six sensors distributed over its length. If the sensors provide accurate data on the subsurface temperature profile, and the thermal conductivity of the soils is measured, it is possible to correct for the time-varying surface boundary condition. However, it is common practice to attach the thermocouple sensors to a metal rod, which is then driven into the soils (Hurwitz et al., 2012; Olmsted et al., 1986). The perturbation introduced to the near-surface temperature profile caused by the insertion of a highly conductive material, as the metal rod, had not been previously evaluated until now.

The work done to understand the temperature change caused by the near-subsurface conditions in hydrothermal areas has been studied for a few decades now. Nevertheless, no quantitative framework of heat transfer exists for coupled land-air thermal interactions. Recently, Price et al. (2017) published an analytical model that investigates the relationship between the near-surface heat and fluid flow which connects surface temperatures with the conditions at the subsurface. Although the model provides a great quantitative approach to this relationship at steady state conditions, it fails to explain this relationship on a transient scenario where soil and air conditions change with time. This study focuses on improving the common practices used to measure the

temperature profile on the subsurface, and on quantifying the heat exchange at the land surface-air boundary over a period of time.

1.2 Background

1.2.1 Heat Flow

Geothermal areas, and more specifically hot springs, have been studied for centuries. However it was not until the 1950's when scientific data became available (White et al., 1971), with the rise of commercial and research drilling. Since the 1960's a growing interest in geothermal energy and its potential as a source of electricity has helped develop and enhance research methodology to characterize subsurface relationships of heat, rock, fracture, and fluid interaction; as well as methods for extraction of the heat contained in the system (Gringarten et al., 1975).

Amongst the methods currently available for the evaluation of near-surface heat flux, one of the most economical is conducting shallow subsurface temperature surveys, which has been a common practice since the 1980's. Many authors have used measurements of shallow ground temperatures for the study of geothermal and volcanic systems. Some have used these to estimate the heat fluxes, as did Dawson (1964) at the Wairakei geothermal area in New Zealand, by using a "Benseman" calorimeter and through indirect measurements of ground temperatures at 1 meter depths; sustaining these were suitable measurements in dominantly conductive areas, and at shallower depths in hotter parts, where convection is the dominant heat transfer mechanism. From this claim, Sorey and Colvard (1994) used Dawson's method to quantify the heat loss from the ground at Lassen Volcanic National Park, CA. Ingebritsen et al. (2001) included this method in their paper, which reviewed the implications for monitoring of selected sites with hydrothermal discharge in the western United States, as one of the common and reliable techniques for point measurements. Hurwitz et al. (2012) used a similar method to measure the ground temperatures at depths ranging from 2 cm to 1 m at various locations in Yellowstone National Park in order to quantify the heat transfer through conduction up to the surface.

Saba et al. (2007) used ground temperature measurements at over 130 points at 1 meter depth to track the development of a geothermal field after the 2000 volcanic eruption of the Mount Usu,

in Japan. Other studies have tried to examine the structural controls on hydrothermal systems, as did Anderson and Fairley (2008) by taking ground temperature measurements at depths of 10 cm on their work at Mickey Hot Springs in southeast Oregon. Rissmann et al. (2011) also used indirect measurements of surface heat flow through surveys of soil temperature, at depths between 15 cm and 1 m, in order to evaluate the structural controls on the Ohaaki hydrothermal system, in New Zealand. Other investigations have used geostatistical analysis of hot springs along with ground temperature measurements to develop models for the distribution of fault permeability in the Borax Lake fault, located in southeast Oregon (Fairley et al., 2003; Fairley and Hinds, 2004; Heffner and Fairley, 2006).

Outside the geothermal and volcanic systems ground temperature measurements have been used to assess slope failure from shallow groundwater (Furuya et al., 2006), to determine permafrost distribution in arctic regions (Smith, 1975), in studies of seismic noise and ground temperature (Gordeev et al., 1992), and have also been used in archeological studies. For example, Mori et al. (1999) used an experimental temperature measurement of the ground in order to confirm whether they could provide information on the existence of subsurface archaeological remains.

Thompson (1960) suggests, as a well known fact, that diurnal and seasonal changes have an effect on ground temperatures, but says that regular measurements of temperatures in the same location show no apparent diurnal effect, at Wairakei. Olmsted et al. (1986) argue that although it is easier to obtain temperature measurements near the surface than at greater depths, there is a tradeoff in the reliability of the measurements by doing so, because of effects unrelated to geothermal heat flow such as solar fluctuations, topography, vegetation, albedo, amongst others. In their paper they review various surveys where measurements between 1 and 2 meters were made. They provide sources, from other studies that evaluate the degree of importance of perturbing factors unrelated to geothermal heat flow as depth decreases, that agree with their argument for a high influence on the temperatures recorded at shallow depths (e.g. Poley and Steveninck, 1970; Kappelmeyer and Haenel, 1974; Olmsted, 1977; Lovering and Goode, 1963).

Lubenow et al. (2016) argue that ground temperatures are an inexpensive, widely used, and flexible approach to investigate shallow subsurface processes. They provide the basis for conducting temperature surveys at depths of under 1 m, which is to minimize the influence of changing atmospheric conditions and more specifically diurnal temperature variations. It is understood that

this assessment arises from a known result that the amplitude of periodic temperature variation decreases with depth (Carslaw and Jaeger, 1959).

However, Lubenow et al. (2016) argue that although it would be nice to limit atmospheric influences on the measured ground temperatures, it is limiting in other ways. To get measurements of at least 1 m depth, most often there needs to be augering and digging, which is time and effort consuming, can be quite intrusive, and in many locations even restricted or prohibited; not to mention the added thermal perturbation by the act of creating a hole. By contrast, shallow measurements (≤ 25 cm) can be preferred because of their depth of penetration and short equilibrium times, which allow for hundreds or even thousands of daily measurements, in addition they are much less invasive. In their paper they have found through geostatistical analysis that their results suggested that the shallow temperature measurement distribution was not particularly sensitive to variations in the surface boundary condition.

1.2.2 Temperature Probes

Most subsurface ground temperature measurements are made through the use of a temperature probe, often possessing more than one temperature sensor throughout its length. In this study I evaluate whether any of the probes that have been used may be adequate for the initial purpose of our study. Aspects from all the probes described below were used for the creation of the probes used in our study.

All the probes that I either tested or examined, have common characteristics. They are all between 1 foot and 1 meter in length. And all of them have temperature sensors or thermocouples throughout their length, either all spaced closely towards one end of the probe; or further spaced throughout their length.

The first probe I examined from the literature was one described by Hurwitz et al. (2012). They used a probe of $\frac{3}{8}$ inch (0.95 cm) thickness made out of stainless steel, with four type K thermocouple sensors placed throughout its length from 5 cm to 100 cm. This device measured the ground temperatures at depths ranging from 2 cm to 1 m, this variation in depth was due to the uneven and occasionally very hard ground, at various locations in Yellowstone National Park. Refer to Figure 1.1 as a reference. They took measurements every 2 seconds for periods ranging

from 8 to 15 minutes after insertion to ensure near thermal equilibrium of the soils after insertion of the probe, which is why they only used the last 40 samples from each of the sensors readings for application on their calculations of equilibrium temperature and standard deviations for each sensor.

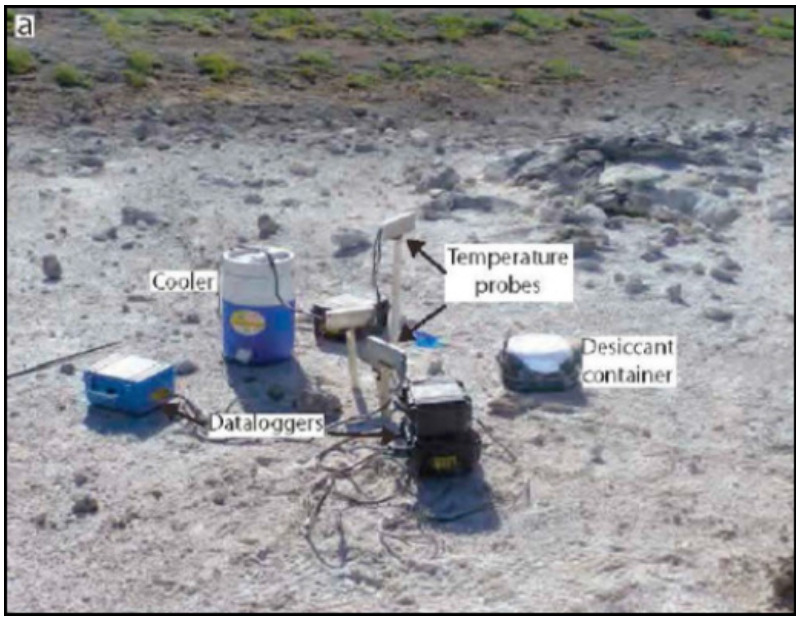

Figure 1.1: **Stainless Steel Probe - Hurwitz.** Reprinted from "Heat flow in vapor dominated areas of the Yellowstone Plateau Volcanic Field: Implications for the thermal budget of the Yellowstone Caldera", (Figure. 6a), by S. Hurwitz, R. N. Harris, C. A. Werner, and F. Murphy, 2012, *Journal of Geophysical Research: Solid Earth*, 117(B10).

On the basis of the Hurwitz et al. (2012) study, the method used in it, and the results from it, I became interested in seeing whether or not the material of the probe would have a significant effect on the heat transferred through the probe to the shallower depths, and if the effect of this could be modifying the heat flux calculations that were obtained by the used of this method. In order to find out whether or not this was a possibility, we evaluated a thermocouple probe made by Omega; it was a stainless steel probe, 24 inches (60.96 cm) long, and $\frac{3}{16}$ inches (0.47 cm) of diameter, with 6 sensors distributed throughout its lower extent. The first sensor located at the bottom of the probe, and the remaining sensors spaced 1.75 inches (4.44 cm) from each other; making the last sensor 8.75 inches (22.22 cm) from the bottom end of the probe. Each sensor has a corresponding labelled thermocouple termination for easy identification, and each termination has a K-type connection to a specific Data Logger. Such sensor appears to be currently discontinued; however, similar probes of different lengths are still being manufactured (i.e. PP6-36-K-U-18 resembles this probe the most

out of all their current products (Omega, 2017). Refer to Figure 1.2 as a reference. The experiments conducted with this probe are further explained in Chapter 2.

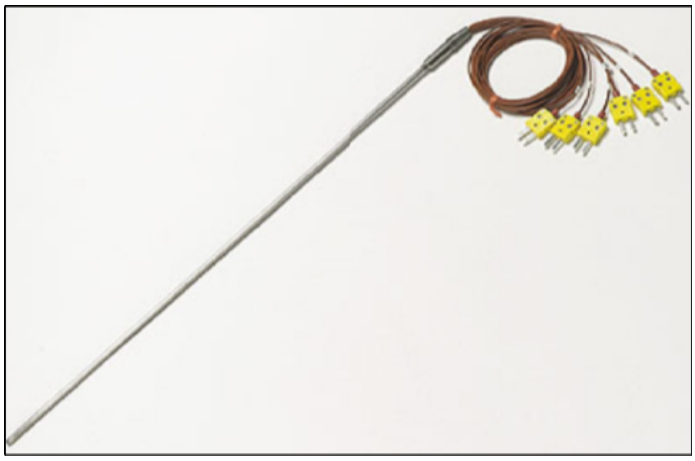

Figure 1.2: **Stainless Steel Probe - Omega.** Reprinted from *Omega TM*, n.d., 2017, from https://www.omega.com/*pptstPP*3*P*P6*P*P10.html#description.

Another probe I examined from the literature after my first experiment was one made by Ramón Naranjo from the USGS, Nevada Water Science Center, in association with Alpha Mach (Naranjo and Turcotte, 2015). This probe is one meter in length, with 6 autonomous temperature sensors (Maxim, Inc. Ibuttons, each with internal storage and battery) at depths of 0, 10, 20, 50, 75, and 100 cm from the top. The probe is made out of a $\frac{3}{4}$ inch (1.9 cm) thick PVC pipe (Naranjo, 2015). Refer to Figure 1.3 as a reference. Unfortunately, after asking the main author for further reference on the probes, we found out that although they have served their purpose perfectly at recording temperatures at streams floors, they are not made for high temperature systems, as the material that encases them is not fit to withstand these temperatures, and the possible sensor types can only read up to temperatures of 125 ˚C.

Another probe I examined and considered using, was one from a private provider, Decagon, an incorporation from whom our research group purchases different instruments. The probe is referred to as the "Th3-v Soil Temperature Profile Probe" from UMS, now associated with Decagon, and both now falling under METER . This probe is one meter in length and 2 cm in diameter, with 6 autonomous temperature sensors, at depths of 5, 10, 20, 30, 50, and 100 cm from the top. The probe is made out of glass-fibre reinforced plastic, and each sensor element has direct contact to a 1 cm high stainless steel ring which is embedded into the tube, which ensures each sensor to have direct contact with the soil. And the probe has a "sensor cable" that, when completely buried, lies

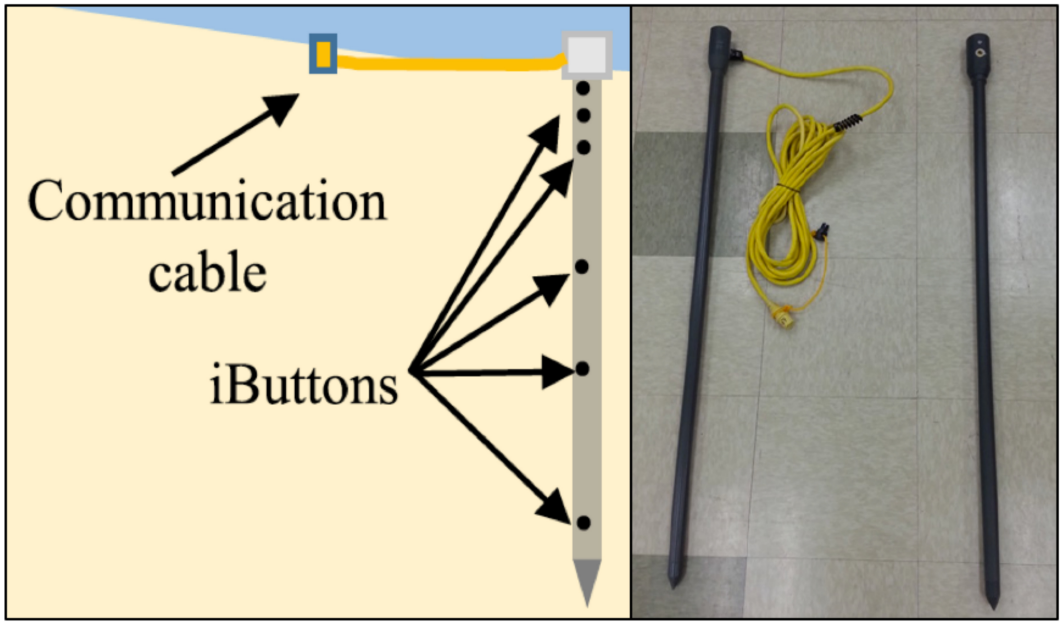

Figure 1.3: **Stream Temperatures Probe - Naranjo.** • Left: Reprinted from "A new temperature profiling probe for investigating groundwater-surface water interaction", (Figure 1-section), by R. Naranjo and R. Turcotte, 2015, *Water Resources Research*, vol.51(9), p.7790 – 7797. • Right: Reprinted from *A multi-depth temperature probe for investigating subsurface heat transport*,R. Naranjo, 2015, from https://mn.water.usgs.gov/uzig/$UZIG_Spring_2$015.2.pdf.

at 8 cm depth (UMS-tk/ma, 2008). Refer to Figure 1.4 as a reference. From all probes examined, this was the one I thought would yield the best results based on its material, length, recording capacities, and make. However, we were not able to purchase, or even try it, due to its high cost ($800.00).

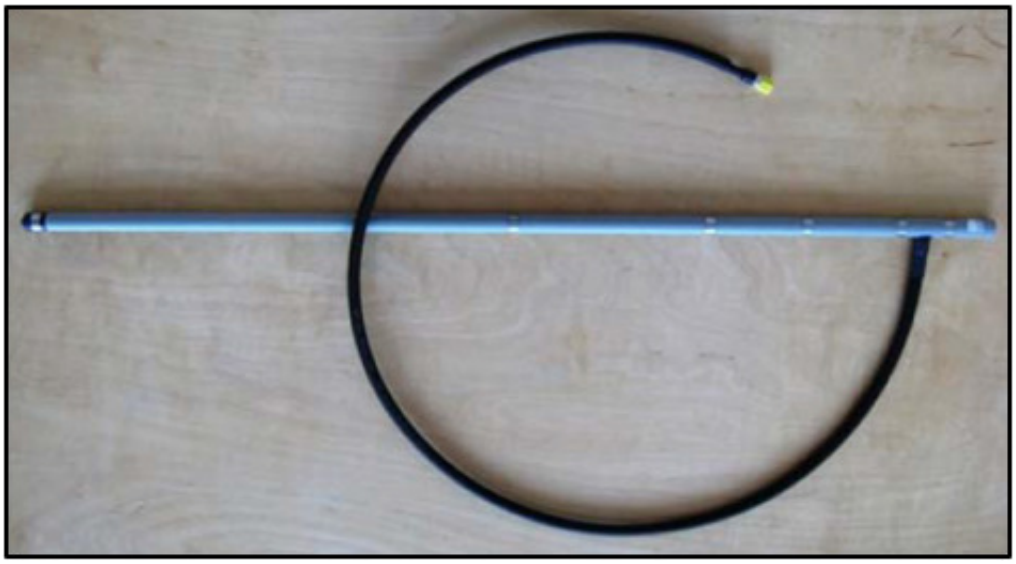

Figure 1.4: **Soil Temperature Profile Probe - UMS.** Reprinted from "Th3-v Soil Temperature Profile Probe - User Manual", (Figure. 1), by UMS, 2008, *UMS - user manuals.*

The last probe we tried was a "Wildfire probe". This probe was redesigned by a group of undergraduate students from the mechanical engineering department at the University of Idaho in 2013, with the help and sponsorship from the USDA Forestry Service, mainly with the help of Pete Robichaud, who I had the pleasure to meet and work with for a short time (Mindworks-Wikipedia, 2015). The Wildfire probe was originally designed by the Forest Service, and the students helped redesign it for better efficiency. This probe is meant to be buried in the ground before a wildfire passes over, and measures the temperature at different depths in the soil. This information becomes important for analysis because the carbon released by a fire coats the soil and causes it to be water-repellent, which will then lead to flooding and inevitable erosion (Certini, 2005). The characteristics needed for the probes were size and weight, as they must be carried long distances to the site of wildfires. The research group of students was able to redesign the probes dimensions, coming up with a stainless steel, hollow, rectangular probe of 12 inches (30.48 cm) in length, a 2 by 2 inch (5.08 by 5.08 cm) cross sectional view, and a weight of 3 pounds. The probe contains both thermocouples and data loggers inside it; and the thermocouples, which can be drawn out of the probe once it is in place, are at 1, 2, 3, 4, 6, and 8 cm depths from the top. The probe is meant to withstand temperatures of at least up to 80 ℃ at least. Refer to Figure 1.5 as a reference.

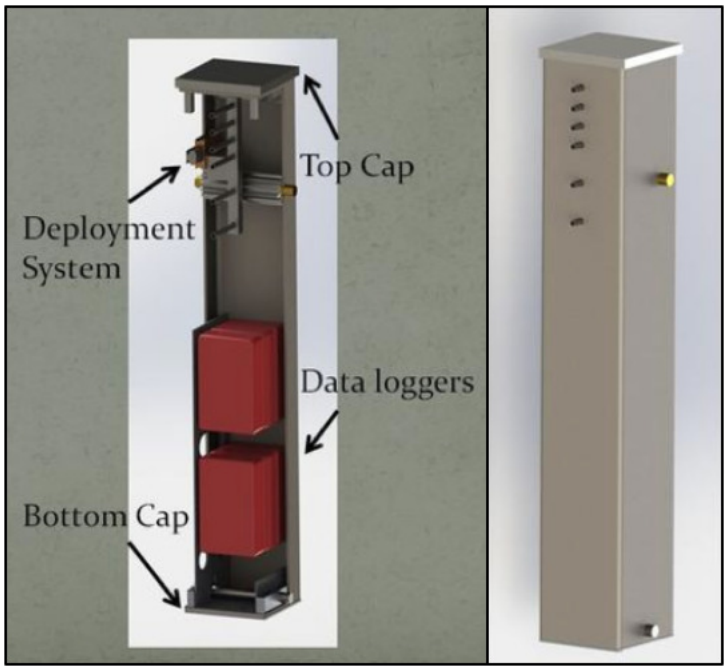

Figure 1.5: **Wildfire Temperature Probe**
Reprinted from *Mindworks Wikipedia*, n.d., 2015, from http://mindworks.shoutwiki.com/wiki/$Wildfire_temperature_probe$.

The Wildfire probe was appealing as the whole system is contained internally. However, it is fairly invasive (2 in^2), and quite heavy if we were to carry and deploy several in the field. Currently the probe is not for sale, and there are only about 10 in possession of the USDA Forestry Service, in Moscow, ID. Nonetheless, it was fantastic to get some experimentation with one of these. The experiments conducted with this probe are further explained in Chapter 2.

1.2.3 Quantifying the System and Time Series Measurements

Various researchers have noticed the potential for hydrothermal fluids to transport heat to the near-surface soils in geothermal systems. Several of them have provided the geothermal community with qualitative and semiquantitative uses of the elevated surface temperatures observed. Ingebritsen et al. (1989) examined the conductive heat flow in young volcanic rocks of the Cascade range of the the northwestern USA, and found a large area (between 44°00′ and 45°15′ N) of near zero heat flux in the younger (<6 Ma) rocks, an amount considerably lower than the heat being carried by the older rocks nearby. They attribute this loss of heat to the capture of it by lower temperature groundwater flow or by "yet-unidentified" thermal fluids.

Following this study, Manga (1998) presented a quantitative model of advective heat transport by lateral groundwater flow in the region, and they suggest from this that at least half of the background heat flux (the missing heat flux), which is equivalent to 56 mW/m^2, is being carried and later discharged by springs, despite their low temperatures of about 3.5 ˚C. This quantitative model analysis was further refined by Manga and Kirchner (2004), who suggested that if groundwater velocities are sufficiently high, most of the subsurface heat transport, and hence any background heat flux observed in an area, could be transported through advection. They suggest that the temperatures from the springs can then be used to infer the geothermal heat flux while accounting for three processes: the conversion of gravitational potential energy to heat through viscous dissipation, the conduction of heat to or from the Earth's surface, and geothermal warming; and they particularly attributed the first process's analysis a great potential for error if it is poorly done.

Burns et al. (2016) presented an extended analysis that applied the Manga and Kirchner (2004) 1-D quantitative model to the Eastern Snake River Plain (ESRP) aquifer, by generalizing the viscous heat generation term, which allowed application to anisotropic, porous media of arbitrary

geometry. They found from the model that geothermal warming and the conduction of heat to or from the Earth's surface had a greater fraction of the energy budget in most regions of the aquifer, but that the viscous dissipation of heat was, most likely, important for the aquifer in the headwaters region just a bit SW of the Yellowstone Plateau.

All of the studies mentioned above have considered the transport of heat by "slightly geothermal waters" (Burns et al., 2016), where the temperature of the groundwater is just slightly elevated above the average air temperature. For all these studies the thermal perturbation at the land surface is small, even in the cases where heat losses to the atmosphere make up a significant portion of the heat budget. Working in geothermal systems changes how the three processes suggested by Manga and Kirchner (2004) will interplay. Price et al. (2017) recently presented a quantitative framework, connecting surface temperature observations with conditions in the subsurface in a hydrothermal system located at Burgdorf Hot Springs, in the Payette National Forest. Price et al. (2017) do a fantastic job at presenting a simple, yet elegant quantification of the system, and suggest that the temperatures observed may be highly correlated to the Biot number (β), as opposed to the heat flux in the shallow subsurface.

Although all of these "geothermal" studies mentioned above seek to understand the heat budget and which mechanisms are more or less responsible for the expression of heat at any one location, given the scope of their corresponding study, they are all based under steady state conditions. None of these studies provide a data analysis or method regarding the change in heat flux, or other variables related to the system, through time.

Other studies in the geosciences have used time series measurements and the analysis of these to answer their scientific questions. Farbrot et al. (2007) present the first quantitative description of mountain permafrost in Iceland, obtained through analysis of four ground temperature time series recording from 2004-2006, which were established at shallow boreholes at high altitude in central and eastern Iceland. Through the simple 1-D model which reproduces the measured ground temperature patterns and simulates possible future climate scenarios, the results indicated that permafrost degradation will occur at these sites within decades, depending on the chosen scenarios and ice content. Another study which takes into account time series measurements and temperatures, describes long-term permafrost temperature and climate change in the northeastern Canadian High Arctic ($77° - 82.5°$ N) through the measurements obtained at four sites that have deep temperature

logs (Taylor et al., 2006). They found through their results of temperatures recorded over 20 years that the permafrost ground temperatures have increased 0.3° - 0.5℃/decade, compared to 0.6℃/decade for air temperatures; and they suggest this could be attributed to an increase of snow accumulation of 22 cm/decade, acting as an insulator from the colder atmospheric temperatures.

Another study by Keisling et al. (2017) used sediment samples collected at one centimeter intervals at Lake El'gygytgyn located in Arctic Russia. From these they analyzed samples every 10 cm throughout the composite core, resulting in a climatic reconstruction with about 2 thousand years resolution. With the resulting samples they were able to use the distribution of branches glycerol dialkyl glycerol tetraethers (brGDGTs) and the isotopic composition of plant leaf waxes to get a sense of the climatic evolution during the late Pliocene; and hence they were able to see a change in vegetation and temperatures through time, which they suggest is a cause of changing boundary conditions, including sea level, sea ice, and pCO_2. This study did not directly do time series measurements, but inferred them through their methodology.

It is by these studies and their achievements that I was motivated to combine the current geothermal measurement methodology with a time series modeling approach. In this study I develop a method used for ground temperature measurement in geothermal areas, and use the data obtained from it to provide an approach for quantification of the geothermal system under transient conditions.

1.3 First Experiment

1.3.1 Sampling Technology

As outlined in the previous section, it is apparent that estimating the heat flux at the land surface in geothermal areas is a useful, yet difficult task. The most accurate way to estimate the heat flux in any set amount of time extending over a few hours, that accounts for the difference in thermal conductivity of the soils, and the time-varying atmospheric condition, is to install a vertical sequence of thermocouple sensors in the shallow subsurface. Such a tool is usually a probe consisting of four to six sensors which are evenly distributed throughout its length, this being between 50 cm and 1 meters long.

In order for the research group to make use of such a probe we needed to first acquire one, and later test its accuracy. My advisor, Dr. Fairley, was given one by a colleague at the Idaho National Laboratories (INL) on one of his visits. The specific probe is an Omega stainless steel probe, 24 inches (60.96 cm) long, and $\frac{3}{16}$ inches (0.47 cm) of diameter, with 6 sensors distributed throughout its lower extent. The specifics of the sensor are detailed in section 1.2.2.

After our acquisition of the probe, we needed a mechanism to test its accuracy simulating conditions from our desired systems. A system which would replicate a vertical soil arrangement, with some heat source at depth, a way to control the temperature of both the atmosphere and the heat source, and some control measurement device. We created such a system in the laboratory through the use of affordable, and easy to access materials.

- Heating System:

    1. Hot plate: Heat source.
    2. Twelve inch inner (30.48 cm) diameter cast iron pan: Distributes the heat evenly throughout the surface.
    3. Eight inch (20.32 cm) square aluminum plate: Transfers heat quickly to the vertical sequence.

- Vertical Sequence:

    1. Eight inch diameter and 30 inch (76.2 cm) length PVC pipe: To contain our soils. A material which is also not very conductive.
    2. Thermal bubble roll: Used to insulate the PVC pipe from the atmospheric temperature and maintain inner temperature.
    3. Sand sized unconsolidated material: Our soil for the purpose of this experiment. It was much easier to acquire, and would not change the experiment's main goal if our soil was unconsolidated.
    4. Four drilled holes (about 2 mm thick) evenly spaced within the vertical sequence: These were drilled in order to insert the thermocouples, which would be our control system.

- Thermocouples and Date Loggers: [1] [2]

    1. Omega - K-Type Ready-Made Insulated Thermocouples with Kapton (5SC Series): Thermocouples inserted into the drilled holes made in the vertical sequence nearly to the extent of the pipe's radius, to come as close as possible to the measurements that would be seen from the Probe.
    2. Probe: The probe described above, which was inserted in the middle of pipes diameter to its full length.
    3. Extra thermocouples - One extra Omega K-Type ready-made insulated thermocouple (5SC Series): Recording the room temperature throughout the duration of the experiment.
    4. Data Loggers: 11 Onset U12-014 data loggers. One attached to every thermocouple termination connection.

Refer to the Figures 1.6 and 1.7 for internal and external layout correspondingly.

1.3.2 Experimental Set-up and Duration

The first experiment was conducted on April 07^{th}, 2016, and it lasted a total of 24 hours. For the first 10 hours the system was exposed to constant heat from the bottom, and the remaining 14 hours letting the system cool down, in order to get some recovery data. Table 1.1 shows the depths of each sensor within the vertical sequence. Table 1.2 shows times of experiment alterations, as well as temperature recordings every 30 minutes of the soil profile at the surface, of the room, of the aluminum plate, and of the cast iron pan. It is important to clarify that each thermocouple sensor (either in the vertical sequence, in the probe, or outside the system) was connected to its respective data logger and temperatures were being recorded every 45 seconds.

[1] "Thermocouples are used to measure temperatures by using two dissimilar conductors that contact each other in a circuit. In K type thermocouples, these conductors are chromel and alumel. A voltage is produced when the temperature at the contact point between the two conductors differs from the temperature at the reference points in other parts of the circuit. The measured voltage produced can be used to calculate the desired temperature when the temperature reference is known" (Lubenow, 2014)

[2] To ensure high-quality, and reproducible measurements, all thermocouples/probes sensors were calibrated in ice- and boiling-water baths before the start of the laboratory work (Lubenow et al., 2016). According to the National Institute Standards and Technology (NIST).

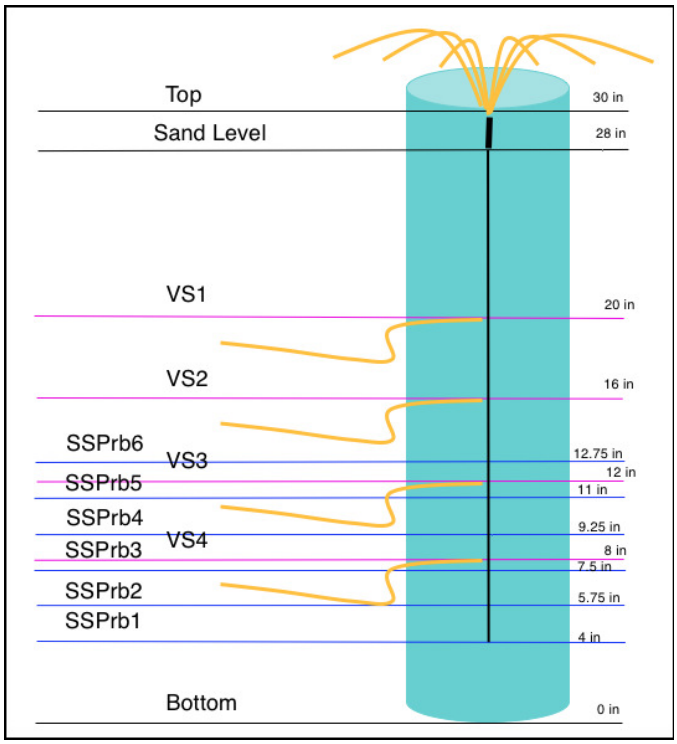

Figure 1.6: **Internal Set-up - 1st Experiment.** Each temperature sensor is labelled and its depth is marked by: blue lines for probe's sensors, and pink lines for vertical sequence's sensors (ex: **SSPrb1** is the deepest sensor in the inserted probe).

Figure 1.7: **External Set-up - 1st Experiment.**

Table 1.1: Depths of thermocouple sensors throughout vertical soil sequence.

Thermocouple Label or Marker	**Depth** (inches, 0 = bottom)
Aluminum Plate	0.00 in (0.00 cm)
SSPrb1	4.00 in (10.16 cm)
SSPrb2	5.75 in (14.60 cm)
SSPrb3	7.50 in (19.05 cm)
VS4	8.00 in (20.32 cm)
SSPrb4	9.25 in (23.49 cm)
SSPrb5	11.00 in (27.94 cm)
VS3	12.00 in (30.48 cm)
SSPrb6	12.75 in (32.38 cm)
VS2	16.00 in (40.64 cm)
VS1	20.00 in (50.80 cm)
Sand Level	28.00 in (71.12 cm)

Table 1.2: Experimental Timeline.

Time and Date	**Event**	**Temperatures:** (˚C) Room ($\mathbf{T_r}$), Soil surface ($\mathbf{T_{ss}}$), Aluminum plate ($\mathbf{T_{Alp}}$), and Cast Iron Pan ($\mathbf{T_{cip}}$)
04/07/2016: 0754	Start Experiment - Hot Plate on highest setting without vertical sequence.	$\mathbf{T_r}$**:** 20.9 ˚C
0824	Placed cast iron pan on top of hot plate and vertical sequence inside cast iron pan.	$\mathbf{T_r}$**:** 20.9 ˚C, $\mathbf{T_{ss}}$**:** 20.9 ˚C
0854	Temperature Recording.	$\mathbf{T_r}$**:** 21.0 ˚C, $\mathbf{T_{ss}}$**:** 21.0 ˚C, $\mathbf{T_{Alp}}$**:** 94.5 ˚C, $\mathbf{T_{cip}}$**:** 59.9 ˚C

Continued on next page

Table 1.2 – *Continued from previous page*

Time and Date	**Event**	**Temperatures:** (˚C) Room ($\mathbf{T_r}$), Soil surface ($\mathbf{T_{ss}}$), Aluminum plate ($\mathbf{T_{Alp}}$), and Cast Iron Pan ($\mathbf{T_{cip}}$)
0924	Temperature Recording.	$\mathbf{T_r}$**:** 21.2 ˚C, $\mathbf{T_{ss}}$**:** 21.2 ˚C, $\mathbf{T_{Alp}}$**:** 108.4 ˚C, $\mathbf{T_{cip}}$**:** 80.8 ˚C
0954	Temperature Recording.	$\mathbf{T_r}$**:** 21.0 ˚C, $\mathbf{T_{ss}}$**:** 21.3 ˚C, $\mathbf{T_{Alp}}$**:** 111.0 ˚C, $\mathbf{T_{cip}}$**:** 81.0 ˚C
1024	Temperature Recording.	$\mathbf{T_r}$**:** 20.9 ˚C, $\mathbf{T_{ss}}$**:** 21.3 ˚C, $\mathbf{T_{Alp}}$**:** 125 ˚C, $\mathbf{T_{cip}}$**:** 85.6 ˚C
1054	Temperature Recording and turned heat down 10% - setting “9”.	$\mathbf{T_r}$**:** 21.0 ˚C, $\mathbf{T_{ss}}$**:** 21.4 ˚C, $\mathbf{T_{Alp}}$**:** 144.9 ˚C, $\mathbf{T_{cip}}$**:** 100.8 ˚C
1124	Temperature Recording.	$\mathbf{T_r}$**:** 21.0 ˚C, $\mathbf{T_{ss}}$**:** 21.5 ˚C, $\mathbf{T_{Alp}}$**:** 145.0 ˚C, $\mathbf{T_{cip}}$**:** 113.1 ˚C
1154	Temperature Recording.	$\mathbf{T_r}$**:** 20.9 ˚C, $\mathbf{T_{ss}}$**:** 21.7 ˚C, $\mathbf{T_{Alp}}$**:** 144.5 ˚C, $\mathbf{T_{cip}}$**:** 118.0 ˚C
1224	Temperature Recording.	$\mathbf{T_r}$**:** 20.8 ˚C, $\mathbf{T_{ss}}$**:** 21.9 ˚C, $\mathbf{T_{Alp}}$**:** 125.0 ˚C, $\mathbf{T_{cip}}$**:** 118.0 ˚C
1254	Temperature Recording.	$\mathbf{T_r}$**:** 20.9 ˚C, $\mathbf{T_{ss}}$**:** 21.3 ˚C, $\mathbf{T_{Alp}}$**:** 132.3 ˚C, $\mathbf{T_{cip}}$**:** 114.0 ˚C
1324	Temperature Recording.	$\mathbf{T_r}$**:** 20.9 ˚C, $\mathbf{T_{ss}}$**:** 22.2 ˚C, $\mathbf{T_{Alp}}$**:** 137.0 ˚C, $\mathbf{T_{cip}}$**:** 107.0 ˚C

Continued on next page

Table 1.2 – *Continued from previous page*

Time and Date	**Event**	**Temperatures:** (˚C) Room ($\mathbf{T_r}$), Soil surface ($\mathbf{T_{ss}}$), Aluminum plate ($\mathbf{T_{Alp}}$), and Cast Iron Pan ($\mathbf{T_{cip}}$)
1354	Temperature Recording.	$\mathbf{T_r}$**:** 20.9 ˚C, $\mathbf{T_{ss}}$**:** 22.3 ˚C, $\mathbf{T_{Alp}}$**:** 136.8 ˚C, $\mathbf{T_{cip}}$**:** 115.6 ˚C
1400	Probe Insertion: At the middle of the vertical sequence's diameter.	
1424	Temperature Recording.	$\mathbf{T_r}$**:** 20.9 ˚C, $\mathbf{T_{ss}}$**:** 22.2 ˚C, $\mathbf{T_{Alp}}$**:** 138.9 ˚C, $\mathbf{T_{cip}}$**:** 106.0 ˚C
1454	Temperature Recording.	$\mathbf{T_r}$**:** 20.9 ˚C, $\mathbf{T_{ss}}$**:** 22.4 ˚C, $\mathbf{T_{Alp}}$**:** 135.5 ˚C, $\mathbf{T_{cip}}$**:** 105.5 ˚C
1524	Temperature Recording.	$\mathbf{T_r}$**:** 20.9 ˚C, $\mathbf{T_{ss}}$**:** 22.4 ˚C, $\mathbf{T_{Alp}}$**:** 139.2 ˚C, $\mathbf{T_{cip}}$**:** 112.0 ˚C
1554	Temperature Recording.	$\mathbf{T_r}$**:** 20.9 ˚C, $\mathbf{T_{ss}}$**:** 22.7 ˚C, $\mathbf{T_{Alp}}$**:** 137.6 ˚C, $\mathbf{T_{cip}}$**:** 117.0 ˚C
1600	Probe removal.	
1624	Temperature Recording.	$\mathbf{T_r}$**:** 20.9 ˚C, $\mathbf{T_{ss}}$**:** 22.7 ˚C, $\mathbf{T_{Alp}}$**:** 139.3 ˚C, $\mathbf{T_{cip}}$**:** 118.0 ˚C
1654	Temperature Recording.	$\mathbf{T_r}$**:** 21.0 ˚C, $\mathbf{T_{ss}}$**:** 22.9 ˚C, $\mathbf{T_{Alp}}$**:** 145.2 ˚C, $\mathbf{T_{cip}}$**:** 119.3 ˚C

Continued on next page

Table 1.2 – *Continued from previous page*

Time and Date	**Event**	**Temperatures:** (˚C) Room ($\mathbf{T_r}$), Soil surface ($\mathbf{T_{ss}}$), Aluminum plate ($\mathbf{T_{Alp}}$), and Cast Iron Pan ($\mathbf{T_{cip}}$)
1724	Temperature Recording.	$\mathbf{T_r}$**:** 21.0 ˚C, $\mathbf{T_{ss}}$**:** 23.0 ˚C, $\mathbf{T_{Alp}}$**:** 135.4 ˚C, $\mathbf{T_{cip}}$**:** 112.0 ˚C
1754	Temperature Recording.	$\mathbf{T_r}$**:** 21.0 ˚C, $\mathbf{T_{ss}}$**:** 23.0 ˚C, $\mathbf{T_{Alp}}$**:** 141.6 ˚C, $\mathbf{T_{cip}}$**:** 112.7 ˚C
1800	Turned hot plate off.	
1824	Temperature Recording.	$\mathbf{T_r}$**:** 21.0 ˚C, $\mathbf{T_{ss}}$**:** 23.1 ˚C, $\mathbf{T_{Alp}}$**:** 71.2 ˚C, $\mathbf{T_{cip}}$**:** 69.9 ˚C
04/08/2016: 1115 - 1210	Data recovery.	

1.3.3 Results and Discussion

From the first trial I expected to see similar temperature measurements from the "control - vertical sequence" thermocouples as those from the thermocouples in the probe. However, I saw that the temperatures recorded from the thermocouples in the probe were much higher. As an example, comparing thermocouples "VS4" and "SSPrb3" from Figure 1.6, we can see they are laying nearly at the same depth, so they should record similar temperatures; yet we can see below, in Figure 1.8, that the temperature measurements from "SSPrb3" are nearly 35 ˚C higher than those of "VS4" from times 1400 until 1600 (times during which the probe was inserted). This was a marker for us that something askew right, either with the probe or with the system.

It is also curious that the temperatures kept rising as recorded by all the VS thermocouples

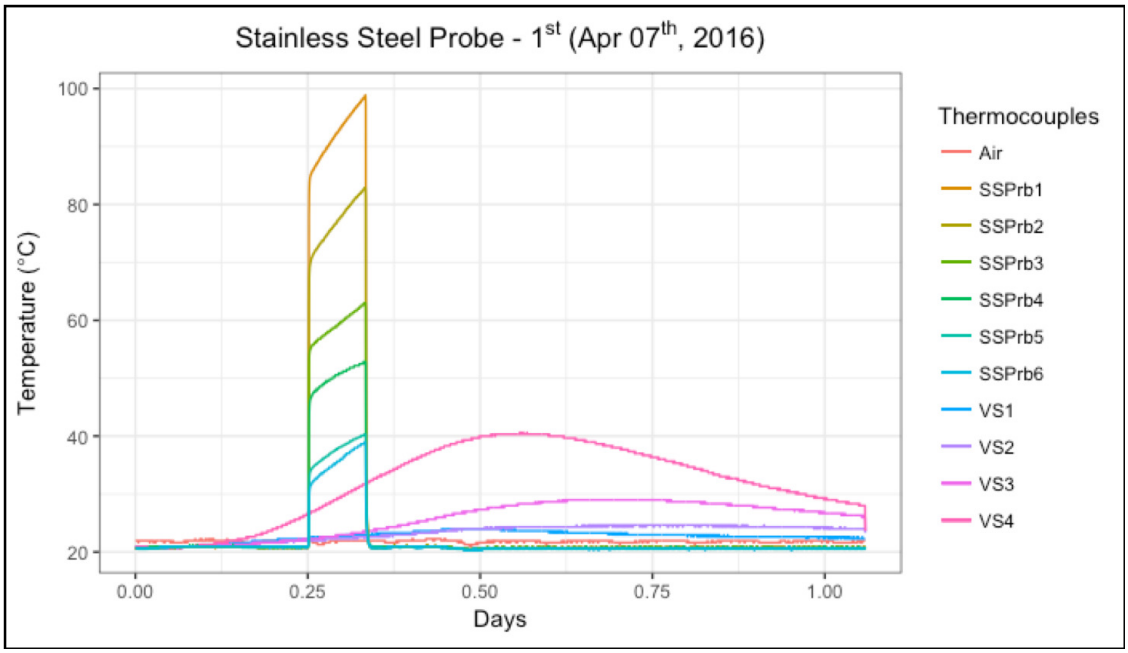

Figure 1.8: **Compiled Data from all Thermocouples** - 1st Experiment.

past the time when we turned the hot plate off. This is represented in Figure 1.8 at day ≈ 0.42 (time we turned the hot plate off), and the further temperature rise after day ≈ 0.42 until day ≈ 0.6 (times of maximum heat observed for the specific thermocouple). In conductive heat transfer once the source of heat stops emitting heat, the particles touching the source start cooling also, and the particles next to those particles will cool as well, and so on. Hence, we should see a decline in temperatures all throughout the sequence once the heat source is turned off. The rate of decline depends highly on the material through which heat is traveling, and its respective physical conditions, and also on the atmospheric temperature (Bergman and Incropera, 2011).

As baffled as I was about this odd phenomenon, I did some research of what could have possibly caused this rise in temperature. I found out that polyvinyl chloride (PVC) is very unstable under high heat. PVC will start dehydrochlorination at a temperature of 100 ˚C, temperature at which release of HCl happens, and this release causes an autocatalytic reaction. PVC will further decompose when temperatures reach 140 ˚C; and it will even melt when temperatures reach 160 ˚C (Titow, 2012). These properties explain why we would see a rise in the temperature for several hours past the time we had turned the heat source off; but they also meant we needed to change either the materials we were working with (PVC), or we would need to control the temperatures from our heat source to be under 100 ˚C. Because its feasibility, cost, and its ability to recreate

natural conditions, we chose the latter option.

1.3.3.1 Error Analysis

In any scientific experimental work, there is always a potential for error. Such error means the inevitable uncertainty that is related to all measurements (Taylor, 1997). Under such premise, I evaluated what the uncertainty may be for certain measurements done in our experimental work.

1. **Temperature Measurements - Thermocouple Readings:** All of our temperature measurements, were made with Omega-K-type thermocouple sensors, either from individual mini connectors, or from the stainless steel probe's thermocouples. Both of these thermocouple types show a percentage of uncertainty of 0.75%, number obtained from product manuals (Omega, 2018).

2. **Thermal Conductivity ($\mathbf{K_T}$) Vertical Sand Sequence:** I used the standard thermal conductivity value (Bergman and Incropera, 2011) for dry sands in all the experiments where the vertical sand sequence was used. And, although I probably should have taken the thermal conductivity of the sediments I used with the KD2 Pro our group has (from Decagon), and taken enough samples to get an averaged consistent reading, there is certain uncertainty from the value Bergman and Incropera (2011) provide. Apparently the best measurement for dry sands is 0.25, with an uncertainty of $\pm$ 0.05. This is a rather rough measurement estimate, with a percentage of uncertainty of 20%, but it is understood that there is a large diversity in sand sediments; what minerals they contain can affect the values seen, and the compaction of the grains can also make a difference.

Aside from errors with the uncertainty which attends each measurement, there are a few possibilities where other kinds of error were introduced while experimenting.

3. **Equipment Malfunction:** Different equipment pieces could have malfunctioned, hence causing our system's desired functioning to be deficient. These pieces of equipment were: Hot plate, PVC pipe's insulation, data loggers (although unlikely). As long as our direct measuring tools (temperature sensors) did not malfunction, I believe we would have been able to see such errors.

4. **Human Error:** I may have calculated the distances between thermocouples's holes wrong when making the vertical sequence. It is hard to get exact values, and easy to drill one or two millimeters off. I also could have wrongfully estimated when the experiments reached equilibrium, which I used to calculate values for heat flux. I could have also made wrongful distance measurements when placing the stainless steel probe tested (SSPrb) down the vertical sequence sands.

1.3.4 Second Set of Trials

Figure 1.9 exhibits the damage caused at the bottom of the PVC pipe, which acted as my vertical sequence. In order to continue using the same materials from the last experiment I had to empty the soil out of the column, turn it upside down, attach what used to be the top of the column (now the bottom) to the aluminum plate, and add the sediments back inside the newly constructed column. As a consequence of this, the depths at which the VS thermocouples had been were now different, as can be seen in Figure 1.10.

Figure 1.9: **Damage to the PVC pipe from the 1st experiment.**

The second trial of the first experiment was conducted from April 24th until April 27th, lasting a total of 72 hours. For the first 48 hours the system was exposed to constant heat from the bottom without exceeding 60 ˚C as a precaution, and the remaining 24 hours letting the system cool down, in order to get some recovery data. We decided to lengthen the time of the experiment

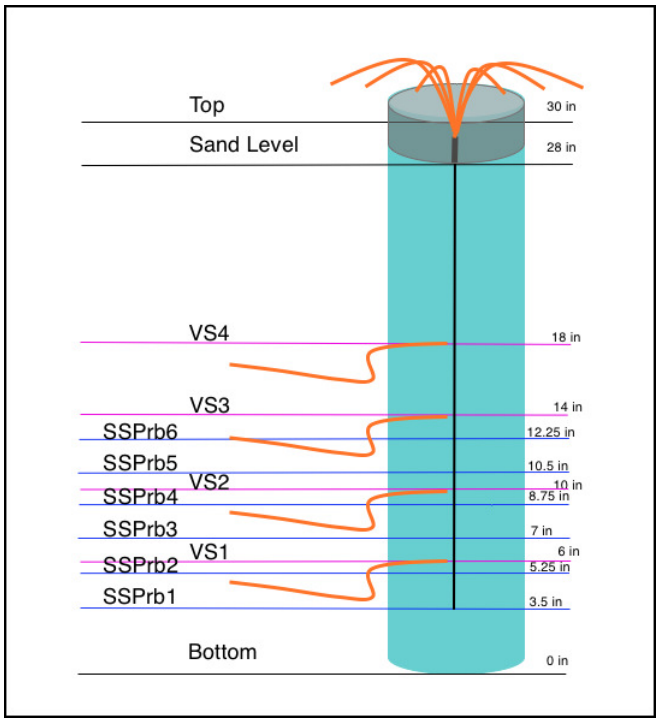

Figure 1.10: **Internal Set-up - 1st Experiment, 2nd Trial.** Each temperature sensor is labelled and its depth is marked by: blue lines for probe's sensors, and pink lines for vertical sequence's sensors (ex: **SSPrb1** is the deepest sensor in the inserted probe).

in order to certify the proper response time of the thermocouples. Holman and Gajda (2001) said that if the response time is slow in comparison with the rate of change of the temperature that you are measuring, then the thermocouple will not be able to truly represent the response to the temperature fluctuations. The amount of time was calculated using the Fourier number and the time required equation below (t). We can assume steady state when the Fourier number is greater than 1, have 95% confidence level the system is steady at Fourier numbers of 3, and have a 99.3% confidence level the system is steady at Fourier numbers of 5, which is why I used this number for our calculations (Omega, 1993). Refer to the calculations below for the properties of the material used at 300 K and for the time needed to assume steady state.

- $K_T = 0.27 \frac{W}{mK}$
- $\rho = 1515 \frac{Kg}{m^3}$
- $c_p = 800 \frac{J}{KgK}$
- $Fo = 5$
- $D = 8$ in
- $r = 4$ in $= 10.16$ cm $= 0.1016$ m
- $\alpha = \frac{K_T}{\rho c_p} = 2.2277 \text{ x } 10^{-7} \frac{m^2}{s}$
- $L_c^2 = (\frac{r}{2})^2 = 2.58064 \text{ x } 10^{-}3m^2$
- $t = \frac{FoL_c^2}{\alpha} = 57921.6232$ seconds $= 16.09$ hours

Table 1.3 shows the depths at which each sensor was within the vertical sequence. Table 1.4 shows times of experimental alterations, or temperatures recorded by hand occasionally. Alike the first trial of this experiment each thermocouple sensor (either in the vertical sequence, or in the probe, or outside the system) was connected to its respective data logger, and temperatures were being recorded every 45 seconds.

Table 1.3: Depths of thermocouple sensors throughout vertical soil sequence - 2nd Trial.

Thermocouple Label or Marker	**Depth** (inches, 0 = bottom)
Aluminum Plate	0.00 in (0.00 cm)
SSPrb1	4.00 in (10.16 cm)
SSPrb2	5.75 in (14.60 cm)
VS1	6.00 in (15.24 cm)
SSPrb3	7.50 in (19.05 cm)
SSPrb4	9.25 in (23.49 cm)
VS2	10.00 in (25.40 cm)
SSPrb5	11.00 in (27.94 cm)
SSPrb6	12.75 in (32.38 cm)
VS3	14.00 in (35.56 cm)
VS4	18.00 in (45.72 cm)
Sand Level	28.00 in (71.12 cm)

Table 1.4: Experimental Timeline - 2nd Trial.

Time and Date	**Event**	**Temperatures:** of Cast Iron Pan Only (˚C)
04/24/16 - 1245	Placed cast iron pan on hot plate and the vertical sequence inside the cast iron. And turned the hot plate on at about 4.5 heat emittance out of 10.	
04/25/16 - 1245	Probe Insertion: At the middle of the vertical sequence's diameter.	50 ˚C
04/26/16 - 1245	Turned hot plate off .	52 ˚C
04/27/16 - 1245 through 1315	Data recovery.	

1.3.5 Results and Discussion of the Second Trial

After this trial I expected to see a perfect system, where temperatures rose after I turned the hot plate (source) on, and an increase of temperature seen until reaching equilibrium, where temperatures would remain constant until the hot plate was turned off. Then I would see a decline of temperature measurements in all sensors. I also expected the temperatures measured from the sensors in the probe to be similar to those recorded by the vertical sequence thermocouples. The former expected outcome was just as predicted, Figure 1.11 below shows the times at which the thermocouples were recording, and the temperatures follow our predictions. However, the second expected outcome did not go as foreseen. Figure 1.11 shows how temperatures recorded by all of the sensors in the probe are much higher than those recorded by the vertical sequence thermocouples. If we take "SSPrb2" for example, which is very near the depth of "VS1", we see "SSPrb2" has temperature measurements of about 17 ˚C higher at all times since the probe was inserted and until I turned the hot plate off.

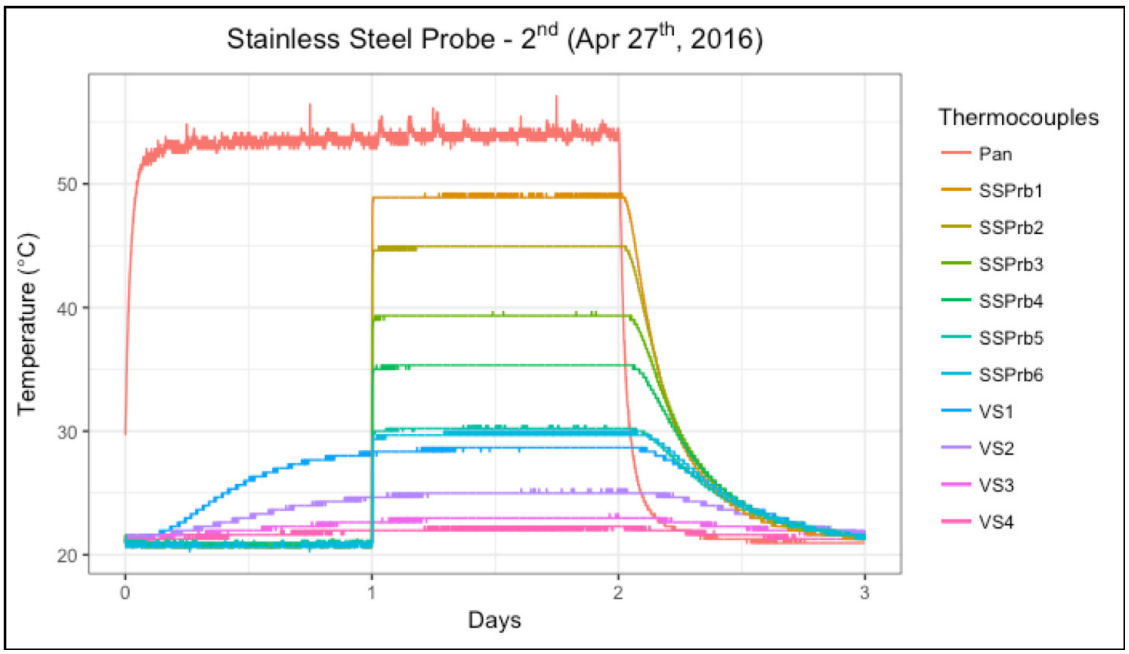

Figure 1.11: **Compiled Data from all Thermocouples** - 1st Experiment, 2nd Trial.

In order to see the effect in the heat flux measurements from using this probe we calculated the conductive heat flux based on the temperatures recorded from the probe's sensors versus the

conductive heat flux based on the temperatures recorded from the vertical sequence thermocouples. The time at which we took the temperatures was after equilibrium had happened, and the temperature used was an average from all temperatures taken from the time after reaching equilibrium and until the hot plate was turned off. Our results below show a heat flux calculation much higher for the probe's sensors than that from the vertical sequence thermocouples.

Probe q":	**Vertical Sequence** q":
$q" = -K_T \frac{dT}{dx}$	$q" = -K_T \frac{dT}{dx}$
$q" = -0.27 \frac{W}{mK}$ x $\frac{19.038K}{0.2225m}$	$q" = -0.27 \frac{W}{mK}$ x $\frac{6.484K}{0.3048m}$
$q" = 23.103 \frac{W}{m^2}$	$q" = 5.744 \frac{W}{m^2}$

From the data obtained in the trials from this experiment I can suggest that the highly-conductive materials from the stainless steel metal rod have a strong impact on the temperatures recorded and therefore have an effect on the calculated heat flux. From this, I can also suggest that some of the studies previously done with the use of such rods have erroneous heat flux calculations. In the following chapter I cover our attempt to construct a more viable option that serves to accurately estimate the heat flux in the shallow subsurface.

1.3.5.1 Error Analysis

1. **Temperature Measurements - Thermocouple Readings:** All of our temperature measurements, were made with Omega-K-type thermocouple sensors, either from individual mini connectors, or from the stainless steel probe's thermocouples. Both of these thermocouple types show a percentage of uncertainty of 0.75%, number obtained from product manuals (Omega, 2018).

2. **Thermal Conductivity (K_T) Vertical Sand Sequence:** I used the standard thermal conductivity value (Bergman and Incropera, 2011) for dry sands in all the experiments where the vertical sand sequence was used. And, although I probably should have taken the thermal conductivity of the sediments I used with the KD2 Pro our group has (from Decagon), and taken enough samples to get an averaged consistent reading, there is certain uncertainty from

the value Bergman and Incropera (2011) provide. Apparently the best measurement for dry sands is 0.25, with an uncertainty of ± 0.05. This is a rather rough measurement estimate, with a percentage of uncertainty of 20%, but it is understood that there is a large diversity in sand sediments; what minerals they contain can affect the values seen, and the compaction of the grains can also make a difference.

Aside from errors with the uncertainty which attends each measurement, there are a few possibilities where other kinds of error were introduced while experimenting.

3. **Equipment Malfunction:** Different equipment pieces could have malfunctioned, hence causing our system's desired functioning to be deficient. These pieces of equipment were: Hot plate, PVC pipe's insulation, data loggers (although unlikely). As long as our direct measuring tools (temperature sensors) did not malfunction, I believe we would have been able to see such errors.

4. **Human Error:** I may have calculated the distances between thermocouples's holes wrong when making the vertical sequence. It is hard to get exact values, and easy to drill one or two millimeters off. I also could have wrongfully estimated when the experiments reached equilibrium, which I used to calculate values for heat flux. I could have also made wrongful distance measurements when placing the stainless steel probe tested (SSPrb) down the vertical sequence sands. And, I could have made wrongful calculations for the heat flux shown above.

Chapter 2: Improvement of Measuring Equipment

2.1 Introduction

Given the results from our previous experiment, I noticed the need for a better ground temperature measurement tool. As covered in section 1.2.2, you can see that from the probes that were reviewed in the literature and those that were tested, none of them truly fit into the categories needed for us to use in the field, or some even in the lab. Those categories being:

- Easy to transport.
- Light weight.
- Robust and sturdy.
- Material needs to be heat resistant.
- Material can not be very heat conductive.
- Affordable to make, or to purchase.

Given the lack of available probes, and our need to find the temperature distribution and the heat flux at the shallow subsurface in geothermal areas, we decided to create our own probes.

2.2 Making of New Probes and Experiment

2.2.1 Sampling Technology

We believe, based on the work from Olmsted et al. (1986), Dawson (1964), Carslaw and Jaeger (1959), Lubenow et al. (2016), amongst others mentioned in section 1.2., that although it is useful to take ground temperature measurements below 1 m depth to minimize the effects from atmospheric conditions in the ground temperature readings, if we are taking continuous and periodic readings for a lapse of time longer than a day or two we can see these effects and account for them accordingly. Hence our probe is only a 25 inches (63.50 cm) long; which made it easier to meet the other criteria outlined above.

The creation of our probe was made with the help of the staff from the facilities department from the University of Idaho. They helped us with the material specifics that were used, as well as the overall design. The probe we created is made out of Nylon 6 plastic, a polyamide. This material is exemplary because of the strong bonds that make it, its robustness, and its thermal conductivity (Textile-Fashion-Study, 2013), which is nearly as conductive as the soils we were working in lab with, and as the epoxy used for the sealing of the probe's groove. The Table below (2.1) shows thermal properties of probe's materials, of the common sediments the probes would be in contact with, and other types of rocks for reference.

Table 2.1: Thermal Properties of Different Materials - values obtained from Bergman and Incropera (2011).

Material	**Upper Working Temperatures** (˚C)	**Thermal Conductivity** (K_T - $\frac{W}{mK}$)
Polyamide - Nylon 6	$\backsim$ 150 ˚C	$\backsim 0.26\frac{W}{mK}$
Epoxy Adhesive	$\backsim$ 150 ˚C	$\backsim 2.00\frac{W}{mK}$
Stainless Steel	$\backsim$ 1200 ˚C	$\backsim 16.50\frac{W}{mK}$
Coal, anthracite		$\backsim 0.26\frac{W}{mK}$
Sand		$\backsim 0.27\frac{W}{mK}$
Soil		$\backsim 0.60\frac{W}{mK}$
Clay		$\backsim 1.30\frac{W}{mK}$
Sandy Soil		$\backsim 1.80\frac{W}{mK}$
Limestone		$\backsim 2.15\frac{W}{mK}$
Sandstone		$\backsim 2.90\frac{W}{mK}$
Quartzite		$\backsim 5.38\frac{W}{mK}$

The probe is a cylindrical rod, 25 inches (63.50 cm) long, and 1 inch (2.54 cm) in diameter. The last inch and a half (3.81 cm)of its length has a conic shape, and throughout its length the probe has a groove, a hollow space of about 3.5 mm. Refer to Figure 2.1 for visualization of the rod, prior to completion or design. Inside the groove I laid 3 Omega K-Type ready-made insulated thermocouples with kapton (5SC Series); the first thermocouple sensor lies at 21 inches (53.34 cm) from the top, the second at 15 inches from the top, and the third at 9 inches from the top, each spaced 6 inches from the following one. Each thermocouple sensor lies outside the "encasing" (groove) of the probe, the connecting cable goes inside the encasing until it reaches the top of the probe, where it simply exits. At the termination of each thermocouple we attached a data logger when recording measurements (11 Onset U12-014 data loggers). The groove was filled with "clear weld" epoxy adhesive, due to its thermal resistivity (Table 2.1) and adhesive properties. Refer to Figure 2.2 for visualization of the probe after completion. The overall cost for the probe was around $75.00.

Figure 2.1: **Plastic Probe** - prior to completion of design.

In order to test the made probe, we used the same sampling laboratory set-up used in section 1.3. More specifically, we used the same set up as the one outlined in section 1.3.1 for the heating system, for the vertical sequence, and for the thermocouples and data loggers inside the vertical sequence. For the internal set up of the overall experiment the only thing that changed was the probe used. Instead of the Omega Stainless Steel probe, we placed our Nylon Plastic Probe, otherwise referred to as PPrb. Refer to Figure 2.3 for visualization of internal set-up of the current experiment.

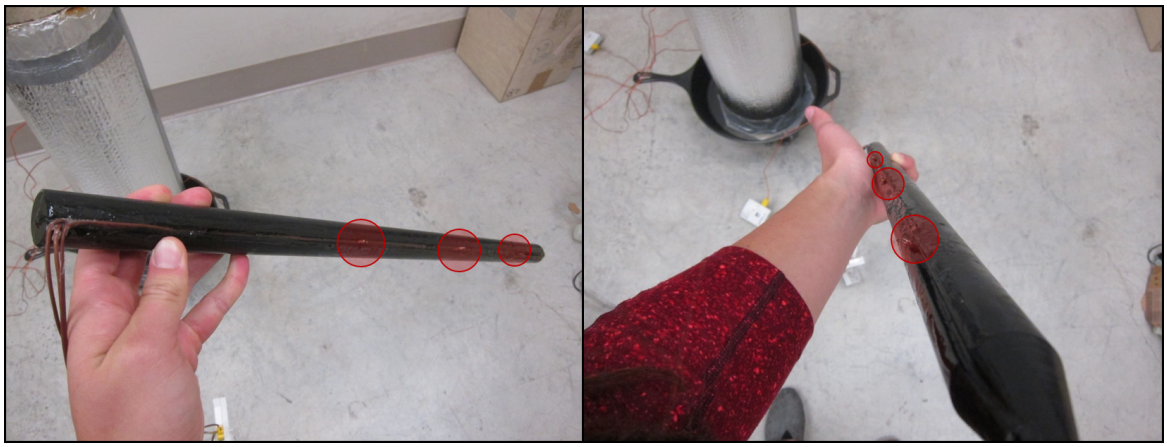

Figure 2.2: **Plastic Probe** - after completion. The red circles represent where the thermocouple sensors are located in the probe.

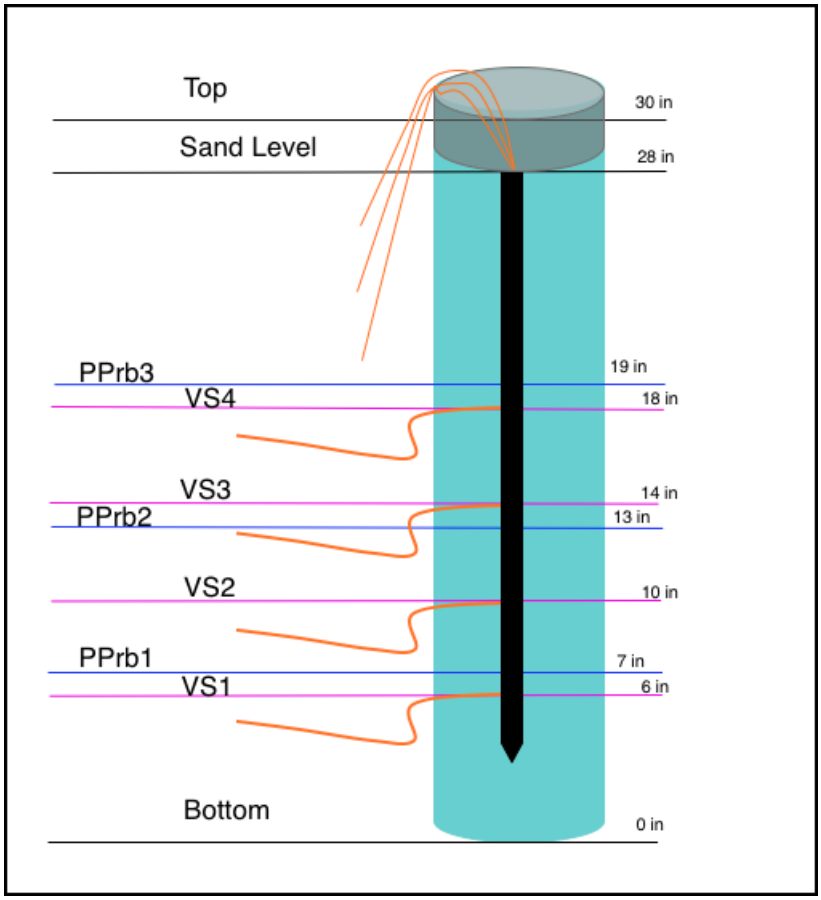

Figure 2.3: **Internal Set-up - Plastic Probe Experiment.** Each temperature sensor is labelled and its depth is marked by: blue lines for probe's sensors, and pink lines for vertical sequence's sensors (ex: **PPrb1** is the deepest sensor in the inserted probe).

2.2.2 Experimental Set-up and Duration

The experiment was conducted on September 15th, 2016, and it lasted a total of 72 hours. For the first 48 hours the system was exposed to constant heat from the bottom without exceeding 50 ˚C as a precaution, and the remaining 24 hours letting the system cool down, in order to get some recovery data. Hence, making it the same time of heat exposure as the second experiment we did with the stainless steel probe. Table 2.2 shows the depths at which each sensor was within the vertical sequence. Table 2.3 shows times of experimental alterations, or temperatures recorded by hand occasionally. As the last two experiments conducted under the same laboratory set up, but with a different probe, each thermocouple (either in the vertical sequence, or in the probe, or outside the system) was connected to its respective data logger, and temperatures were being recorded every 45 seconds.

Table 2.2: Depths of thermocouple sensors throughout vertical soil sequence - PPrb.

Thermocouple Label or Marker	**Depth** (inches, 0 = bottom)
Aluminum Plate	0 in (0.00 cm)
VS1	6 in (15.24 cm)
PPrb1	7 in (17.78 cm)
VS2	10 in (25.40 cm)
PPrb2	13 in (33.02 cm)
VS3	14 in (35.56 cm)
VS4	18 in (45.72 cm)
PPrb3	19 in (48.26 cm)
Sand Level	28 in (71.12 cm)

2.2.3 Results and Discussion

After this experiment our expected results were that the heat flux calculated through the vertical sequence thermocouples, and the one calculated through the probe's thermocouples would be similar, if not the same. And, just like in the previous experiments we also expected to see an increase in temperatures in all the vertical sequence thermocouples until reaching equilibrium and then a constant temperature reading until the hot plate was turned off, at which point we expected to see a decrease in temperature throughout the whole system. It turns out, that in this experiment both of our expectations were fulfilled. Refer to Figure 2.4 for a graph of the data.

Table 2.3: Experiment Timeline - PPrb.

Time and Date	**Event**	**Temperatures:** of Cast Iron Pan Only (˚C)
09/15/16 - 0920	Placed cast iron pan on hot plate and the vertical sequence inside the cast iron. And turned the hot plate on at about 3.5 heat emittance out of 10.	
09/16/16 - 0925	Probe Insertion: At the middle of the vertical sequence's diameter.	43 ˚C
09/17/16 - 0953	Turned hot plate off .	44 ˚C
09/18/16 - 0943 through 1005	Data recovery.	

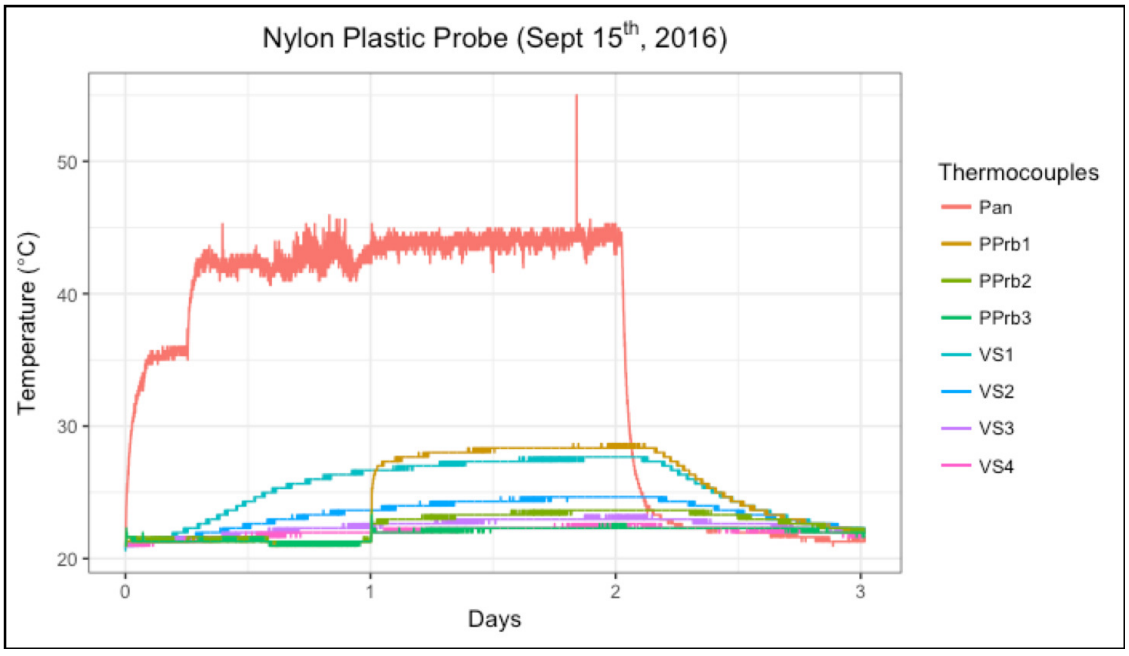

Figure 2.4: **Compiled Data from all Thermocouples** - Plastic Probe Experiment.

In order to see the effect in the heat flux measurements from using out new nylon probe, we calculated the conductive heat flux based on the temperatures recorded from the probes sensors

versus the conductive heat flux based on the temperatures recorded from the vertical sequence thermocouples. The time at which we took the temperatures was after equilibrium had happened, and the temperature used was an average from all temperatures taken from the time after reaching equilibrium and until the hot plate was turned off. Our results below show similar values for both cases.

Nylon Probe q": **Vertical Sequence** q":

$q" = -K_T \frac{dT}{dx}$ $q" = -K_T \frac{dT}{dx}$

$q" = -0.27 \frac{W}{mK}$ x $\frac{6.051K}{0.3048m}$ $q" = -0.27 \frac{W}{mK}$ x $\frac{5.172K}{0.3048m}$

$q" = 5.3604 \frac{W}{m^2}$ $q" = 4.5815 \frac{W}{m^2}$

From the data obtained in this experiment I can suggest that the material in which the temperature sensors are encased in, is of major relevance. The probe I made is ideal for measuring temperatures in the shallow subsurface of geothermal areas given its weight, its material, and its manufacturing cost, which is not as elevated as some of the other probes we though of using as a research group.

2.2.3.1 Error Analysis

1. **Temperature Measurements - Thermocouple Readings:** All of our temperature measurements, were made with Omega-K-type temperature sensors. These thermocouple type shows a percentage of uncertainty of 0.75%, number obtained from product manuals (Omega, 2018).

2. **Thermal Conductivity (K_T) Vertical Sand Sequence:** I used the standard thermal conductivity value (Bergman and Incropera, 2011) for dry sands in all the experiments where the vertical sand sequence was used. And, although I probably should have taken the thermal conductivity of the sediments I used with the KD2 Pro our group has (from Decagon), and taken enough samples to get an averaged consistent reading, there is certain uncertainty from the value Bergman and Incropera (2011) provide. Apparently the best measurement for dry sands is 0.25, with an uncertainty of ± 0.05. This is a rather rough measurement estimate,

with a percentage of uncertainty of 20%, but it is understood that there is a large diversity in sand sediments; what minerals they contain can affect the values seen, and the compaction of the grains can also make a difference.

Aside from errors with the uncertainty which attends each measurement, there are a few possibilities where other kinds of error were introduced while experimenting.

3. **Equipment Malfunction:** Different equipment pieces could have malfunctioned, hence causing our system's desired functioning to be deficient. These pieces of equipment were: Hot plate, PVC pipe's insulation, data loggers (although unlikely). As long as our direct measuring tools (temperature sensors) did not malfunction, I believe we would have been able to see such errors.

4. **Human Error:** I also could have wrongfully estimated when the experiments reached equilibrium, which I used to calculate values for heat flux. I could have also made wrongful distance measurements when placing the plastic probe tested (PPrb) down the vertical sequence sands. And, I could have made wrongful calculations for the heat flux shown above.

2.3 Field Experiment

Following the making of our Nylon 6 probe, we decided to do a field experiment in a geothermal area, and see what kind of information we could recover from our device. The initial idea was to have a temperature grid of about 20 squared meters, with a temperature probe inserted in the ground at every meter. This way we could get a fairly large areal extent to determine possible structural controls on the hydrothermal fluid flow paths in the area; and, through the probes' time series temperature measurements we would be able to understand what the effect from atmospheric conditions was on the soils in the temporal component.

However, although the probe had a low manufacturing cost, the expense would have added up quickly if we had decided to make 400 probes, and it would have been time consuming to put all of them together for the time we had an hand. So, given our resources, I made another 2 probes, and decided to make a similar field experiment but to a smaller scale, where the 3 probes were inserted into the ground and sat 1 meter from each other.

2.3.1 Burgdorf Hot Springs, ID - Site Description

Burgdorf Hot Springs is a rustic resort located in the Payette National Forest on the Burgdorf-French Creek Road. It is approximately 50 km north of the town of McCall, in Valley County, ID, USA (Figure 2.5). The area is in a region of Late Cretaceous granitic intrusive complexes that are associated with the Salmon River suture zone. These complexes were later deformed by the Late Cretaceous western Idaho shear zone (Giorgis et al., 2008). Unfortunately, there is little geological information available from this site or even the area surrounding it, at least 30 miles in all directions; and, to my knowledge the only geological map of the area is the 1:250,000 - *Geologic Map of the Elk City Quadrangle, Idaho* (Mitchell and Bennett, 1979). This map's details are quite blurry and hard to decipher, and the map does not provide much information to the scale I need for this project.

From site inspection by Mitchell et al. (1984), thermal waters discharge from two spring vents positioned near the toe of a hillslope, covered with Quaternary alluvium and glacial debris in its lower and middle portions. Its upper portions consist of Cretaceous granitic outcrops (Young and Mitchell, 1973). Currently, thermal groundwaters discharge into two spring boxes that feed a larger gravel bottomed pool, which is the "main pool" of the resort. From the pool this water then drains into French Creek, a perennial stream (Price et al., 2017).

2.3.2 Experimental Set-up and Duration

This site was chosen by our group based on a few factors:

1. Proximity: The site was relatively near our school (University of Idaho, Moscow, ID), and hence it would be easy to go there and back in one single day, if required.

2. Geothermal System: This was an area with known hydrothermal fluids, and had a heat output greater than average from its soils.

3. Previous Work: Our group had experience working at the site during the Summer of 2015. We had performed a temperature survey, and a seismic survey at the same site we chose for our current temperature grid.

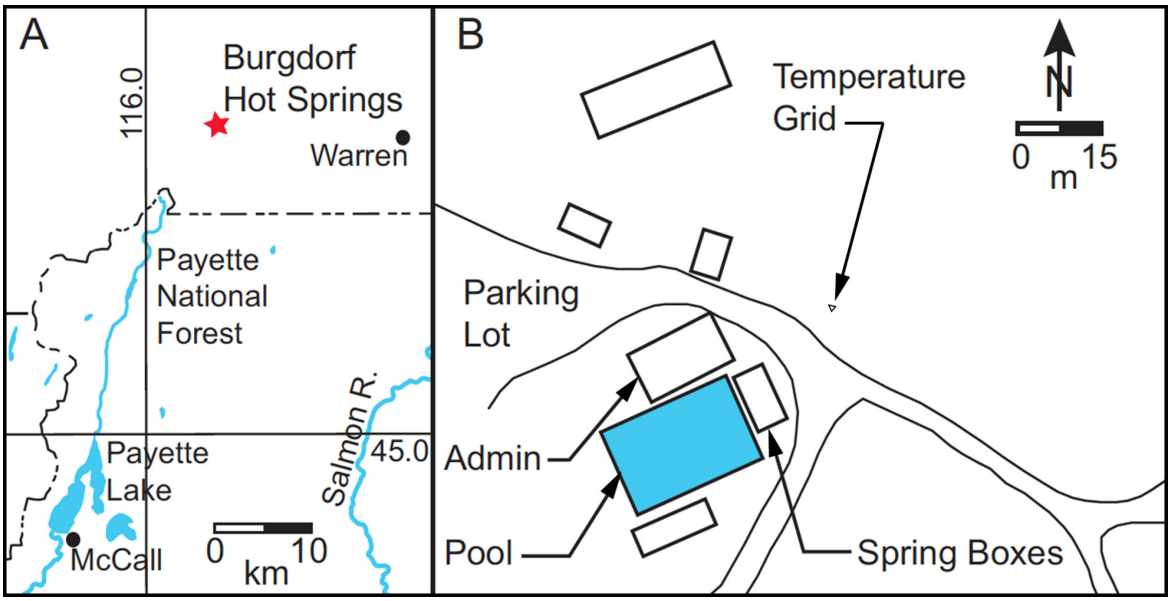

Figure 2.5: **Layout and location map of the study area - Burgdorf.** - (a)Location of the site, approximately 50 km north of McCall, ID, in the Payette National Forest (45.27608N, 115.91388W). (b) Detail map showing the placement of the temperature grid (triangular shape) in relation to the major structures at the site. → Adapted from "Interpretation of Ground Temperature Anomalies in Hydrothermal Discharge Areas", (Figure. 1), by A. N. Price, C. R. Lindsey, and J. P. Fairley, 2017, *Water Resources Research.*

4. Permission: Given we had done work at the site previously, we were able to contact the owners of the site rapidly, and they were happy to collaborate and help us once again.

Table 2.4: Field Experiment Specifics - Location, and Dates.

Aspect	**Details**
Start Date	October 21st, 2016
End Date	November 08th, 2016
Coordinate System	UTM Zone 11T - 5014302.55 N - 585251.29 E
Datum	NAD83
Elevation	1,868 m
Total Days	18.125 days

The specific location of the temperature grid site was chosen because it was within the previous temperature grid our group had done in 2015, and because the path for the thermal groundwaters fell right underneath the site, based on the results obtained from that study (Price et al., 2017). The amount of days chosen was based on how fast we could get there, and how soon we needed to be back prior to road closure; while still obtaining enough data that portrayed the daily, and potentially even the weekly, change in atmospheric conditions.

On October 21st, 2016, my advisor and one of my research group members, Jerry Fairley and Cary Lindsey respectively, and I, went to our chosen site (refer to Table 2.4 for specifics) and inserted the 3 probes, as Figure 2.5 shows (spaced 1 meter from each other, and leaving 4 inches (10.16 cm) from their length above ground for easier removal). We also set up the stainless steel probe, which we used in the the first couple of experiments described in section 1.3 of this thesis, near the center of the grid, just to to see what kind of readings we would get from it. Directly above the grid we set up a Davis Cup Anemometer from Decagon, now the METER Group, along with a stainless steel HOBO Onset waterproof data logger temperature sensor, to record atmospheric temperatures and wind speeds. Ultimately we took 10 readings of the thermal conductivity of the soils from the first few centimeters using the KD2 Pro Thermal Properties Instrument, also from Decagon. Figure 2.6a. shows the set up of the temperature grid from an aerial view, and Figure 2.6b. shows the set up from a cross sectional view. Figure 2.7a shows a picture of the set up after the insertion of the probes, and setting of the anemometer and the air temperature sensor; and Figure 2.7b shows a picture of the set up 18 days later.

While setting up our probes and starting the data loggers attached to each sensor, we found out that the deepest sensor from probe number 3 was no longer measuring any temperatures. I believe this could have been either from malfunctioning in the wire's length at insertion, or damaging of the sensor's tip. The rest of the sensors were still recording temperatures without any change, and they were what we considered "normal" readings. Recording of temperatures from data loggers started at 1139. And the data loggers were left to record every 45 seconds until recovery, 18 days later. After starting the data loggers we took the thermal conductivity and surficial temperature (5-10 cm) measurements using the KD2 Pro. Table 2.5 below shows the results for those measurements, and the locations for each measurement can be seen from Figure 2.6a.

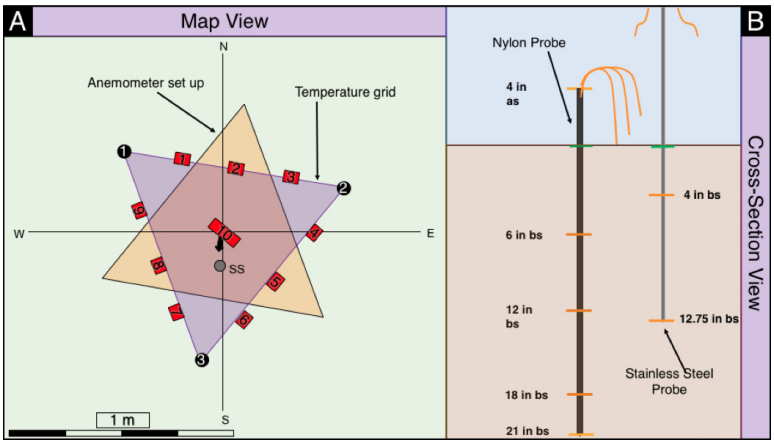

Figure 2.6: **Field Experiment Set-up - Burgdorf.** (a)Aerial View: Red boxes correspond to locations where we took thermal conductivity measurements. Black circles correspond to locations of each of the 3 probes. (b) Cross-Sectional View: Depths indicate height above or below surface at which each sensor falls depending on the probe type.

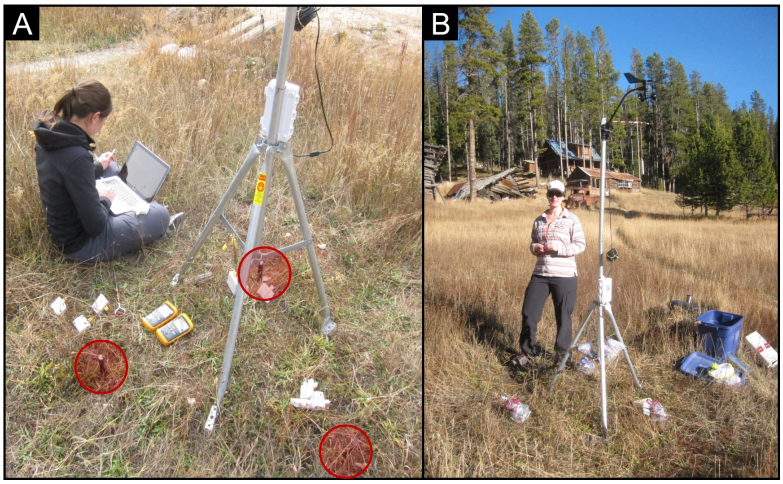

Figure 2.7: **Field Experiment - Burgdorf.** (a) Gabriela Villegas starting data loggers after insertion of probes and setting of anemometer. The red circles correspond to the location of the probes. (b) Meg Aunan 18 days after set up, experiment instruments are intact.

2.3.3 Results and Discussion of the Field Experiment

On November 08th, 2016, another one of my research group members, Meg Aunan, and I, went back into the field to recover our probes and our data. The first thing we did was recover the data from all the data loggers, then take the anemometer apart, and then recover the inserted probes. When we tried to recover the probes we encountered a bit of an issue, as it was incredibly hard to get a good grip on them and pull them out of the ground. Thankfully, one of the staff

Table 2.5: Surficial Temperatures and Thermal Conductivity.

Location Number	**Temperature** (˚C)	**Thermal Conductivity** (K_T - $\frac{W}{mK}$)
1	12.31 ˚C	0.889 $\frac{W}{mK}$
2	12.33 ˚C	0.850 $\frac{W}{mK}$
3	12.26 ˚C	0.888 $\frac{W}{mK}$
4	12.46 ˚C	1.071 $\frac{W}{mK}$
5	12.42 ˚C	0.922 $\frac{W}{mK}$
6	12.78 ˚C	0.987 $\frac{W}{mK}$
7	12.49 ˚C	1.021 $\frac{W}{mK}$
8	12.32 ˚C	0.829 $\frac{W}{mK}$
9	12.40 ˚C	0.969 $\frac{W}{mK}$
10	12.65 ˚C	1.022 $\frac{W}{mK}$

members from the Hot Springs Resort was able to help us dig the 3 plastic probes out, and by doing so, we damaged the top layer of the soil a bit. Refer to Figure 2.8 to see the damage to the soil.

Post recovery of the temperature measurements from the data loggers, and recovery of the probes we took the thermal conductivity and surficial temperature (5-10 cm) measurements using the KD2 Pro once more. Table 2.6 below shows the results for those measurements; and the locations for each measurement were the same as those made at the time of deployment, 18 days prior. The specific locations can be seen in Figure 2.6a.

From this field experiment we expected to see an increase in temperature as depth increased within the soil profile, and we expected to see daily oscillations in temperature in all the probes' sensors. We also expected to see the amplitude from the oscillation to decrease with depth, as the surficial conditions would have a lesser effect on the subsurface temperature.

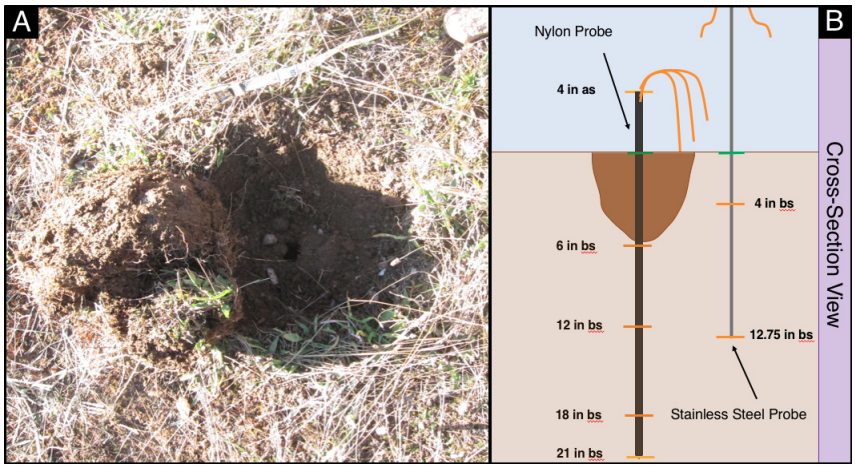

Figure 2.8: **Field Experiment Pick-up - Burgdorf.** (a) Soil damage at pick up in order to retrieve probe (about 8 inches (20.32 cm) diameter). (b) Cross-sectional view of damage to the soil at pick up (bs: below surface; as: above surface).

Table 2.6: Surficial Temperatures and Thermal Conductivity - at pick-up.

Location Number	**Temperature** (˚C)	**Thermal Conductivity** (K_T - $\frac{W}{mK}$)
1	13.06 ˚C	0.840 $\frac{W}{mK}$
2	13.44 ˚C	0.881 $\frac{W}{mK}$
3	13.92 ˚C	0.880 $\frac{W}{mK}$
4	14.20 ˚C	0.932 $\frac{W}{mK}$
5	13.38 ˚C	0.983 $\frac{W}{mK}$
6	13.65 ˚C	0.934 $\frac{W}{mK}$
7	13.11 ˚C	1.263 $\frac{W}{mK}$
8	14.36 ˚C	0.904 $\frac{W}{mK}$
9	13.37 ˚C	1.077 $\frac{W}{mK}$
10	13.71 ˚C	0.853 $\frac{W}{mK}$

In the following figures, we can see the resulting temperatures recorded by all the sensors, as well as the speed of the wind from our anemometer. Figure 2.9 shows all temperatures recorded by all thermocouples: the air's, the 3 plastic probes' (3 sensors each, except the one that got damaged (PPrb3D)), and the stainless steel probe's (2 sensors used). For greater clarity Figures 2.10 - 2.13 show air temperatures along with the temperatures recorded by the stainless steel probe's sensors, the first plastic probe (NW), the second plastic probe (SW), and the third plastic probe (NE), respectively. Figure 2.14 shows the wind speed data. And Figures 2.15 - 2.17 show the air temperatures along with the temperatures recorded by the shallow sensors, middle depth sensors, and deep sensors from the 3 plastic probes (correlated by depth in the ground).

Figure 2.9: **Compiled Data from all Probes' Sensors** - Burgdorf Field Experiment.

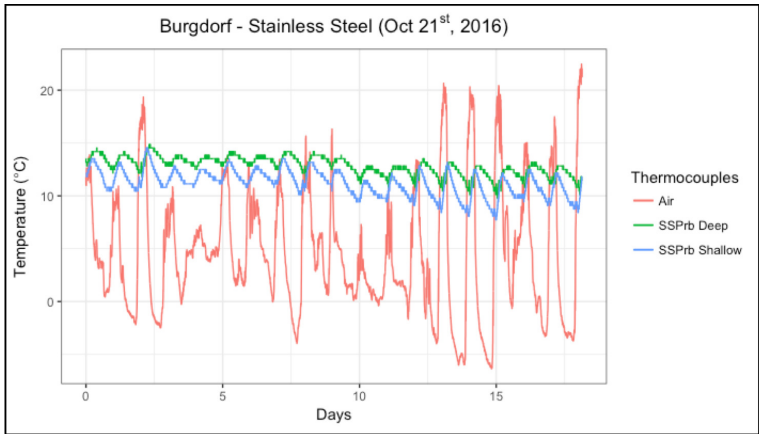

Figure 2.10: **Compiled Data from Stainless Steel Probe Sensors (1 and 6)** - Burgdorf Field Experiment.

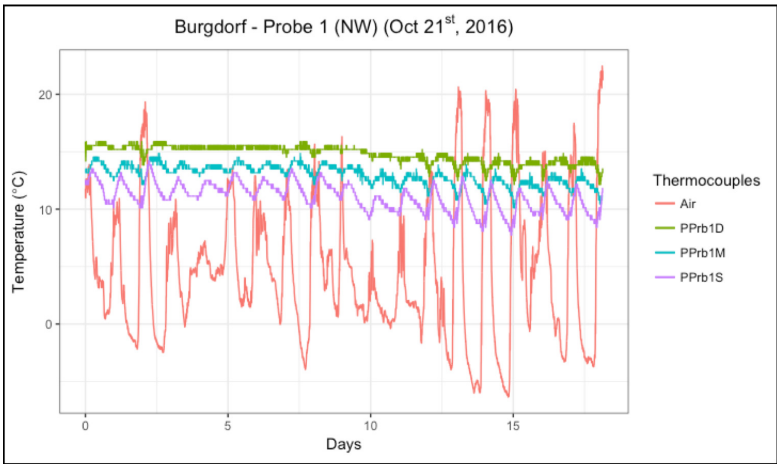

Figure 2.11: **Compiled Data from Plastic Probe - 1 (NW) Sensors** - Burgdorf Field Experiment.

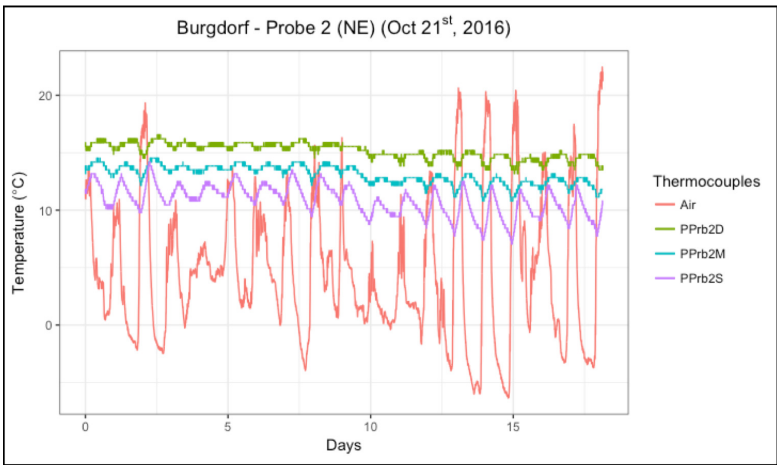

Figure 2.12: **Compiled Data from Plastic Probe - 2 (SW) Sensors** - Burgdorf Field Experiment.

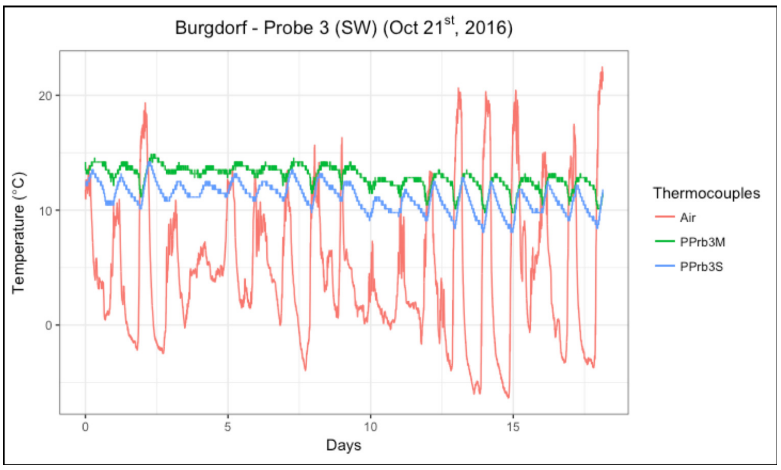

Figure 2.13: **Compiled Data from Plastic Probe - 3 (NE) Sensors** - Burgdorf Field Experiment.

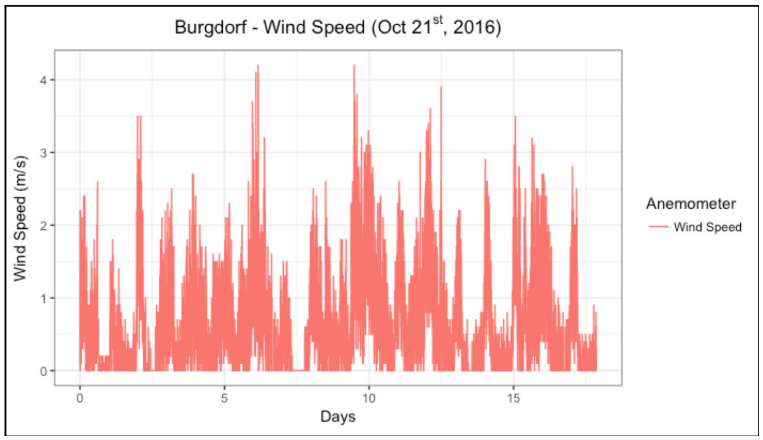

Figure 2.14: **Compiled Data from Anemometer** - Burgdorf Field Experiment.

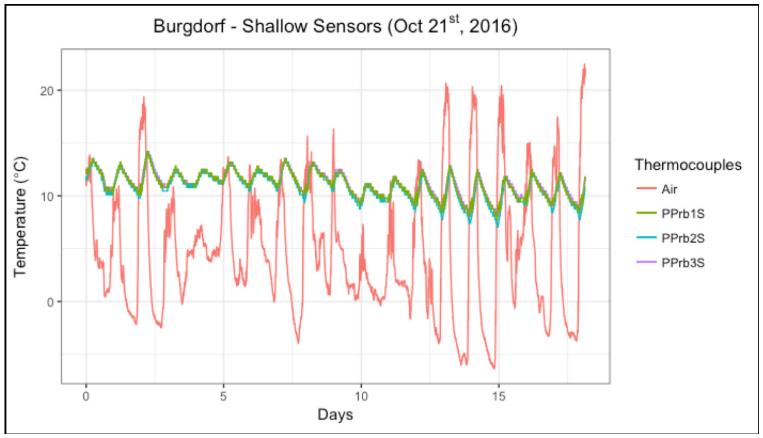

Figure 2.15: **Compiled Data from all the Plastic Probes Shallow Sensors** - Burgdorf Field Experiment.

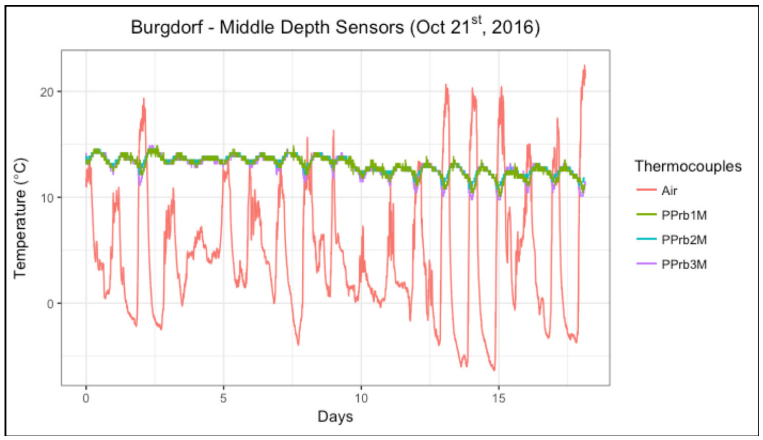

Figure 2.16: **Compiled Data from all the Plastic Probes Middle Depth Sensors** - Burgdorf Field Experiment.

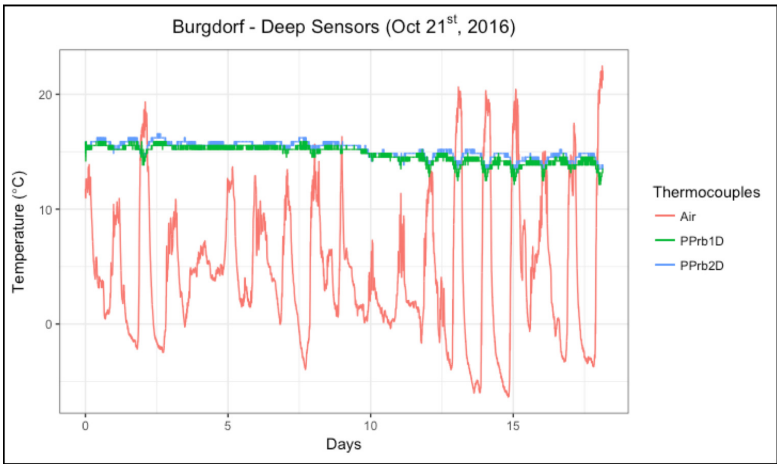

Figure 2.17: **Compiled Data from all the Plastic Probes Deep Sensors** - Burgdorf Field Experiment.

From these figures we can see a few important things:

1. The temperature increases as depth increases.

2. There are daily oscillations in temperature, these are very clear in the air temperature, but are present at all depths at which we had a sensor.

3. The oscillations' amplitude decreased, however, as the depth of the sensors increased, as we expected would happen.

4. The coldest temperatures of the day, recorded by the air's thermocouple, seem to have an

effect in the soil's temperature; this is seen throughout the sensors at all depths at which we were recording. However, the time of day at which we see the coldest temperatures in the soil do not match the time of day at which we see the coldest temperatures above the surface. The former happen a few hours after the latter, and the deeper the sensors were, the later the time we see the coldest temperatures with respect with the temperatures above the surface. The same pattern happens for warm temperatures recorded on the surface.

5. There is a cold front seen at around day 10 (Oct 31st) and this is recorded by all thermocouples. Unfortunately, weather station number 109560, located at the town of Warren, ID, (about 12 km East from our field location), which is the closest station from the Western Regional Climate Center has no daily record for temperature or precipitation for year 2016 (WRCC, 2018a,b). However their average temperature and precipitation for the two months were listed at weather station 105708 (at McCall, ID, 50 km South of our location). For October: Average temperature was 7.3 ˚C, and precipitation was 7.9 cm; and for November they were 2.75 ˚C, and 4.4 cm respectively. According to "Weather Underground", a weather website, the precipitation at McCall, ID, for the days of October 30th - November 05th was as follows: 0.15 cm, 0.18 cm, 0.23 cm, 2.54 cm, 2.8 cm, 2.54 cm, and 2.8 cm (Weather-Underground, 2018). This change in precipitation, perhaps, could have caused the temperature decrease we see in the latter half of the days the experiment took place.

6. We see little effect from the wind on the daily temperatures recorded at all soils depths. It appears to affect the air temperatures during the day, slightly, but does not seem to have an effect anywhere in the subsurface.

7. Unfortunately, we do see small temperature variations from atmospheric conditions on the temperatures recorded at all depths, and this leads me to believe that the length of our probes is not sufficient to eliminate the any potential influence from atmospheric conditions. We knew this was a likely possibility, nonetheless, and are aware of what these results will do to our analysis.

Most of these observations, were part of our expectations, and were for the most part understood. A few other ones were surprising, yet, not extraordinary. However, after doing this experiment, and from trying to understand the overall system (from which I could not find a heat flux that wasn't an average of all the records, yet), I realized there was a greater need for a model

that would represent a system like this one, that accounted for diurnal changes, and that accounted for the transfer of heat through the soils as well as the transfer of heat through the air.

We also realized that I needed to test our probes under extreme conditions. Although they worked sufficiently well for this experiment, and suffered minor damage, they did cause a bit of a problem at recovery. It was unclear what other aspects from our probes could be deficient, so the following experiment we conducted was to subject them to very extremely acid and hot conditions for a period of time longer than 3 days (refer to section 2.4.).

2.3.3.1 Error Analysis

1. **Temperature Measurements - Thermocouple Readings:** All of our temperature measurements, were made with Omega-K-type thermocouple sensors, either from individual mini connectors, or from the stainless steel probe's thermocouples. Both of these thermocouple types show a percentage of uncertainty of 0.75%, number obtained from product manuals (Omega, 2018).
2. **Thermal Conductivity ($\mathbf{K_T}$) of Sediments at Burgdorf:** From the recorded thermal conductivity values taken at our grid in Burgdorf Hot Springs (refer to Figure 2.5 and 2.6), we could determine that the thermal conductivity in our whole grid is about 0.945 with an uncertainty of $\pm$ 0.116. This is a percentage uncertainty of about 12.3%, but that seems normal given not all of our measurements were taken exactly at the same location.

Aside from errors with the uncertainty which attends each measurement, there are a few possibilities where other kinds of error were introduced while experimenting.

3. **Equipment Malfunction:** Different equipment pieces could have malfunctioned, hence causing our system's desired functioning to be deficient. These pieces of equipment were: Data loggers (although unlikely), anemometer, KD2Pro. As long as our direct measuring tools (temperature sensors, Davis cup, and KD2Pro sensor) did not malfunction, I believe we would have been able to see such errors.
4. **Human Error:** I could have made wrongful distance measurements when placing the plastic probes (PPrb), or the stainless steel probe (SSPrb) tested down the soils at our site (one probe

may have been slightly deeper that the other 2). I could have measured the distances between each probe wrong also.

2.4 Sulfuric acid

As I said in the previous paragraph, if we were going to deploy our made plastic probes in geothermal systems of any kind, we needed to be prepared for extreme conditions, such as high heat and acidity for a long period of time. In order to simulate such an environment in the laboratory, I needed to create a different system than the one used for the previous laboratory experiments. The environment needed to be constantly heated (near boiling temperatures), ideally from all directions (assuming soil contact with hydrothermal fluids in the field) except the surface, and the soils used needed to have a low pH at all times. Such an environment was difficult to create and keep at equilibrium, however I came up with something that worked sufficiently well.

2.4.1 Sampling Technology

- Heating System

    1. Hot Plate: Heat Source, which was kept on a high setting throughout the length of the experiment.

- "Contained System"

    1. 2000 mL Beaker (B_2): This beaker rested directly on top of the hot plate. It contained the water, which was the heating medium for the actual system.
    2. 1000 mL Long Beaker (B_1): This beaker was held by the support system, and hence was inside the 2000 mL beaker, touching the water inside it, but not touching any of the sides. It also contained the sulfuric acid rich silica sand.
    3. Silica Sand (Mesh 70-30): This was the sediment used to simulate soils in the field. Initially we had a more diverse sand sized sediment, but given its calcareous material content, we found it was not ideal for this experiment, as it kept balancing the acidity and making the sediment's pH neutral.

4. Sulfuric Acid (H_2SO_4) in solution: At normality of about 0.05. The original mix was diluted with dionized water to reach this normality. At this normality the pH was about 1-1.5, which is the most acid our research group has seen the hot springs to be.
5. Water: Heating medium - (bain-marie: water bath).

- Support System:

1. Support Stand with rod: About 50 cm long rod.
2. Clamp Holder: An extra clamp holder adjusted to the support stand to hold the extra rod.
3. Extra rod: An extra rod adjusted to the clamp holder. From this rod I hung the "water" temperature sensor.
4. Extra Wide Adjustable 3-prong Clamp: Borrowed from the chemistry department supplies. This clamp held the 1000 mL beaker.

- Probes, Thermocouples, and Data Loggers: [3]

1. Stainless Steel Probe: Described in section 1.3.1. We wanted to test how this probe would do under such an environment as well as our made probes.
2. Plastic (Nylon 6) Probe: Described in section 2.2.1. The main purpose of this experiment was to test how this probe withstood such environment.
3. Omega - K-Type Ready-Made Insulated Thermocouples with Kapton (5SC Series): We used two of these thermocouples to record temperatures also. We were curious to see how they performed under such environments as well.
4. Omega - K-Type Ready-Made Insulated Thermocouples with Glass Braid (5LSC Series): We used one of these thermocouple to record temperatures. We wanted to see if the material would have any effect in comparisson with the Kapton covered thermocouples.
5. Data Loggers: 11 Onset U12-014 data loggers. One attached to every thermocouple termination connection. We only had one of the sensors from the plastic probe recording temperatures because the other two were too high up that were not submerged under

[3] To ensure high-quality, and reproducible measurements, all thermocouples/probes were calibrated in ice- and boiling-water baths before the start of the laboratory work (Lubenow et al., 2016). According to the National Institute Standards and Technology (NIST).

the soil - hence only one data logger was attached to a termination here. And we only had two data loggers attached to the stainless steel probe sensors, one from the deepest sensor, and one from the shallowest sensor.

6. Data Loggers - Water and Air: U12 Stainless steel HOBO Onset waterproof data logger temperature sensor. These two data logger temperature sensors were used to record temperatures of the water and the air respectively.

- Extra materials needed for measurements during experiment's duration:

1. Fume Hood: We conducted this experiment under a fume hood, to prevent any fumes expelled to remain in the laboratory room.
2. Weight Scale: Precise weight scale to the nearest mg. Used to add sulfuric acid to the 1000 mL beaker when needed, as it evaporated with the heat exerted on the beaker.
3. Glass pH Probe for hot environments: Used to test soil pH prior and during the experiment to check it remained acid enough. Also used after the experiment to test the sediments neutralization process for its disposal.
4. Deionized Water: Used to clean any surfaces needed in the experiment.
5. Baking Soda ($NaHCO_3$): Used after the experiment to neutralize the sediments and be able to dispose of them.
6. Citric Acid ($C_6H_8O_7$): Used after the experiment to neutralize the sediments and be able to dispose of them.
7. Plastic Tub: Used after the experiment, as a place to neutralize the sediments in and later be able to dispose of them.
8. Extra Laboratory Instruments: Gloves, goggles, robe, additional beakers, mixing instruments, kim wipes, NaOH.

Refer to the Figures 2.18 and 2.19 for internal and external layout of this experiment correspondingly.

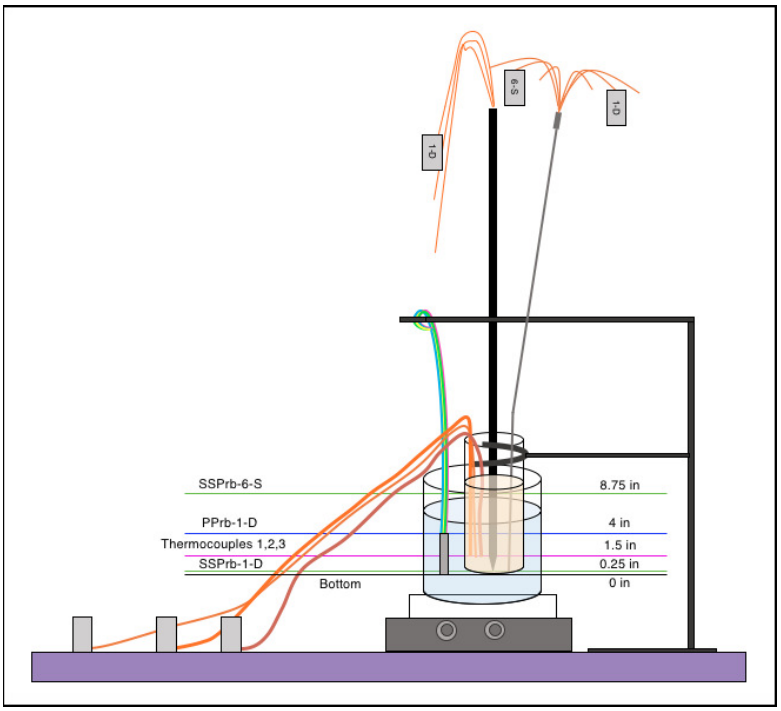

Figure 2.18: **Internal Set-up - H_2SO_4 Experiment.** Each temperature sensor is labelled and its depth is marked by: blue lines for plastic probe's sensors, pink lines for individual thermocouples, and green lines for stainless steel probe's sensors. The plastic and stainless steel probe, and the individual thermocouples are inserted into the saturated sand beaker; which is submerged in the water beaker, which is in turn being heated by the hot plate directly underneath (ex: **PPrb-1-D** is the deepest sensor in the inserted plastic probe).

Figure 2.19: **External Set-up - H_2SO_4 Experiment.**

2.4.2 Experimental Set-up and Duration

This experiment was conducted on March 27th, 2017, and it lasted a total of 120 hours. During these hours I added cold water to the 2000 mL beaker in many occasions to keep the system under bain-marie; and I added H_2SO_4 in solution to the 1000 mL beaker several times to keep the system at constant liquid saturation. Table 2.7 shows the depths at which each thermocouple and sensor fell (having the "bottom" being the bottom of the 1000 mL beaker). Table 2.8 shows times of experiment alterations or "events", as well as randomly spaced temperature recordings of the water and of the soil. It is important to clarify that temperature sensor (either a single wire, or inside either the probe, or outside of the system) was connected to its respective data logger and temperatures were being recorded every 45 seconds.

From this experiment I expected to see uniform temperatures in all 3 single wire thermocouples. And slightly lower temperatures progressing upwards in our system (refer to Figure 2.18). I also expected all probes and single wire thermocouples to have no physical damage done to them from the high heat or acidity.

Table 2.7: Depths of thermocouple sensors throughout experimental set-up H_2SO_4.

Thermocouple Label or Marker	**Depth** (inches)	
Bottom of 1000 mL beaker	0.00 in	(0.00 cm)
Bottom of 2000 mL beaker	-2.50 in	(6.35 cm)
Hot Plate	-2.60 in	(6.60 cm)
SSPrb-1-Deep	0.25 in	(0.635 cm)
Thermocouple 1, 2, 3.	1.50 in	(3.81 cm)
PPrb-1-Deep	4.00 in	(10.16 cm)
SSPrb-6-Shallow	8.75 in	(22.22 cm)
Top of Soil - inside 1000 mL beaker	9.00 in	(22.86 cm)

Table 2.8: Experiment Timeline - H_2SO_4 Experiment (1000 mL Beaker (B_1), 2000 mL (B_2); Water (W), and Sand (S)).

Time and Date	**Event**	**Weight** (grams)	**Temperature** (℃)
03/27/17 - 1040 - 1140	Weighted the two beakers first.	**B_1:** 345.46 g **B_2:** 448.73 g	
	Weighted with 660 mL sand (B_1).	**B_1:** 1130.68 g	
	Weighted with 660 mL sand & 320 mL H_2SO_4 (B_1).	**B_1:** 1454.74 g	
	Weighted with 1315 mL water and stirrer (B_2).	**B_2:** 1771.09 g	
	pH of saturated sand (B_1): **2.18**.		
03/27/17 - 1100	Launched data loggers.		
03/27/17 - 1123	Insertion of thermocouples and Probes.	**B_1:** 2139.02 g	
03/27/17 - 1154	Turning hot plate on. Heat setting: 7; Stirring: 4.		
03/27/17 - 1156	Temperature Check.		**W:** 24.0 ℃ **S:** 20.0 ℃
03/27/17 - 1220	Temperature Check.		**W:** 83.2 ℃ **S:** 58.0 ℃

Continued on next page

Table 2.8 – *Continued from previous page*

Time and Date	**Event**	**Weights** (grams)	**Temperatures** (˚C)
03/27/17 - 1325	Temperature Check. Reduce Heat setting: 6. Added 250 mL water (B_2).		**W:** 98.0 ˚C **S:** 70.0 ˚C
03/27/17 - 1500	Temperature Check. Reduce Heat setting: 5. Added 400 mL water (B_2). Added 20 mL H_2SO_4 (B_1).	**B_1:** 2121.75 g	**W:** 97.9 ˚C **S:** 67.0 ˚C
03/27/17 - 1621	Temperature Check.		**W:** 87.0 ˚C **S:** 67.0 ˚C
03/27/17 - 1653	Temperature Check. Added 150 mL water (B_2).		**W:** 88.2 ˚C **S:** 66.3 ˚C
03/27/17 - 2045	Temperature Check. Reduce Heat setting: 4.5. Added 300 mL water (B_2).	**B_1:** 2030.54 g	**W:** 93.4 ˚C **S:** 66.0 ˚C

Continued on next page

Table 2.8 – *Continued from previous page*

Time and Date	**Event**	**Weights** (grams)	**Temperatures** (˚C)
	Added 100 mL H_2SO_4 (B_1).		
03/28/17 - 0739	Temperature Check.	**B_1:** 2037.43 g	**W:** 88.0 ˚C **S:** 45.0 ˚C
	Added 800 mL water (B_2).		
	Added 40 mL H_2SO_4 (B_1).		
03/28/17 - 1053	Temperature Check.		**W:** 85.5 ˚C **S:** 79.8 ˚C
	Added 200 mL water (B_2).		
	Added 60 mL H_2SO_4 (B_1).		
03/28/17 - 1307	Temperature Check.	**B_1:** 2043.42 g	**W:** 80.0 ˚C **S:** 69.0 ˚C
	Added 100 mL water (B_2).		
	Added 100 mL H_2SO_4 (B_1).		
03/28/17 - 1819	Temperature Check.	**B_1:** 2111.93 g	**W:** 86.7 ˚C **S:** 76.6 ˚C
	Added 400 mL water (B_2).		
03/28/17 - 2216	Temperature Check.		**W:** 83.7 ˚C **S:** 79.1 ˚C
	Added 200 mL water (B_2).		

Continued on next page

Table 2.8 – *Continued from previous page*

Time and Date	**Event**	**Weights** (grams)	**Temperatures** (˚C)
03/29/17 - 0903	Temperature Check.	**B_1:** 1990.28 g	**W:** 87.5 ˚C **S:** 48.9 ˚C
	Added 1000 mL water (B_2).		
	Added 140 mL H_2SO_4 (B_1).		
03/29/17 - 1223	Temperature Check.		**W:** 79.6 ˚C **S:** 77.7 ˚C
	Added 100 mL water (B_2).		
03/29/17 - 1502	Temperature Check.	**B_1:** 2063.62 g	**W:** 88.3 ˚C **S:** 73.5 ˚C
	Added 475 mL water (B_2).		
	Added 80 mL H_2SO_4 (B_1).		
03/30/17 - 0740	Temperature Check.	**B_1:** 2075.53 g	**W:** 93.0 ˚C **S:** 59.0 ˚C
	Added 750 mL water (B_2).		
	Added 60 mL H_2SO_4 (B_1).		
03/30/17 - 1300	Temperature Check.	**B_1:** 2051.55 g	**W:** 86.3 ˚C **S:** 74.2 ˚C
	Added 350 mL water (B_2).		

Continued on next page

Table 2.8 – *Continued from previous page*

Time and Date	**Event**	**Weights** (grams)	**Temperatures** (˚C)
03/30/17 - 1905	Added 90 mL H_2SO_4 (B_1). Temperature Check. Added 425 mL water (B_2).	**B_1:** 2069.50 g	**W:** 88.0 ˚C **S:** 73.2 ˚C
03/31/17 - 0728	Added 75 mL H_2SO_4 (B_1). Temperature Check. Added 1040 mL water (B_2).	**B_1:** 2051.90 g	**W:** 86.3 ˚C **S:** 51.4 ˚C
03/31/17 - 1333	Added 85 mL H_2SO_4 (B_1). Temperature Check. Added 350 mL water (B_2).	**B_1:** 2066.27 g	**W:** 86.8 ˚C **S:** 83.2 ˚C
03/31/17 - 2305	Added 70 mL H_2SO_4 (B_1). Temperature Check. Added 675 mL water (B_2).	**B_1:** 2062.94 g	**W:** 91.3 ˚C **S:** 64.9 ˚C

Continued on next page

Table 2.8 – *Continued from previous page*

Time and Date	**Event**	**Weights** (grams)	**Temperatures** (˚C)
04/01/17 - 1010 04/01/17 - 1100	Added 80 mL H_2SO_4 (B_1). Temperature Check & turn hot plate off. Stop logging from data loggers.	**B_1:** 2061.43 g	**W:** 95.1 ˚C **S:** 59.4 ˚C

Below, in Figure 2.20, we see two pictures, the one on the left shows how I weighted the equipment constituting the inside of B_1 (1000 mL beaker). And the picture on the right shows me taking a temperature measurement of the sand. Both of these pictures were taken the first day of the experiment.

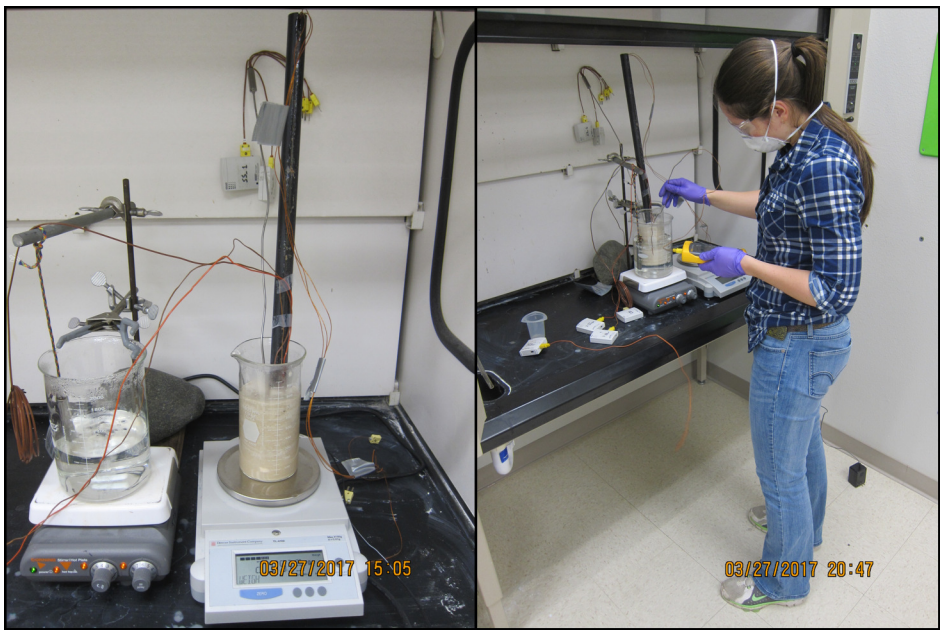

Figure 2.20: **Weigh in - H_2SO_4 Experiment.**

2.4.3 Results and Discussion

From the graph below (Figure 2.21), all temperature sensors recording the times when I added cold water to the experiment, and even when I added the H_2SO_4. All measurements seem reasonable and go according to our expectations except the temperatures recorded by the shallowest sensor from the stainless steel probe (SSPrb Shallow). We can see that for the most part the temperatures recorded by it exceed those from the water, which I can only think to attribute to the highly conductive material of the probe.

From this experiment I also saw that all thermocouples and probes were intact, no damage was done by the low pH or by the heat under which they were subjected. This result means that the material of our probes is not a problem, and they can be deployed in a setting under similar conditions, which is what we were hoping would happen.

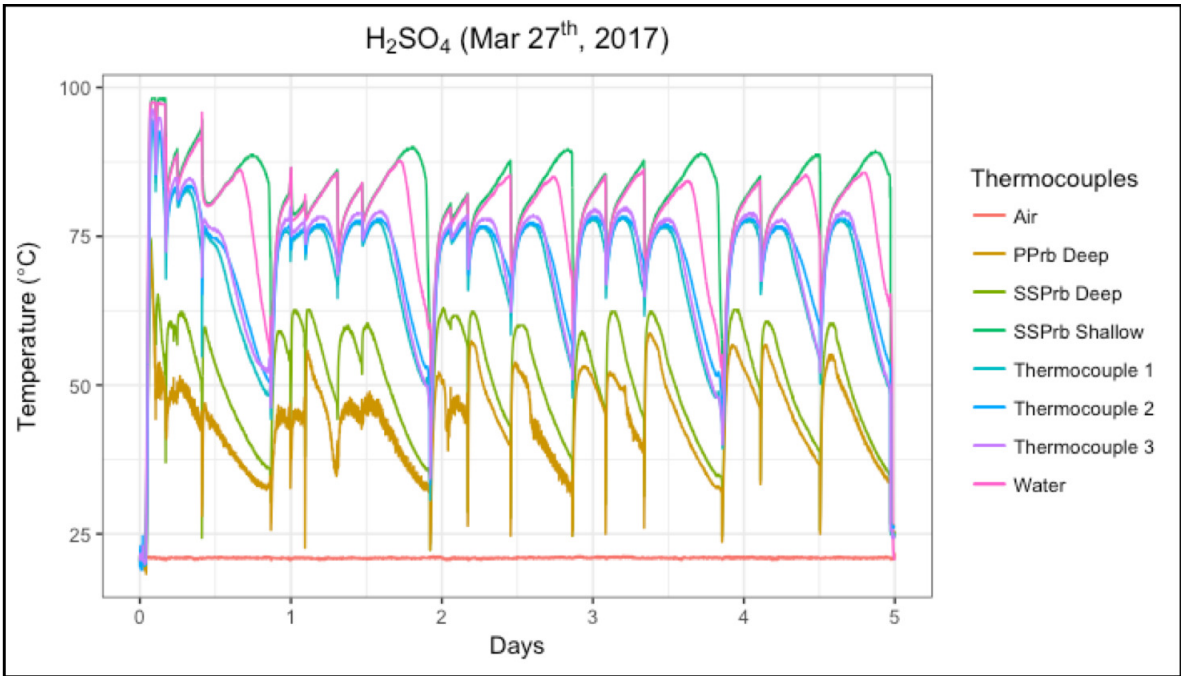

Figure 2.21: **Compiled Data from all the Thermocouples and Probes' Sensors** - H_2SO_4 Field Experiment.

2.4.3.1 Error Analysis

1. **Temperature Measurements - Thermocouple Readings:** All of our temperature measurements, were made with Omega-K-type temperature sensors, or with K type thermocouples inside the stainless steel probe. Both of these thermocouple types show a percentage of uncertainty of 0.75%, number obtained from product manuals (Omega, 2018).

2. **Equipment Malfunction:** Different equipment pieces could have malfunctioned, hence causing our system's desired functioning to be deficient. These pieces of equipment were: Hot plate, scale, fume hood, data loggers (although unlikely). As long as our direct measuring tools (temperature sensors) did not malfunction, I believe we would have been able to see such errors.

3. **Human Error:** I could have also made wrongful distance measurements when placing the plastic probe tested (PPrb), stainless steel probe (SSPrb), or individual thermocouples down in the saturated sands beaker (B_1). I could have read individual weights wrong when weighting the equipment. I could have dissolved the sulfuric acid too much or too little (to reach the desired normality of 0.05N), to have done this I could have wrongfully used the pH probe.

2.5 Wildfire probe

The last experiment I did was to test another probe's performance compared to our plastic probes. Such probe came to my knowledge thanks to one of my committee members, Dr. Crepeau, who pointed out a project done by the students from the mechanical engineering department a few years back that sought to make the best design for a Wildfire probe which measured temperatures in the first 10 cm of the subsurface during and after a fire. The project was done in association and was funded by the USDA Forestry Service in Moscow, ID. The reason I did this experiment was partly due to curiosity, but also because if the heat flux results from the Wildfire probe were similar to those from our probe, the Forest Service and the students from the mechanical engineering department could be good resources for collaboration and improvement of our probes' design. The specifics on this probe are on section 1.2.2.

2.5.1 Sampling Technology

For this experiment we used the same sampling equipment as we did for the experiments outlined in sections 1.3, and 2.2. We simply compared the Wildfire probe's efficiency with our "control system" (vertical sequence).The only difference in instrumentation was the probe used, and the data loggers for each sensor from the probe; these data loggers come encased inside the probe already (Figure 1.5).

2.5.2 Experimental Set-up and Duration

This experiment was conducted on May 11$^{\text{th}}$, 2017, and it lasted 96 hours. In this experiment, as opposed to the other two done under the same system, we had to bury the probe in the sand sequence prior to the start of the experiment. The probe's dimensions were too large to simply insert once the system had reached equilibrium, as we did with the previous two experiments, which is why all the sensors record increasing temperatures in a rather continuous way throughout the first day. Table 2.9 shows the depths at which each sensor was within the vertical sequence, whether a sensor from the vertical sequence or from the Wildfire probe. It is important to clarify that each thermocouple sensor (either in the vertical sequence, or checking the pan's or air's temperature) was connected to its respective data logger and temperatures were being recorded every 45 seconds. And, that the sensors from the Wildfire probe were in turn connected to their specific data loggers, but these ones recorded temperatures every 15 seconds (not all at the same seconds). This fact becomes important when seeing the extend to which we could manipulate the data.

The data loggers were launched at noon on May 11th, and stopped at noon on May 15th. The heat setting on the hot plate was kept at 5 throughout the first day of the experiment, and then reduced to 4 at the beginning of the second day.

Refer to Figure 2.22 for the internal set-up of this experiment, Figure 2.23 shows an aerial picture of setting up the experiment, and Figure 2.24 show the probes inner look of the sensors with my hand for scale.

Table 2.9: Depths of thermocouple sensors throughout vertical soil sequence - Wildfire Probe Experiment.

Thermocouple Label or Marker	**Depth** (inches, 0 = bottom)
Aluminum Plate	0.0 in (0.00 cm)
VS1	6.0 in (15.24 cm)
VS2	10.0 in (25.40 cm)
WFP1	12.5 in (31.75 cm)
WFP2	12.9 in (32.77 cm)
WFP3	13.3 in (33.78 cm)
WFP4	13.7 in (34.80 cm)
VS3	14.0 in (35.56 cm)
WFP5	14.5 in (36.83 cm)
WFP6	15.3 in (38.86 cm)
VS4	18.0 in (45.72 cm)
Sand Level	28.0 in (71.12 cm)

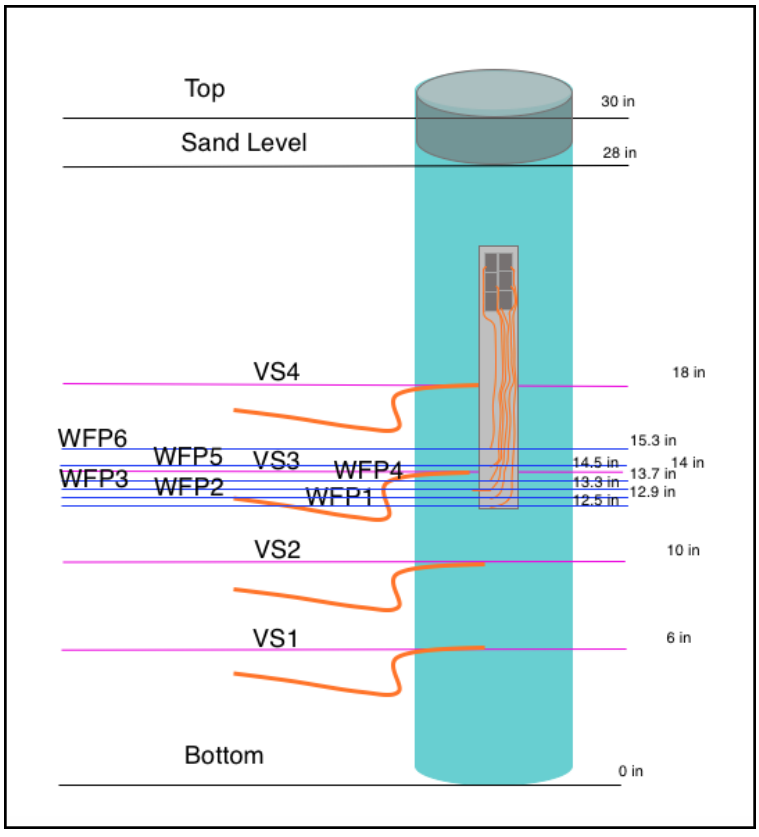

Figure 2.22: **Internal Set-up - Wildfire Probe Experiment.** Each temperature sensor is labelled and its depth is marked (ex: **WFP1** is the deepest sensor in the inserted probe).

Figure 2.23: **External Set-up - Wildfire Probe Experiment.**

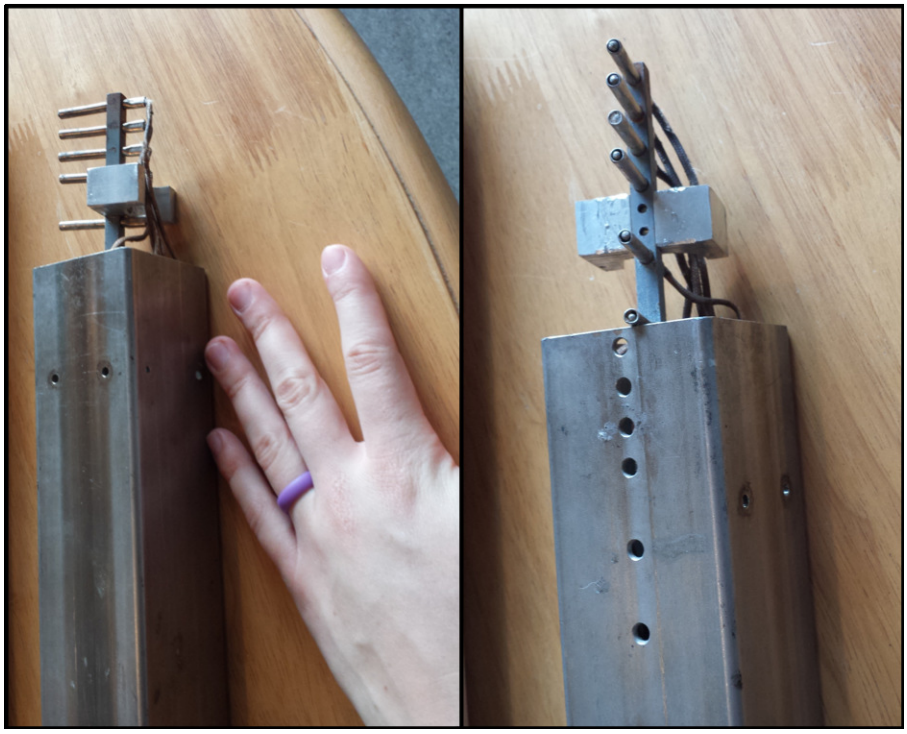

Figure 2.24: **Look of External Probe with Gabriela's hand to scale** - Wildfire Probe Experiment.

2.5.3 Results and Discussion

From the results below (Figure 2.25) we can see that all of the sensors from the Wildfire probe (WFP) measured temperatures very similar to those recorded by VS3 and VS4, both sensors which lay very near the depths at which the WFP's sensors were located. We also see how that the temperatures increase and decrease at about the same increments for all the sensors near the WFP's depth. Unfortunately, sensor "WFP2" did not recover any data, from malfunctioning prior to the experiment, which is why there is no data for that sensor. Finally, below are the heat flux calculations for both "systems". The temperature used was an average from all temperatures taken from the time after reaching equilibrium and until the hot plate was turned off, which matches time of data recovery.

Probe q":	**Vertical Sequence** q":
$q" = -K_T \frac{dT}{dx}$	$q" = -K_T \frac{dT}{dx}$
$q" = -0.27 \frac{W}{mK}$ x $\frac{0.967K}{0.0500m}$	$q" = -0.27 \frac{W}{mK}$ x $\frac{7.729K}{0.3048m}$
$q" = 5.222 \frac{W}{m^2}$	$q" = 6.847 \frac{W}{m^2}$

From the results above, I conclude that the design made for the Wildfire probe seems efficient and the measurements from its sensors were similar to those from the vertical sequence sensors'. Although it is quite a bit invasive to the system, it would be worth investing time and money to design a similar probe that targeted our purposes better. Perhaps one where the sensors were spread out further from each other, and that the encasing was longer and easier to insert into the ground.

2.5.3.1 Error Analysis

1. **Temperature Measurements - Thermocouple Readings:** All of our temperature measurements from the vertical sequence sensors were made with Omega-K-type thermocouples. These thermocouple type shows a percentage of uncertainty of 0.75%, number obtained from

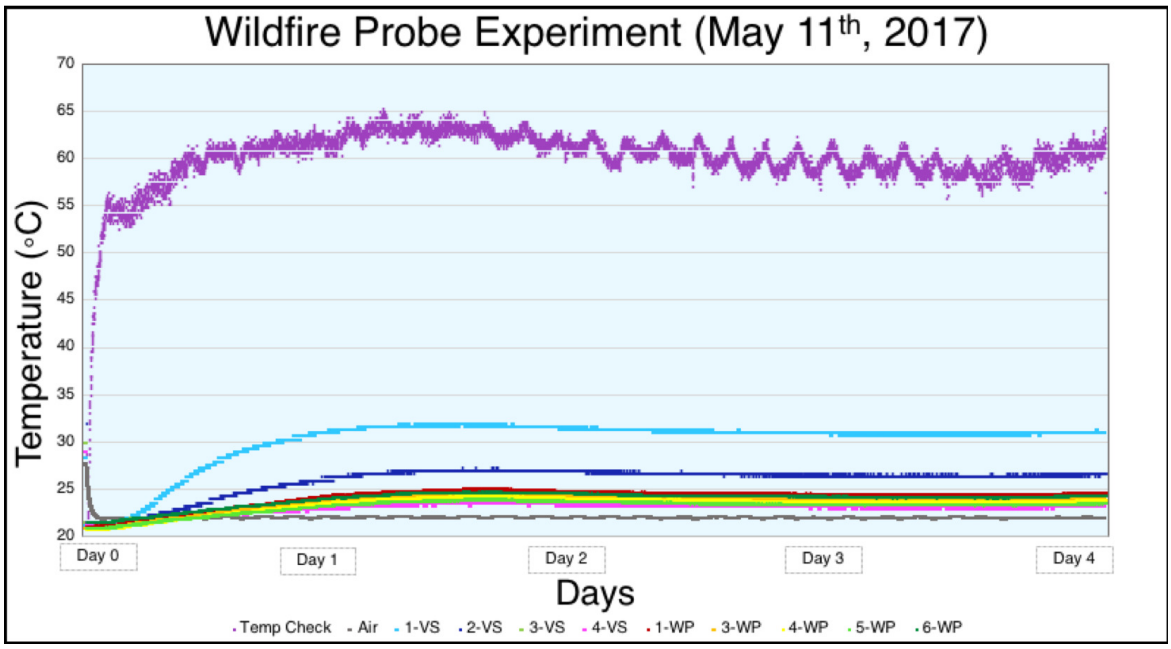

Figure 2.25: **Compiled Data from all the Wildfire Probe and Vertical Sequence Sensors** - Wildfire Probe Experiment.

product manuals (Omega, 2018). The Wildfire probe thermocouples are also K-type, and although I do not know who the maker is, I seem to recall from conversations with Dr. Peter Robichaud when he first showed me the probe that they have a percentage of uncertainty of 0.5% to 1% .

2. **Thermal Conductivity (K_T) Vertical Sand Sequence:** I used the standard thermal conductivity value (Bergman and Incropera, 2011) for dry sands in all the experiments where the vertical sand sequence was used. And, although I probably should have taken the thermal conductivity of the sediments I used with the KD2 Pro our group has (from Decagon), and taken enough samples to get an averaged consistent reading, there is certain uncertainty from the value Bergman and Incropera (2011) provide. Apparently the best measurement for dry sands is 0.25, with an uncertainty of $\pm$ 0.05. This is a rather rough measurement estimate, with a percentage of uncertainty of 20%, but it is understood that there is a large diversity in sand sediments; what minerals they contain can affect the values seen, and the compaction of the grains can also make a difference.

Aside from errors with the uncertainty which attends each measurement, there are a few possibilities where other kinds of error were introduced while experimenting.

3. **Equipment Malfunction:** Different equipment pieces could have malfunctioned, hence causing our system's desired functioning to be deficient. These pieces of equipment were: Hot plate, PVC pipe's insulation, data loggers (although unlikely). As long as our direct measuring tools (temperature sensors) did not malfunction, I believe we would have been able to see such errors.

4. **Human Error:** I also could have wrongfully estimated when the experiments reached equilibrium, which I used to calculate values for heat flux. I could have also made wrongful distance measurements when placing the Wildfire probe tested (WFP) down the vertical sequence sands. And, I could have made wrongful calculations for the heat flux shown above.

Chapter 3: Analytical Model and Solution

3.1 Introduction

In the previous two chapters I have provided an introduction and background on the necessity to obtain more reliable data and the need for a method to analyze it. I have also presented a few experiments done to help us improve our measuring techniques and to constraint the possible error seen in previous work. Through implementation of our findings we mean to either reduce any error, or eliminate it altogether in future work. In this chapter I go over an analytical model made by my advisor, with my aid (J. P. Fairley, personal communication, Fall semester 2017). This model was made after our experimentation, and was inspired by the lack of a quantitative framework for geothermal systems under transient conditions. We wanted to mathematically understand the time dependent relationship between the conduction of heat through the shallow subsurface and the ability to carry such heat through convection at the surface; and we wanted to do this using time-series measurements of temperature data, along with a few additional semi-constant values characteristic of each system.

3.2 Analytical Model

The following model attempts to find the distribution of temperatures in the subsurface as a function of the geothermal gradient and a transient atmosphere forcing at any geothermal location. In the coming subsection I walk through the model's main steps, definitions, and assumptions, and provide an analytical solution for the problem. Appendix A has all steps made for development of this model for further clarification.

3.2.1 Model - Main Steps

As most models do, this one makes a few assumptions about the system:

- Temporally and spatially constant properties (K_T, ρ, c_p, D, etc).

- The heat source is sufficiently deep that the approximation z $\rightarrow \infty$ holds (i.e., semi-infinite half-space (Refer to Figure 3.1)).
- The geothermal heat flux from depth is constant.
- The heat loss at the upper (land surface) boundary is coupled to atmospheric temperatures by a Type III boundary (Robin Boundary [4]) condition.
- Land surface is flat (i.e., no topographic effect; thus can assume 1-D heat transfer).
- Heat transfer in the subsurface is solely by conduction; assume convective heat transfer is negligible.
- Neglect the impact of changes in saturation on thermal properties.
- No sources or sinks in the subsurface (i.e., no lateral flow, etc.).

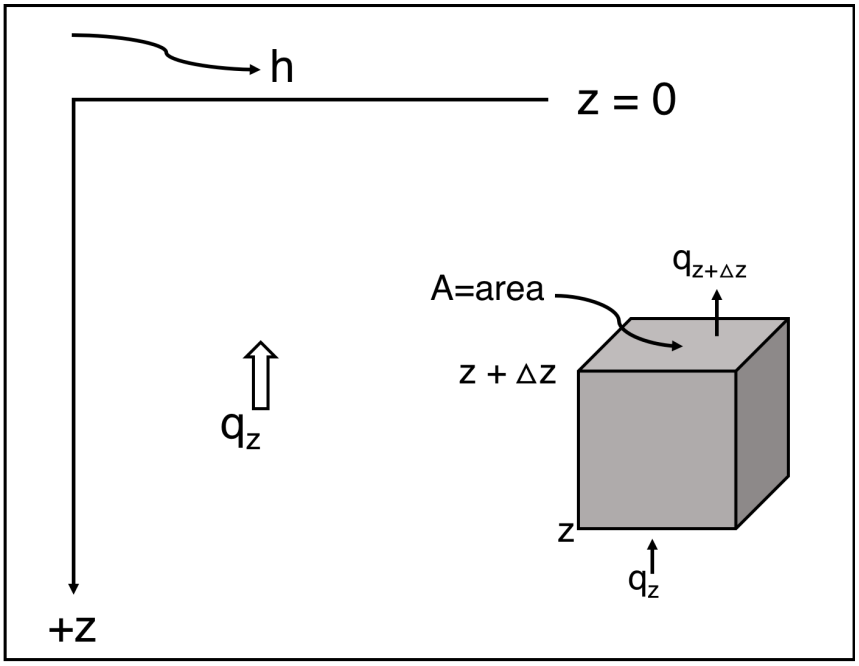

Figure 3.1: **Schematic Diagram of a Geothermal System.** The cube represents a random volume of the system under which we are working. Otherwise called control volume.

[4] This is a boundary condition of the third type, sometimes referred to as Robin condition, or as the *convection* or *convection/conduction condition*. This *convection/conduction condition* is understood as the relationship between heat traveling through the soils by conduction and heat being carried away by the fluid (air in this case) through convection. The relationship states that the rate at which heat is traveling through the soils must equal the rate at which heat is being carried away by the air (Fairley, 2016).

Following the energy balance concept, where energy coming into the system (or model domain) (E_{in}) must equal the outgoing energy (E_{out}), with any differences between those two quantities represented in a change of energy (ΔE) stored in the system (Fairley, 2016):

$$E_{in} = E_{out} + \Delta E$$

Substituting for the appropriate parameters making up each term above; and later taking the limit as the change in depth and change in time approach zero:

$$q_z \cancel{A} \Delta t = q_{z+\Delta z} \cancel{A} \Delta t + \Delta T \rho c_p \cancel{A} \Delta z$$

$$\frac{q_{z+\Delta z} - q_z}{\Delta z} = -\rho c_p \frac{\Delta T}{\Delta t} \qquad \rightarrow$$

$$\lim_{\Delta z, \Delta t \rightarrow\ 0}$$

$$\frac{\partial q_z}{\partial z} = -\rho c_p \frac{\partial T}{\partial t} \tag{1}$$

In equation (1), z is the vertical spatial coordinate (depth), with the boundary at the surface being $z = 0$, and increasing with depth indefinitely. ∂q is the heat flow through our system's control volume, ρ is the density of the material under which our control volume is, c_p is the specific heat capacity of the material, ∂T is the change in temperature seen through our control volume, and ∂t is the change in time.

If we substitute Fourier's Law ($q_z = -K_T \frac{\partial T}{\partial z}$) into equation 1, it becomes:

$$\frac{\partial^2 T}{\partial z^2} = \frac{\rho c_p}{K_T} \frac{\partial T}{\partial t} \tag{2}$$

Where K_T is the thermal conductivity if the material. And, if we introduce the thermal diffusivity term ($D = \frac{K_T}{\rho c_p}$), then our equation 1 turns into:

$$\frac{\partial^2 T}{\partial z^2} = \frac{1}{D} \frac{\partial T}{\partial t} \tag{3}$$

Equation 3 is our governing equation, and it has two boundary conditions:

$$-\mathrm{K_T}\frac{\partial \mathrm{T}}{\partial \mathrm{t}}(\mathrm{z}\to\infty,\mathrm{t}) = \mathrm{q_z} \tag{4}$$

$$-\mathrm{K_T}\frac{\partial T}{\partial \mathrm{t}}(\mathrm{z}=0,\mathrm{t}) = \mathrm{h}[\mathrm{T}(\mathrm{z}=0,\mathrm{t}) - \mathrm{T}_\infty(\mathrm{t})] \tag{5}$$

Equation 5 represents the boundary condition at the land surface, where h is the heat transfer coefficient, typically used in heat transfer by convection. We can expand equation 5 and redefine the transient air temperature term ($\mathrm{T}_\infty(\mathrm{t})$), or temperature of the atmosphere far from the land surface boundary; by making this transient behavior into a cyclical phenomenon based on daily changes at the land surface.

$$\frac{\partial \mathrm{T}}{\partial \mathrm{z}}(\mathrm{z}=0,\mathrm{t}) + \frac{\mathrm{h}}{\mathrm{K_T}}[\mathrm{T}(\mathrm{z}=0,\mathrm{t}) - \mathrm{T_o} - \sum_{\mathrm{n}=1}^{\infty}\mathrm{A_n}\sin(\frac{2n\pi t}{p}) + \mathrm{B_n}\cos(\frac{2\mathrm{n}\pi\mathrm{t}}{\mathrm{p}})] = 0 \tag{6}$$

Rewriting the Fourier series as a complex Fourier series:

$$\mathrm{T}_\infty(\mathrm{t}) = \sum_{\mathrm{n}=-\infty}^{\infty}\mathrm{C_n}e^{\frac{2\mathrm{in}\pi\mathrm{t}}{\mathrm{p}}} \tag{7}$$

Where:

$$\mathrm{C_n} = \tfrac{\mathrm{B_n}-\mathrm{iA_n}}{2} \quad ; \quad \mathrm{n}>0$$

$$\mathrm{C_n} = \mathrm{T_o} \quad ; \quad \mathrm{n}=0$$

$$\mathrm{C_n} = \tfrac{\mathrm{B_n}+\mathrm{iA_n}}{2} \quad ; \quad \mathrm{n}<0$$

Equation 7 will be useful later, after development of our initial governing equation and boundary conditions. Now, we define the following nondimensional variables and parameters:

$$\theta = \frac{T - T_o}{T_o} \qquad \xi = \frac{z}{z_c}$$

$$\tau = \frac{t}{t_c} \qquad \epsilon \equiv \frac{q_z\sqrt{Dp}}{K_T T_o}$$

$$\beta = \frac{h\sqrt{Dp}}{K_T} \qquad \Gamma_n = \begin{cases} \frac{B_n - iA_n}{2T_o} & ; \quad n>0 \\ 0 & ; \quad n = 0 \\ \frac{B_n + iA_n}{2T_o} & ; \quad n<0 \end{cases}$$

$$t_c = p \qquad z_c = \sqrt{D_p}$$

From the equations above, θ is defined as the nondimensional temperature, ξ as the nondimensional vertical spatial coordinate, τ as the nondimensional time, β as the Biot number, which quantifies the rate at which heat can be removed from the boundary by convection in comparison to the rate at which heat can be brought to the boundary by conduction (Price et al., 2017). The remaining parameters, ϵ, Γ_n, χ, κ, t_c, and z_c, represent other variables and their relationship to each other, but their definition helps keep the model clean and easier to follow.

From the definition of these terms above, we can rewrite our governing equation and boundary conditions, equations 3, 4, and 5, into:

$$\frac{\partial^2\theta}{\partial\xi^2} = \frac{z_c^2}{Dt_c}\frac{\partial\theta}{\partial\tau} \tag{8}$$

$$\frac{\partial\theta}{\partial\xi}(\xi \to \infty, \tau) = -\frac{q_z z_c}{K_T T_o} \tag{9}$$

$$\frac{T_o}{z_c}\frac{\partial\theta}{\partial\xi}(\xi = 0, \tau) + \frac{h}{K_T}[T_o\theta(\xi = 0, \tau) + T_o - T_o] = \frac{h}{K_T}\sum_{n=1}^{\infty} A_n \sin(\frac{2n\pi t_c\tau}{p}) + B_n \cos(\frac{2n\pi t_c\tau}{p}) \tag{10}$$

Developing 8, 9, and 10, they become:

$$\frac{\partial^2\theta}{\partial\xi^2} = \frac{\partial\theta}{\partial\tau} \tag{11}$$

$$\frac{\partial\theta}{\partial\xi}(\xi \to \infty, \tau) = -\epsilon \tag{12}$$

$$\frac{\partial\theta}{\partial\xi}(\xi = 0, \tau) + \beta\theta(\xi = 0, \tau) = \beta \sum_{\mathrm{n}=1}^{\infty} \frac{\mathrm{A_n}}{\mathrm{T}_o} \sin(2\mathrm{n}\pi\tau) + \frac{\mathrm{B_n}}{\mathrm{T_o}} \cos(2\mathrm{n}\pi\tau) \tag{13}$$

Using the result from equation 7 and redefining equation 13, we get:

$$\frac{\partial\theta}{\partial\xi}(\xi = 0, \tau) + \beta\theta(\xi = 0, \tau) = \beta \sum_{\mathrm{n}=-\infty}^{\infty} \Gamma_{\mathrm{n}}\ e^{2\mathrm{in}\pi\tau} \tag{14}$$

Equations 11, 12, and 14, as our new field equation. The first step is to simplify the problem by inspecting a single forcing frequency:

$$\frac{\partial^2\theta_{\mathrm{n}}}{\partial\xi^2} = \frac{\partial\theta_{\mathrm{n}}}{\partial\tau} \tag{15}$$

$$\frac{\partial\theta_n}{\partial\xi}(\xi \to \infty, \tau) = -\epsilon \tag{16}$$

$$\frac{\partial\theta_{\mathrm{n}}}{\partial\xi}(\xi = 0, \tau) + \beta\theta_{\mathrm{n}}(\xi = 0, \tau) = \beta\Gamma_{\mathrm{n}}\ e^{2\mathrm{in}\pi\tau} \tag{17}$$

After we do this, we can sum-up all the frequencies by superposition by decomposing the solution for θ_{n} into a **linear** solution that accounts for one of the boundary conditions (in this case, $\frac{\partial\theta}{\partial\xi} = -\epsilon$), and a transient portion, $\theta_{\mathrm{n,t}}$.

$$\theta_{\mathrm{n}}(\xi,\tau) = \theta_{\mathrm{n,T}}(\xi,\tau) + \mathrm{A}\xi + \mathrm{B} \tag{18}$$

→ Then:

$\frac{\partial\theta}{\partial\xi} = \frac{\partial\theta_T}{\partial\xi} + \mathrm{A}$ And, $\frac{\partial^2\theta}{\partial\xi^2} = \frac{\partial^2\theta_{\mathrm{T}}}{\partial\xi^2} + 0$

$\frac{\partial\theta}{\partial\tau} = \frac{\partial\theta_{\mathrm{T}}}{\partial\tau} + \xi\frac{\partial\mathrm{A}}{\partial\tau} + \frac{\partial\mathrm{B}}{\partial\tau}$ And, $\frac{\partial^2\theta_{\mathrm{T}}}{\partial\xi^2} = \frac{\partial\theta_{\mathrm{T}}}{\partial\tau} + \xi\frac{\partial\mathrm{A}}{\partial\tau} + \frac{\partial\mathrm{B}}{\partial\tau}$

→ And, from the boundary conditions. From equation 16:

$\frac{\partial\theta}{\partial\xi}(\xi\to\infty,\tau) = \frac{\partial\theta_{\mathrm{T}}}{\partial\xi}(\xi\to\infty,\tau) + \mathrm{A} = -\epsilon$ ⇒ $\frac{\partial\theta_{\mathrm{T}}}{\partial\xi}(\xi\to\infty,\tau) = 0$

⇒ $\mathbf{A} = -\epsilon$

→ From equation 17:

$\frac{\partial\theta}{\partial\xi}(\xi=0,\tau) + \mathrm{A} + \beta[\theta_{\mathrm{T}}(\xi=0,\tau) + \cancel{\mathrm{A}\xi} + \mathrm{B}] = \beta\Gamma_{\mathrm{n}}\, e^{2\mathrm{in}\pi\tau}$

$\frac{\partial\theta}{\partial\xi}(\xi=0,\tau) + \beta\theta_{\mathrm{T}}(\xi=0,\tau) + \mathrm{A} + \beta\mathrm{B} = \beta\Gamma_{\mathrm{n}}\, e^{2\mathrm{in}\pi\tau}$

$\frac{\partial\theta}{\partial\xi}(\xi=0,\tau) + \beta\theta_{\mathrm{T}}(\xi=0,\tau) = \beta\Gamma_{\mathrm{n}}\, e^{2\mathrm{in}\pi\tau}$ ⇒ $\mathrm{A} + \beta\mathrm{B} = -\epsilon + \beta\mathrm{B} = 0$

⇒ $\beta\mathrm{B} = \epsilon$

⇒ $\mathbf{B} = \frac{\epsilon}{\beta}$

→ From equation 18, and the steps taken since, the **steady state** solution:

$$\theta_{\mathrm{n}}(\xi,\tau) = \theta_{\mathrm{n,T}}(\xi,\tau) + \frac{\epsilon}{\beta} - \epsilon\xi \tag{19}$$

$$\theta_{\mathrm{n}}(\xi,\tau) = \underbrace{\frac{\epsilon}{\beta}(1-\beta\xi)} + \theta_{\mathrm{n,T}}(\xi,\tau) \tag{20}$$

→ Furthermore, for **transient behavior**:

$$\xi \frac{\partial \mathrm{A}}{\partial \tau} = 0 \qquad \text{And:} \qquad \frac{\partial \mathrm{B}}{\partial \tau} = 0$$

→ Which means equation 15, 16, and 17, will be:

$$\frac{\partial^2 \theta_{\mathrm{T}}}{\partial \xi^2} = \frac{\partial \theta_{\mathrm{T}}}{\partial \tau} \tag{21}$$

$$\frac{\partial \theta_{\mathrm{T}}}{\partial \xi}(\xi \to \infty, \tau) = 0 \tag{22}$$

$$\frac{\partial \theta_{\mathrm{T}}}{\partial \xi}(\xi = 0, \tau) + \beta \theta_{\mathrm{T}}(\xi = 0, \tau) = \beta \Gamma_{\mathrm{n}}\, e^{2\mathrm{in}\pi\tau} \tag{23}$$

→ If we let:

$\theta_{\mathrm{T}}(\xi, \tau) = \chi(\xi)\, e^{\mathrm{in}\pi\tau} \quad \Rightarrow \quad \frac{\partial \theta_T}{\partial \xi} = \chi'\, e^{2\mathrm{in}\pi\tau}$

$\Rightarrow \quad \frac{\partial^2 \theta_{\mathrm{T}}}{\partial \xi^2} = \chi''\, e^{2\mathrm{in}\pi\tau}$

$\Rightarrow \quad \frac{\partial \theta_T}{\partial \tau} = 2\mathrm{in}\pi\, \chi\, e^{2\mathrm{in}\pi\tau}$

→ Substituting the above steps in equation 21:

$\chi''\, e^{2\mathrm{in}\pi\tau} = 2\mathrm{in}\pi\, \chi\, e^{2\mathrm{in}\pi\tau} \quad \Rightarrow$

$$\chi'' - 2\mathrm{in}\pi\, \chi = 0 \tag{24}$$

→ The Boundary Conditions, equations 22 and 23, decompose to:

$\chi'(\xi \to \infty)\, e^{2\mathrm{in}\pi\tau} = 0 \quad \Rightarrow \quad \chi'(\xi \to \infty) = 0$

→ And:

$\chi'(\xi = 0)e^{2\mathrm{in}\pi\tau} + \beta\chi(\xi = 0)e^{2\mathrm{in}\pi\tau} = \beta\Gamma_{\mathrm{n}}e^{2\mathrm{in}\pi\tau}$

$$\Rightarrow \qquad \chi'(\xi = 0) + \beta\chi(\xi = 0) = \beta\Gamma_{\mathrm{n}}$$

→ Where:

$$\chi = e^{\kappa\xi} \qquad \Rightarrow \qquad \chi' = \kappa e^{\kappa\xi} \qquad \Rightarrow \qquad \chi'' = \kappa^2 e^{\kappa\xi}$$

→ Once we substitute the definition for χ in equation 24, we get:

$$\kappa^2 e^{\kappa\xi} - 2\mathrm{in}\pi\ \kappa^2 e^{\kappa\xi} = 0 \qquad \Rightarrow \qquad \kappa^2 = 2\mathrm{in}\pi \qquad \Rightarrow \qquad \kappa = \pm\sqrt{2\mathrm{in}\pi}$$

→ Which redefines χ to be:

$$\chi = e^{\pm\sqrt{2\mathrm{in}\pi}\xi} \qquad \Rightarrow \qquad \chi = e^{\pm\sqrt{\mathrm{i}}\sqrt{2\mathrm{n}\pi}\xi}$$

→ This step is somewhat confusing. Again, refer to Appendix A for further steps. If we express $\sqrt{\mathrm{i}}$ from the equation right above as:

$\sqrt{\mathrm{i}} = \mathrm{a} + \mathrm{ib}, \qquad \Rightarrow$ Then: $\qquad \sqrt{i} = \frac{\sqrt{2}}{2}(1 + \mathrm{i})$

→ Which redefines χ to be:

$$\chi = e^{\pm\frac{\sqrt{2}}{2}(1+\mathrm{i})\sqrt{2\mathrm{n}\pi}\xi} \qquad \Rightarrow \qquad \chi = e^{\pm(1+\mathrm{i})\sqrt{\mathrm{n}\pi}\xi}$$

→ Therefore:

$$\chi = \mathrm{C}_1\ e^{(1+\mathrm{i})\sqrt{\mathrm{n}\pi}\xi} + \mathrm{C}_2\ e^{-(1+\mathrm{i})\sqrt{\mathrm{n}\pi}\xi} \tag{25}$$

→ From the boundary conditions at $\xi \to \infty$, $\mathrm{C}_1 = 0$:

$$\chi = \mathrm{C}_2\ e^{-(1+\mathrm{i})\sqrt{\mathrm{n}\pi}\xi} \qquad \Rightarrow \qquad \chi' = -(1 + \mathrm{i})\ \mathrm{C}_2\ \sqrt{\mathrm{n}\pi}\ e^{-(1+\mathrm{i})\sqrt{\mathrm{n}\pi}\xi}$$

→ From the boundary conditions at $\xi = 0$:

$$-(1 + \mathrm{i})\mathrm{C}_2\ \sqrt{\mathrm{n}\pi} + \beta\mathrm{C}_2 = \beta\Gamma_{\mathrm{n}} \qquad \Rightarrow \qquad \mathrm{C}_2 = \frac{\beta\Gamma_{\mathrm{n}}}{\beta - (1+\mathrm{i})\sqrt{\mathrm{n}\pi}}$$

→ Solving this, we get:

$$C_2 = \frac{\beta\Gamma_n\ (\beta - \sqrt{n\pi}) + i\beta\Gamma_n\ \sqrt{n\pi}}{(\beta - \sqrt{n\pi})^2 + n\pi} \tag{26}$$

→ Or:

$C_2 = a_n + ib_n$ ⇒ Where: $a_n = \frac{\beta\Gamma_n\ (\beta - \sqrt{n\pi})}{(\beta - \sqrt{n\pi})^2 + n\pi}$

⇒ And: $b_n = \frac{\beta\Gamma_n\ \sqrt{n\pi}}{(\beta - \sqrt{n\pi})^2 + n\pi}$

→ So χ is:

$$\chi(\xi) = (a_n + ib_n)\ e^{-(1+i)\sqrt{n\pi}\xi} \tag{27}$$

→ Furthermore, if we substitute equation 27 into our previous definition of $\theta_T(\xi, \tau)$ (step following equation 23), we get:

$$\theta_T(\xi, \tau) = (a_n + ib_n)\ e^{-(1+i)\sqrt{n\pi}\xi}\ e^{2in\pi\tau}$$

$$\theta_T(\xi, \tau) = (a_n + ib_n)\ e^{-\sqrt{n\pi}\xi - i(\sqrt{n\pi}\xi - 2n\pi\tau)}$$

→ Summing over all of the frequencies:

$$\theta_T(\xi, \tau) = \sum_{n=-\infty}^{\infty} \theta_n(\xi, \tau)$$

$$\theta_T(\xi, \tau) = \underline{\sum_{n=-\infty}^{\infty} (a_n + ib_n)\ e^{-\sqrt{n\pi}\xi - i(\sqrt{n\pi}\xi - 2n\pi\tau)}}$$

→ Finally, add on the "steady" solution from equation 20 for the full expression:

$$\theta_T(\xi, \tau) = \underbrace{\frac{\epsilon}{\beta}(1 - \beta\xi)}_{} + \underline{\sum_{n=-\infty}^{\infty} (a_n + ib_n)\ e^{-\sqrt{n\pi}[\xi + i(\xi - \sqrt{n\pi}2\tau)]}} \tag{28}$$

From the solution to the analytical model above we can solve numerically what the temperature distribution will be from a certain system, as a function of the geothermal gradient and a transient atmospheric forcing. It is worth noting that such a result is useful at any location that presents similar conditions, and where the assumptions made for this model may also apply.

3.3 Numerical Solution

With the above solution to our problem, it is possible to input values for the known variables and through a numerical solution get the temperature distribution through the subsurface profile. I wanted to do this by learning a computer language through which I could do this (python). I was going to use our data values from the Burgdorf hot springs field experiment, but unfortunately, the time at hand and the complexity of the analytical solution, made it difficult to come up with a numerical answer to this problem. I will continue to try this in the future, with means of publishing our results from it.

Chapter 4: Conclusions

Throughout the last 3 chapters I have given an overview of previous work done in geothermal areas. I have presented you with different studies that covered: understanding where the heat comes from and how it propagates, how it can be measured and how good these methods can be, and what has been the extent of quantifying different geothermal systems. I also presented my experimental work done in the lab and in the field: testing different measuring tools, testing these tools under extreme environments in the lab, and measuring real life temperature data in the field using some of these tools. Lastly I presented an analytical model which, when applied to a geothermal system, will find the distribution of temperatures in the subsurface as a function of the geothermal gradient and of a transient atmosphere forcing.

In this chapter I present my conclusions about this project.

4.1 Experiments - Conclusions

From the experiments I did, as from any scientific experiment, it is worth mentioning that no experiment ever proves something, it simply suggests from the analysis done to the experimental data that there is some result or some behavior (Taylor, 1997), which is what I meant to do throughout this project.

- As a result to background reading and through our analysis of the temperature distribution throughout the profile of the probes we measured under experimentation, we suggest that the material used to encase the thermocouples of a probe highly influences the temperatures seen at each sensor of the probe's profile. The sensors inside those probes made out of more thermally conductive materials will experience a greater impact from the temperature carried by conduction through the probe than would sensors inside probes with low thermal conductivity.
- The Plastic (Nylon) Probes (PPrb) created by our research team are inexpensive and easy to make, effective at recording temperatures, and not very invasive, as opposed to other probes that require holes be dug with an auger prior to insertion. This allows for use of the probes in

geothermal areas more subject or restricting to environmental harm (ex: Yellowstone National Park).

- The PPrb is light in weight and not too large. It is also robust enough to resist being hammered into the ground without bending or breaking.

- The PPrb does not seem to be harmed in any physical or functional way by long (i.e. weeks) exposure under environments of high heat and acidity. In this case, the Stainless Steel Probe (SSPrb), or the individual mini-connector K-Type thermocouples did not seem to be affected either when exposed to these extreme environments.

- The PPrb needs some improvement to make it an even better tool. First of all, a recovery mechanism would be beneficial. Either by having a wider grip at the top of the probe (closest to land surface), and this part would always stay above surface; or it could have a pulling mechanism similar to that used to pull and remove a wine cork from the bottle for the first time. I view the initial option more likely.

- Another improvement for the PPrb would be to create an encasing mechanism for the 3 data loggers attached to each probe when recording temperatures. This does not seem too hard or expensive; in fact there are a few options already available, as cases for electronics that can be deployed in the field for months and even years. It would be ideal, however, to get or create the smallest, yet best case that fits our needs.

- The Wildfire Probe (WFP) is a good probe for its purpose. It does not fit our needs in the same way, as it is heavy, a bit bulky, and a bit too short. It is however, useful that it encases all parts of the measuring equipment inside the stainless steel casing. The relationships with the USDA Forestry Service, and the mechanical engineering students are definitely good partnerships for future work together, and perhaps even to improve the PPrb's mechanism based on our needs.

- The depth at which our PPrb's thermocouples were at still felt some change based on atmospheric conditions variations in the field. The effect from atmospheric conditions was reduced as depth increased throughout the soil profile, but it would be worth testing a longer probe of similar material and making where the thermocouples were placed at greater depths to see when atmospheric conditions no longer had an effect on the soil temperatures measured.

Thankfully the analytical model should account for these changes sensed, and hence, this becomes a less relevant issue; depending on what the probes were used for I suppose.

4.2 Model - Conclusions

- The analytical model developed by my advisor, Jerry Fairley, and myself, helps us know what the distribution of heat is through the subsurface profile in a geothermal setting over time, and it takes into account the heat carried through conduction in the soils, and the heat being removed by the air above the surface. This model, alike any model, is accompanied by several assumptions, which should be noted whenever a researcher is thinking of applying it to their data.

- Greater emphasis should be put in understanding the model both mathematically and in terms of finding a numerical solution for it. Any students using this model for their research should be aware of this.

4.3 Planning - Conclusions

- Greater planning needs to be done for further lab research: Researching materials' thermal resistance prior to exposing them to high or low heat, which they are not meant to withstand. Preferably measuring thermal conductivity of the sediments manually, as opposed to obtaining an average from the sediments found in the literature. Keeping a uniform schedule for all experiments that vary minimally. Keeping constant conditions for all experiment that vary minimally.

- Further funding should have been sought out to test other probes, and to make more plastic probes for a greater temperature grid. This is always hard to plan, but it should have been expected of me to encounter this issue along the road.

- Further time should have been spent at learning computer languages to solve linear differential equations, and more specifically to simulate numerically our analytical model solution, with values from our field site data. This will continue to be done after completion of my degree, in strife to publish this work.

References

Anderson, T. R. and Fairley, J. P. (2008). Relating permeability to the structural setting of a fault-controlled hydrothermal system in southeast oregon, usa. *Journal of Geophysical Research: Solid Earth*, 113(B5).

Bergman, T. L. and Incropera, F. P. (2011). *Fundamentals of heat and mass transfer*. John Wiley & Sons.

Burns, E. R., Ingebritsen, S. E., Manga, M., and Williams, C. F. (2016). Evaluating geothermal and hydrogeologic controls on regional groundwater temperature distribution. *Water Resources Research*, 52(2):1328–1344.

Carslaw, H. S. and Jaeger, J. C. (1959). Conduction of heat in solids. *Oxford: Clarendon Press, 1959, 2nd ed.*

Certini, G. (2005). Effects of fire on properties of forest soils: a review. *Oecologia*, 143(1):1–10.

Dawson, G. (1964). The nature and assessment of heat flow from hydrothermal areas. *New Zealand journal of geology and geophysics*, 7(1):155–171.

Fairley, J. (2016). *Models and Modeling: An Introduction for Earth and Environmental Scientists*. John Wiley & Sons.

Fairley, J., Heffner, J., and Hinds, J. (2003). Geostatistical evaluation of permeability in an active fault zone. *Geophysical Research Letters*, 30(18).

Fairley, J. P. and Hinds, J. J. (2004). Rapid transport pathways for geothermal fluids in an active great basin fault zone. *Geology*, 32(9):825–828.

Farbrot, H., Etzelmüller, B., Schuler, T. V., Guomundsson, Á., Eiken, T., Humlum, O., and Björnsson, H. (2007). Thermal characteristics and impact of climate change on mountain permafrost in iceland. *Journal of Geophysical Research: Earth Surface*, 112(F3).

Furuya, G., Suemine, A., Sassa, K., Komatsubara, T., Watanabe, N., and Marui, H. (2006). Relationship between groundwater flow estimated by soil temperature and slope failures caused by heavy rainfall, shikoku island, southwestern japan. *Engineering geology*, 85(3-4):332–346.

Giorgis, S., McClelland, W., Fayon, A., Singer, B. S., and Tikoff, B. (2008). Timing of deformation and exhumation in the western idaho shear zone, mccall, idaho. *Geological Society of America Bulletin*, 120(9-10):1119–1133.

Gordeev, E., Saltykov, V., Sinitsin, V., and Chebrov, V. (1992). Relationship between heating of the ground surface and high-frequency seismic noise. *Physics of the earth and planetary interiors*, 71(1-2):1–5.

Gringarten, A., Witherspoon, P., and Ohnishi, Y. (1975). Theory of heat extraction from fractured hot dry rock. *Journal of Geophysical Research*, 80(8):1120–1124.

Heffner, J. and Fairley, J. (2006). Using surface characteristics to infer the permeability structure of an active fault zone. *Sedimentary Geology*, 184(3-4):255–265.

Holman, J. P. and Gajda, W. J. (2001). *Experimental methods for engineers*, volume 7. McGraw-Hill New York.

Hurwitz, S., Harris, R. N., Werner, C. A., and Murphy, F. (2012). Heat flow in vapor dominated areas of the yellowstone plateau volcanic field: Implications for the thermal budget of the yellowstone caldera. *Journal of Geophysical Research: Solid Earth*, 117(B10).

Ingebritsen, S., Galloway, D., Colvard, E., Sorey, M., and Mariner, R. (2001). Time-variation of hydrothermal discharge at selected sites in the western united states: implications for monitoring. *Journal of Volcanology and Geothermal Research*, 111(1):1–23.

Ingebritsen, S., Sherrod, D., and Mariner, R. (1989). Heat flow and hydrothermal circulation in the cascade range, north-central oregon. *Science*, 243(4897):1458.

Kappelmeyer, O. and Haenel, R. (1974). Geothermics with special reference to application. *Berlin Gebrueder Borntraeger Geoexploration Monographs Series*, 4.

Keisling, B. A., Castañeda, I. S., and Brigham-Grette, J. (2017). Hydrological and temperature change in arctic siberia during the intensification of northern hemisphere glaciation. *Earth and Planetary Science Letters*, 457:136–148.

Lovering, T. S. and Goode, H. D. (1963). Measuring geothermal gradients in drill holes less than 60 feet deep, east tintic district, utah.

Lubenow, B. L. (2014). *Best practices for shallow ground temperature measurements*. University of Idaho.

Lubenow, B. L., Fairley, J. P., Lindsey, C. R., and Larson, P. B. (2016). Influences on shallow ground temperatures in high flux thermal systems. *Journal of Volcanology and Geothermal Research*, 323:53–61.

Manga, M. (1998). Advective heat transport by low-temperature discharge in the oregon cascades. *Geology*, 26(9):799–802.

Manga, M. and Kirchner, J. W. (2004). Interpreting the temperature of water at cold springs and the importance of gravitational potential energy. *Water Resources Research*, 40(5).

Mindworks-Wikipedia (2015). Wildfire temperature probe. `http://mindworks.shoutwiki.com/wiki/Wildfire_temperature_probe`. [Online; accessed 01.30.2018].

Mitchell, J. C., Bideganeta, K., and Palmer, M. A. (1984). *Stable Isotopic Evaluation of Thermal Water Occurrences in the Weiser and Little Salmon River Drainage Basins and Adjacent Areas, West-central Idaho: With Attendant Gravity and Magnetic Data on the Weiser Area*. Idaho Department of Water Resources.

Mitchell, V. and Bennett, E. (1979). Geologic map of the elk city quadrangle. *Idaho Bureau of Mines and Geology, Moscow ID*.

Mori, M., Kamei, H., Nakai, M., and Kudo, H. (1999). High-density resistivity survey and experimental measurement of subsurface temperatures on hirui-otsuka mounded tomb in ogaki, japan. *Archaeological Prospection*, 6(3):171–178.

Naranjo, R. (2015). A multi-depth temperature probe for investigating subsurface heat transport. `https://mn.water.usgs.gov/uzig/UZIG_Spring_2015.2.pdf`. [Online; accessed 01.30.2018].

Naranjo, R. C. and Turcotte, R. (2015). A new temperature profiling probe for investigating groundwater-surface water interaction. *Water Resources Research*, 51(9):7790–7797.

Olmsted, F., Welch, A. H., and Ingebritsen, S. (1986). Shallow subsurface temperature surveys in the basin and range province, usa?i. review and evaluation. *Geothermics*, 15(3):251–265.

Olmsted, F. H. (1977). Use of temperature surveys at a depth of 1 meter in geothermal exploration in nevada. *US, Geol. Surv., Prof. Pap.;(United States)*, 1044.

Omega (2017). Profile probes made from high-accuracy special-limits-of-error wire. https://www.omega.com/temperature/pdf/PP3_PP6_PP10.pdf. [Online; accessed 01.30.2018].

Omega (2018). Ansi and iec color codes for thermocouples, wire and connectors. https://www.omega.com/temperature/pdf/tc_colorcodes.pdf. [Online; accessed 02.26.2018].

Omega, E. I. (1993). *Omega Technologies Handbook, "Thermocouple Reference Tables"*.

Poley, J. and Steveninck, J. v. (1970). Delineation of shallow salt domes and surface faults by temperature measurements at a depth of approximately 2 metres. *Geophysical Prospecting*, 18(s1):666–700.

Price, A. N., Lindsey, C. R., and Fairley, J. P. (2017). Interpretation of ground temperature anomalies in hydrothermal discharge areas. *Water Resources Research*.

Rissmann, C., Nicol, A., Cole, J., Kennedy, B., Fairley, J., Christenson, B., Leybourne, M., Milicich, S., Ring, U., and Gravley, D. (2011). Fluid flow associated with silicic lava domes and faults, ohaaki hydrothermal field, new zealand. *Journal of Volcanology and Geothermal Research*, 204(1-4):12–26.

Saba, M., Nishida, Y., Takakura, S., Matsushima, N., Mogi, T., et al. (2007). Development of geothermal field following the 2000 eruption of usu volcano as revealed by ground temperature, resistivity and self-potential variations.

Smith, M. W. (1975). Microclimatic influences on ground temperatures and permafrost distribution, mackenzie delta, northwest territories. *Canadian Journal of Earth Sciences*, 12(8):1421–1438.

Sorey, M. L. and Colvard, E. M. (1994). *Measurements of heat and mass flow from thermal areas in Lassen Volcanic National Park, California, 1984-93*. US Geological Survey Menlo Park, CA.

Taylor, A. E., Wang, K., Smith, S. L., Burgess, M. M., and Judge, A. S. (2006). Canadian arctic permafrost observatories: Detecting contemporary climate change through inversion of subsurface temperature time series. *Journal of Geophysical Research: Solid Earth*, 111(B2).

Taylor, J. (1997). *Introduction to error analysis, the study of uncertainties in physical measurements*.

Textile-Fashion-Study (2013). Polyamide fiber, physical and chemical properties of nylon 6. http://textilefashionstudy.com/

polyamide-fiber-physical-and-chemical-properties-of-nylon-6/. [Online; accessed 01.30.2018].

Thompson, G. (1960). Shallow temperature surveying in the wairakei-taupo area. *New Zealand Journal of Geology and Geophysics*, 3(4):553–562.

Titow, W. V. (2012). *PVC plastics: properties, processing, and applications*. Springer Science & Business Media.

UMS-tk/ma (2008). *Th3-v Soil Temperature Profile Probe - User Manual*. UMS.

Weather-Underground (2018). Mccall,id - history. https://www.wunderground.com/history/airport/KMYL/2016/10/31/DailyHistory.html?req_city=McCall&req_state=ID&req_statename=Idaho&reqdb.zip=83638&reqdb.magic=1&reqdb.wmo=99999. [Online; accessed 02.16.2018].

White, D., Muffler, L., and Truesdell, A. (1971). Vapor-dominated hydrothermal systems compared with hot-water systems. *Economic Geology*, 66(1):75–97.

WRCC, W. R. C. C. (2018a). Mccall,id - average of average temperature (degrees fahrenheit). https://wrcc.dri.edu/cgi-bin/cliMAIN.pl?id5708. [Online; accessed 02.16.2018].

WRCC, W. R. C. C. (2018b). Mccall,id - total of precipitation (inches). https://wrcc.dri.edu/cgi-bin/cliMAIN.pl?id5708. [Online; accessed 02.16.2018].

Young, H. W. and Mitchell, J. C. (1973). Geochemistry and geologic setting of selected thermal waters.

Appendix A: Complete Analytical Model - Heat Transfer at Surface Boundary under Transient Conditions

Let me clarify that this model was mainly created and developed by my advisor, with my aid (J. P. Fairley, personal communication, Fall semester 2017).

A.1 Problem

A.1.1 Find

The distribution of temperatures in the subsurface as a function of the geothermal gradient and a transient atmosphere forcing.

A.1.2 Known

- Site geometry
- The time-series temperature of the atmosphere.
- The thermal properties (K_T, ρ, c_p, D) of the near-surface soils.

A.1.3 Assume

- Temporally and spatially constant properties (K_T, ρ, c_p, D, etc).
- Heat source is sufficiently deep that the approximation $z \rightarrow \infty$ holds (i.e., semi-infinite half-space).
- Geothermal heat flux from depth is constant.
- Heat loss at the upper (land surface) boundary is coupled to atmospheric temperatures by a Type III boundary (Robin Boundary) condition.
- Land surface is flat (i.e., no topographic effect; thus can assume 1-D heat transfer).
- Heat transfer is solely by conduction; assume convective heat transfer is negligible.

- Neglect the impact of changes in saturation on thermal properties.
- No sources or sinks in the subsurface (i.e., no lateral flow, etc.).

A.1.4 Approach

Formulate the transient diffusion equation on a semi-infinite half-space with a Robin Boundary Condition at the land surface. Represent the changing air temperatures as a Fourier Series. Decompose the series and solve.

A.2 Energy Balance

$E_{in} = E_{out} + \Delta E$; Expanding the individual terms:

- $E_{in} = q_z A \Delta t$

  Units check: $E_{in} = \frac{J}{m^2 s} m^2 s$

  Units check: $E_{in} = \frac{J}{\cancel{m^2 s}} \cancel{m^2 s}$

  Units check: $E_{in} = J$

- $E_{out} = q_{z+\Delta z} A \Delta t$

  Units check: $E_{out} = \frac{J}{m^2 s} m^2 s$

  Units check: $E_{out} = \frac{J}{\cancel{m^2 s}} \cancel{m^2 s}$

  Units check: $E_{out} = J$

- $\Delta E = \Delta T \rho c_p A \Delta z$

  Units check: $\Delta E = K \frac{Kg}{m^3} \frac{J}{KgK} m^3$

  Units check: $\Delta E = \cancel{K} \frac{\cancel{Kg}}{\cancel{m^3}} \frac{J}{\cancel{Kg} \cancel{K}} \cancel{m^3}$

  Units check: $\Delta E = J$

Substituting:

$$q_z A\Delta t = q_{z+\Delta z} A\Delta t + \Delta T \rho c_p A \Delta z$$

$$q_z \cancel{A}\Delta t = q_{z+\Delta z} \cancel{A}\Delta t + \Delta T \rho c_p \cancel{A} \Delta z$$

$$\frac{q_{z+\Delta z} - q_z}{\Delta z} = -\rho c_p \frac{\Delta T}{\Delta t} \qquad \rightarrow \qquad \lim_{\Delta z, \Delta t \rightarrow\ 0}$$

$$\frac{\partial q_z}{\partial z} = -\rho c_p \frac{\partial T}{\partial t}$$

A.3 Substituting Fourier's Law

$$q_z = -K_T \frac{\partial T}{\partial z}$$

$$\frac{\partial^2 T}{\partial z^2} = \frac{\rho c_p}{K_T} \frac{\partial T}{\partial t} \quad ; \qquad \text{Let:} \qquad D = \frac{K_T}{\rho c_p};$$

Then:

$$\frac{\partial^2 T}{\partial z^2} = \frac{1}{D} \frac{\partial T}{\partial t} \quad ; \qquad -K_T \frac{\partial T}{\partial t}(z = 0, t) = h[T(z = 0, t) - T_\infty(t)]$$

$$-K_T \frac{\partial T}{\partial t}(z \rightarrow \infty, t) = q_z$$

The transient air temperature term can be expanded as:

$$T_\infty(t) = T_o + \sum_{n=1}^{\infty} A_n \sin(\frac{2n\pi t}{p}) + B_n \cos(\frac{2n\pi t}{p})$$

Substituting into the boundary condition at the land surface:

$$-K_T \frac{\partial T}{\partial z}(z = 0, t) = h[T(z = 0, t) - T_o - \sum_{n=1}^{\infty} A_n \sin(\frac{2n\pi t}{p}) + B_n \cos(\frac{2n\pi t}{p})]$$

$$\frac{\partial T}{\partial z}(z = 0, t) + \frac{h}{K_T}[T(z = 0, t) - T_o - \sum_{n=1}^{\infty} A_n \sin(\frac{2n\pi t}{p}) + B_n \cos(\frac{2n\pi t}{p})] = 0$$

Rewrite the Fourier series as a complex Fourier Series:

$$\sin(\frac{2n\pi t}{p}) = \frac{e^{\frac{2in\pi t}{p}} - e^{-\frac{2in\pi t}{p}}}{2i} \quad ; \qquad \cos(\frac{2n\pi t}{p}) = \frac{e^{\frac{2in\pi t}{p}} + e^{-\frac{2in\pi t}{p}}}{2}$$

$$T_\infty(t) = T_o + \sum_{n=1}^{\infty} A_n[\frac{e^{\frac{2in\pi t}{p}} - e^{-\frac{2in\pi t}{p}}}{2i}] + B_n[\frac{e^{\frac{2in\pi t}{p}} + e^{-\frac{2in\pi t}{p}}}{2}]$$

$$T_\infty(t) = T_o + \sum_{n=1}^{\infty} \frac{A_n}{2i}\, e^{\frac{2in\pi t}{p}} - \frac{A_n}{2i}\, e^{-\frac{2in\pi t}{p}} + \frac{B_n}{2}\, e^{\frac{2in\pi t}{p}} + \frac{B_n}{2}\, e^{-\frac{2in\pi t}{p}}$$

$$T_\infty(t) = T_o + \sum_{n=1}^{\infty} \frac{A_n + iB_n}{2i}\, e^{\frac{2in\pi t}{p}} + \frac{iB_n - A_n}{2i}\, e^{-\frac{2in\pi t}{p}}$$

$$T_\infty(t) = T_o + \sum_{n=1}^{\infty} \frac{B_n - iA_n}{2}\, e^{\frac{2in\pi t}{p}} + \frac{B_n + iA_n}{2} e^{-\frac{2in\pi t}{p}}$$

$$T_\infty(t) = \sum_{n=-\infty}^{\infty} C_n e^{\frac{2in\pi t}{p}} \quad ; \qquad C_n = \frac{B_n - iA_n}{2} \quad ; \quad n>0$$

$$C_n = T_o \qquad ; n = 0$$

$$C_n = \frac{B_n + iA_n}{2} \quad ; n<0$$

OK, save this result...

$$\frac{\partial^2 T}{\partial z^2} = \frac{1}{D}\frac{\partial T}{\partial t} \quad ; \qquad \frac{\partial T}{\partial z}(z=0,t) + \frac{h}{K_T}[T(z=0,t) - T_o] = \frac{h}{K_T}\sum_{n=1}^{\infty} A_n \sin(\frac{2n\pi t}{p}) + B_n \cos(\frac{2n\pi t}{p})$$

$$\frac{\partial T}{\partial z}(z=0,t) = -\frac{q_z}{K_T}$$

A.4 Nondimensionalize

Let: $\theta = \frac{T - T_o}{T_o}$; $T = T_o\theta + T_o$; $dT = T_o d\theta$; $d^2T = T_o d^2\theta$

Let: $\xi = \frac{z}{z_c}$; $z = z_c\xi$; $z^2 = z_c^2\xi^2$; $dz = z_c d\xi$; $dz^2 = z_c^2 d\xi^2$

Let: $\tau = \frac{t}{t_c}$; $t = t_c\tau$; $dt = t_c d\tau$

$$\frac{\partial^2\theta}{\partial\xi^2} = \frac{z_c^2}{Dt_c}\frac{\partial\theta}{\partial\tau} \quad ; \qquad \frac{\partial\theta}{\partial\xi}(\xi\to\infty,\tau) = -\frac{q_z z_c}{K_T T_o}$$

And: $\frac{T_o}{z_c}\frac{\partial\theta}{\partial\xi}(\xi=0,\tau) + \frac{h}{K_T}[T_o\theta(\xi=0,\tau) + T_o - T_o] = \frac{h}{K_T}\sum_{n=1}^{\infty} A_n \sin(\frac{2n\pi t_c\tau}{p}) + B_n\cos(\frac{2n\pi t_c\tau}{p})$

Let: $t_c = p$; Then:

$$\frac{\partial^2\theta}{\partial\xi^2} = \frac{z_c^2}{Dp}\frac{\partial\theta}{\partial\tau} \quad ; \qquad \frac{\partial\theta}{\partial\xi}(\xi\to\infty,\tau) = -\frac{q_z z_c}{K_T T_o}$$

And: $\frac{\partial\theta}{\partial\xi}(\xi=0,\tau) + \frac{hz_c}{K_T}[\theta(\xi=0,\tau)] = \frac{hz_c}{K_T}\sum_{n=1}^{\infty}\frac{A_n}{T_o}\sin(2n\pi\tau) + \frac{B_n}{T_o}\cos(2n\pi\tau)$

Let: $z_c = \sqrt{Dp}$; Then:

$\frac{\partial^2\theta}{\partial\xi^2} = \frac{\partial\theta}{\partial\tau}$; $\frac{\partial\theta}{\partial\xi}(\xi\to\infty,\tau) = -\frac{q_z\sqrt{Dp}}{K_T T_o} \equiv -\epsilon$

And: $\frac{\partial\theta}{\partial\xi}(\xi=0,\tau) + (\frac{h\sqrt{Dp}}{K_T})\theta(\xi=0,\tau) = (\frac{h\sqrt{Dp}}{K_T})\sum_{n=1}^{\infty}\frac{A_n}{T_o}\sin(2n\pi\tau) + \frac{B_n}{T_o}\cos(2n\pi\tau)$

Let: $\beta = \frac{h\sqrt{Dp}}{K_T}$; Then:

$\frac{\partial^2\theta}{\partial\xi^2} = \frac{\partial\theta}{\partial\tau}$; $\frac{\partial\theta}{\partial\xi}(\xi\to\infty,\tau) = -\epsilon$

And: $\frac{\partial\theta}{\partial\xi}(\xi=0,\tau) + \beta\theta(\xi=0,\tau) = \beta\sum_{n=1}^{\infty}\frac{A_n}{T_o}\sin(2n\pi\tau) + \frac{B_n}{T_o}\cos(2n\pi\tau)$

A.5 Substituting in the complex Fourier Series Result

$\frac{\partial^2\theta}{\partial\xi^2} = \frac{\partial\theta}{\partial\tau}$; $\frac{\partial\theta}{\partial\xi}(\xi\to\infty,\tau) = -\epsilon$

And: $\frac{\partial\theta}{\partial\xi}(\xi=0,\tau) + \beta\theta(\xi=0,\tau) = \beta\sum_{n=-\infty}^{\infty}\Gamma_n\, e^{2in\pi\tau}$

Where: $\theta = \frac{T-T_o}{T_o}$; $\xi = \frac{z}{\sqrt{Dp}}$; $\tau = \frac{t}{p}$; $\epsilon = \frac{q_z\sqrt{Dp}}{K_T T_o}$; $\beta = \frac{h\sqrt{Dp}}{K_T}$

And:

$$\Gamma_n = \begin{cases} \frac{B_n - iA_n}{2T_o} & ; \quad n>0 \\ 0 & ; \quad n=0 \\ \frac{B_n + iA_n}{2T_o} & ; \quad n<0 \end{cases}$$

The first step in solving the field equation is to simplify the problem to look at the single forcing frequency. Later, we can sum-up all the frequencies by superposition. The problem statement for a single (arbitrary) frequency is:

$\frac{\partial^2\theta}{\partial\xi^2} = \frac{\partial\theta}{\partial\tau}$; $\frac{\partial\theta}{\partial\xi}(\xi\to\infty,\tau) = -\epsilon$

And: $\frac{\partial\theta}{\partial\xi}(\xi=0,\tau) + \beta\theta(\xi=0,\tau) = \beta\sum_{n=-\infty}^{\infty}\Gamma_n\, e^{2in\pi\tau}$

The next step is to decompose the solution for θ_n into a linear solution that accounts for one of the boundary conditions (in this case, $\frac{\partial\theta_n}{\partial\xi} = -\epsilon$) and a transient portion, $\theta_{n,T}$.

Let: $\theta_{\mathrm{n}}(\xi,\tau) = \theta_{\mathrm{n,T}}(\xi,\tau) + \mathrm{A}\xi + \mathrm{B}$; Then:

$\frac{\partial\theta}{\partial\xi} = \frac{\partial\theta_{\mathrm{T}}}{\partial\xi} + \mathrm{A}$; $\frac{\partial^2\theta}{\partial\xi^2} = \frac{\partial^2\theta_{\mathrm{T}}}{\partial\xi^2} + 0$

$\frac{\partial\theta}{\partial\tau} = \frac{\partial\theta_{\mathrm{T}}}{\partial\tau} + \xi\frac{\partial\mathrm{A}}{\partial\tau} + \frac{\partial\mathrm{B}}{\partial\tau}$; $\frac{\partial^2\theta}{\partial\xi^2} = \frac{\partial\theta_{\mathrm{T}}}{\partial\tau} + \xi\frac{\partial\mathrm{A}}{\partial\tau} + \frac{\partial\mathrm{B}}{\partial\tau}$

From the Boundary Conditions:

$\frac{\partial\theta}{\partial\xi}(\xi\to\infty,\tau) = \frac{\partial\theta_{\mathrm{T}}}{\partial\xi}(\xi\to\infty,\tau) + \mathrm{A} = -\epsilon$; $\frac{\partial\theta_{\mathrm{T}}}{\partial\xi}(\xi\to\infty,\tau) = 0$; $\mathrm{A} = -\epsilon$

$\frac{\partial\theta}{\partial\xi}(\xi=0,\tau) + \beta\theta(\xi=0,\tau) = \beta\Gamma_{\mathrm{n}}\, e^{2\mathrm{in}\pi\tau}$

$\frac{\partial\theta}{\partial\xi}(\xi=0,\tau) + \mathrm{A} + \beta[\theta_{\mathrm{T}}(\xi=0,\tau) + \cancel{\mathrm{A}\xi} + \mathrm{B}] = \beta\Gamma_{\mathrm{n}}\, e^{2\mathrm{in}\pi\tau}$

$\frac{\partial\theta}{\partial\xi}(\xi=0,\tau) + \beta\theta_{\mathrm{T}}(\xi=0,\tau) + \mathrm{A} + \beta\mathrm{B} = \beta\Gamma_{\mathrm{n}}\, e^{2\mathrm{in}\pi\tau}$

$\frac{\partial\theta}{\partial\xi}(\xi=0,\tau) + \beta\theta_T(\xi=0,\tau) = \beta\Gamma_{\mathrm{n}}\, e^{2\mathrm{in}\pi\tau}$; $\mathrm{A} + \beta\mathrm{B} = -\epsilon + \beta\mathrm{B} = 0$; $\beta\mathrm{B} = \epsilon$; $\mathrm{B} = \frac{\epsilon}{\beta}$

So, **steady state solution** is underlined:

$\theta_{\mathrm{n}}(\xi,\tau) = \theta_{\mathrm{n,T}}(\xi,\tau) + \frac{\epsilon}{\beta} - \epsilon\xi = \underline{\frac{\epsilon}{\beta}(1-\beta\xi)} + \theta_{\mathrm{n,T}}(\xi,\tau)$

Furthermore, for **transient behavior**: $\xi\frac{\partial\mathrm{A}}{\partial\tau} = 0$; And: $\frac{\partial\mathrm{B}}{\partial\tau} = 0$

So: $\frac{\partial^2\theta_{\mathrm{T}}}{\partial\xi^2} = \frac{\partial\theta_{\mathrm{T}}}{\partial\tau}$; $\frac{\partial\theta_{\mathrm{T}}}{\partial\xi}(\xi=0,\tau) + \beta\theta_{\mathrm{T}}(\xi=0,\tau) = \beta\Gamma_{\mathrm{n}}\, e^{2\mathrm{in}\pi\tau}$; $\frac{\partial\theta_{\mathrm{T}}}{\partial\xi}(\xi\to\infty,\tau) = 0$

Let: $\theta_{\mathrm{T}}(\xi,\tau) = \chi(\xi)\, e^{\mathrm{in}\pi\tau}$; $\frac{\partial\theta_{\mathrm{T}}}{\partial\xi} = \chi'\, e^{2\mathrm{in}\pi\tau}$

$\frac{\partial^2\theta_{\mathrm{T}}}{\partial\xi^2} = \chi''\, e^{2\mathrm{in}\pi\tau}$; $\frac{\partial^2\theta_{\mathrm{T}}}{\partial\xi^2} = 2\mathrm{in}\pi\chi\, e^{2\mathrm{in}\pi\tau}$

Substituting: $\chi''\, e^{2\mathrm{in}\pi\tau} = 2\mathrm{in}\pi\chi\, e^{2\mathrm{in}\pi\tau}$; $\chi'' - 2\mathrm{in}\pi\chi = 0$

The Boundary Conditions decompose to:

$\chi'(\xi=0)\, e^{2\mathrm{in}\pi\tau} + \beta\chi(\xi=0)\, e^{2\mathrm{in}\pi\tau} = \beta\Gamma_{\mathrm{n}}\, e^{2\mathrm{in}\pi\tau}$

$\chi'(\xi=0) + \beta\chi(\xi=0) = \beta\Gamma_{\mathrm{n}}$; $\chi'(\xi\to\infty) = 0$

$\chi'' - 2\mathrm{in}\pi\chi = 0$; $\chi'(\xi=0) + \beta\chi(\xi=0) = \beta\Gamma_{\mathrm{n}}$; $\chi'(\xi\to\infty) = 0$

Let: $\chi = e^{\kappa\xi}$; $\chi' = \kappa e^{\kappa\xi}$; $\chi'' = \kappa^2 e^{\kappa\xi}$

Substituting: $\kappa^2 e^{\kappa\xi} - 2\mathrm{in}\pi e^{\kappa\xi} = 0$; $\kappa^2 = 2\mathrm{in}\pi$; $\kappa = \pm\sqrt{2\mathrm{in}\pi}$

$\chi = e^{\pm\sqrt{2\mathrm{in}\pi}\xi} = e^{\pm\sqrt{\mathrm{i}}\sqrt{2\mathrm{n}\pi}\xi}$

Express $\sqrt{\mathbf{i}}$ in the form: **a+ib:**

$$\sqrt{\mathbf{i}} = \mathbf{a} + \mathbf{ib}$$

$$\mathrm{i} = (\mathrm{a} + \mathrm{ib})^2 = \mathrm{a}^2 - \mathrm{b}^2 + \mathrm{i}2\mathrm{ab}$$

$$\mathrm{i} = (\mathrm{a}^2 - \mathrm{b}^2) + \mathrm{i}2\mathrm{ab}$$

However: $\mathrm{a}^2 - \mathrm{b}^2 = 0$; $\mathrm{a}^2 = \mathrm{b}^2$; $\mathrm{a} = \mathrm{b}$

And: $2\mathrm{ab} = 1$; $2\mathrm{a}^2 = 1$; $\mathrm{a}^2 = \frac{1}{2}$

$\mathrm{a} = \pm\frac{1}{\sqrt{2}}$; $\mathrm{a} = \pm\frac{\sqrt{2}}{2}$

So: $\underline{\sqrt{\mathrm{i}} = \frac{\sqrt{2}}{2}(1+\mathrm{i})}$

$\chi = e^{\pm\frac{\sqrt{2}}{2}(1+\mathrm{i})\sqrt{2\mathrm{n}\pi}\xi}$; $\chi = e^{\pm(1+\mathrm{i})\sqrt{\mathrm{n}\pi}\xi}$

Therefore: $\underline{\chi = \mathrm{C}_1\ e^{(1+\mathrm{i})\sqrt{\mathrm{n}\pi}\xi} + \mathrm{C}_2\ e^{-(1+\mathrm{i})\sqrt{\mathrm{n}\pi}\xi}}$

- From the Boundary Conditions at $\xi \to \infty$, $\mathrm{C}_1 = 0$

  $\chi = \mathrm{C}_2\ e^{-(1+\mathrm{i})\sqrt{\mathrm{n}\pi}\xi}$; $\chi' = -(1+\mathrm{i})\mathrm{C}_2\ \sqrt{\mathrm{n}\pi}e^{-(1+\mathrm{i})\sqrt{\mathrm{n}\pi}\xi}$

- From the Boundary Conditions at $\xi = 0$:

$-(1+\mathrm{i})\mathrm{C}_2\ \sqrt{\mathrm{n}\pi} + \beta\mathrm{C}_2 = \beta\Gamma_\mathrm{n}$; $\mathrm{C}_2\ [\beta - (1+\mathrm{i})\sqrt{\mathrm{n}\pi}] = \beta\Gamma_\mathrm{n}$

$\mathrm{C}_2 = \frac{\beta\Gamma_\mathrm{n}}{\beta-(1+\mathrm{i})\sqrt{\mathrm{n}\pi}}$; $\mathrm{C}_2 = \frac{\beta\Gamma_\mathrm{n}}{(\beta-\sqrt{\mathrm{n}\pi})-i\sqrt{\mathrm{n}\pi}}$; $\mathrm{C}_2 = \frac{(\beta-\sqrt{\mathrm{n}\pi})+\mathrm{i}\sqrt{\mathrm{n}\pi}}{(\beta-\sqrt{\mathrm{n}\pi})+\mathrm{i}\sqrt{\mathrm{n}\pi}}\ \frac{\beta\Gamma_\mathrm{n}}{(\beta-\sqrt{\mathrm{n}\pi})-\mathrm{i}\sqrt{\mathrm{n}\pi}}$

$\mathrm{C}_2 = \frac{\beta\Gamma_\mathrm{n}\ [\beta-\sqrt{\mathrm{n}\pi})+\mathrm{i}\sqrt{\mathrm{n}\pi}}{(\beta-\sqrt{\mathrm{n}\pi})^2+(\sqrt{\mathrm{n}\pi})^2}$; $\mathrm{C}_2 = \frac{\beta\Gamma_\mathrm{n}\ (\beta-\sqrt{\mathrm{n}\pi})+\mathrm{i}\beta\Gamma_\mathrm{n}\ \sqrt{\mathrm{n}\pi}}{(\beta-\sqrt{\mathrm{n}\pi})^2+\mathrm{n}\pi}$

OR:

$C_2 = a_n + ib_n \quad ; \qquad a_n = \frac{\beta\Gamma_n\ (\beta-\sqrt{n\pi})}{(\beta-\sqrt{n\pi})^2+n\pi} \quad ; \qquad b_n = \frac{\beta\Gamma_n\ \sqrt{n\pi}}{(\beta-\sqrt{n\pi})^2+n\pi}$

So: $\chi(\xi) = (a_n + ib_n)\ e^{-(1+i)\sqrt{n\pi}\xi}$

And: $\theta_T(\xi,\tau) = (a_n+ib_n)\ e^{-(1+i)\sqrt{n\pi}\xi}\ e^{2in\pi\tau} \quad ; \qquad \theta_T(\xi,\tau) = (a_n+ib_n)\ e^{-\sqrt{n\pi}\xi-i(\sqrt{n\pi}\xi-2n\pi\tau)}$

Summing over all the frequencies:

$\theta_T(\xi,\tau) = \sum_{n=-\infty}^{\infty}(a_n + ib_n)\ e^{-\sqrt{n\pi}\xi-i(\sqrt{n\pi}\xi-2n\pi\tau)}$

Finally, add on the "steady" solution for the full expression

$$\theta_T(\xi,\tau) = \underline{\frac{\epsilon}{\beta}(1-\beta\xi)} + \sum_{n=-\infty}^{\infty}(a_n + ib_n)\ e^{-\sqrt{n\pi}[\xi+i(\xi-\sqrt{n\pi}2\tau)]}$$

Where: $a_n = \frac{\beta\Gamma_n(\beta-\sqrt{n\pi})}{(\beta-\sqrt{n\pi})^2+n\pi} \quad ; \qquad b_n = \frac{\beta\Gamma_n\sqrt{n\pi}}{(\beta-\sqrt{n\pi})^2+n\pi}$

A.6 Comments

The modulus of the coefficient of the exponential for a given frequency is:

$|a_n + ib_n| = \sqrt{a_n^2 + b_n^2} \quad ; \qquad a_n = \frac{\beta\Gamma_n(\beta-\sqrt{n\pi})}{(\beta-\sqrt{n\pi})^2+n\pi} \quad ; \qquad b_n = \frac{\beta\Gamma_n\sqrt{n\pi}}{(\beta-\sqrt{n\pi})^2+n\pi}$

Since Γ_n is the nondimensional amplitude of the n^{th} frequency, the remaining terms after Γ_n has been factored from the expressions for a_n and b_n is the attenuation (or amplification, however unlikely that may be) of the amplitude as a function of frequency (n) and the surface atmosphere decoupling attributable to the Biot number. Switching notation slightly such that: $a_n \equiv \frac{a_n}{\Gamma_n}$ and $b_n \equiv \frac{b_n}{\Gamma_n}$

$a_n = \frac{\beta(\beta-\sqrt{n\pi})}{(\beta-\sqrt{n\pi})^2+n\pi} \quad ; \qquad a_n = \frac{\beta^2-\beta\sqrt{n\pi}}{\beta^2-2\beta\sqrt{n\pi}+n\pi+n\pi} \quad ; \qquad a_n = \frac{\beta^2-\beta\sqrt{n\pi}}{\beta^2-2\beta\sqrt{n\pi}+2n\pi}$

$b_n = \frac{\beta\sqrt{n\pi}}{(\beta-\sqrt{n\pi})^2+n\pi} \quad ; \qquad b_n = \frac{\beta\sqrt{n\pi}}{\beta^2-2\beta\sqrt{n\pi}+2n\pi}$

$a_n^2 = [\frac{\beta^2-\beta\sqrt{n\pi}}{\beta^2-2\beta\sqrt{n\pi}+2n\pi}]^2 \quad ; \qquad a_n^2 = \frac{(\beta^2-\beta\sqrt{n\pi})(\beta^2-\beta\sqrt{n\pi})}{(\beta^2-2\beta\sqrt{n\pi}+2n\pi)(\beta^2-2\beta\sqrt{n\pi}+2n\pi)}$

$a_n^2 = \frac{\beta^4-\beta^3\sqrt{n\pi}-\beta^3\sqrt{n\pi}+\beta^2 n\pi}{\beta^4-2\beta^3\sqrt{n\pi}+2\beta^2 n\pi-2\beta^3\sqrt{n\pi}+4\beta^2 n\pi-4\beta(n\pi)^{\frac{3}{2}}+2\beta^2 n\pi-4\beta(n\pi)^{\frac{3}{2}}+4(n\pi)^2}$

$$a_n^2 = \frac{\beta^2(\beta^2-2\beta\sqrt{n\pi}+n\pi)}{\beta^4-4\beta^3\sqrt{n\pi}+8\beta^2n\pi-8\beta(n\pi)^{\frac{3}{2}}+4(n\pi)^2}$$

$$b_n^2 = (\frac{\beta\sqrt{n\pi}}{\beta^2-2\beta\sqrt{n\pi}+2n\pi})^2 \quad ; \qquad b_n^2 = \frac{\beta^2n\pi}{(\beta^2-2\beta\sqrt{n\pi}+2n\pi)(\beta^2-2\beta\sqrt{n\pi}+2n\pi)}$$

$$b_n^2 = \frac{\beta^2n\pi}{\beta^4-2\beta^3\sqrt{n\pi}+2\beta^2n\pi-2\beta^3\sqrt{n\pi}+4\beta^2n\pi-4\beta(n\pi)^{\frac{3}{2}}+2\beta^2n\pi-4\beta(n\pi)^{\frac{3}{2}}+4(n\pi)^2}$$

$$b_n^2 = \frac{\beta^2n\pi}{\beta^4-4\beta^3\sqrt{n\pi}+8\beta^2n\pi-8\beta(n\pi)^{\frac{3}{2}}+4(n\pi)^2}$$

So:

$$a_n^2 + b_n^2 = \frac{\beta^2(\beta^2-2\beta\sqrt{n\pi}+2n\pi)}{\beta^4-4\beta^3\sqrt{n\pi}+8\beta^2n\pi-8\beta(n\pi)^{\frac{3}{2}}+4(n\pi)^2}$$

And:

$$\sqrt{a_n^2 + b_n^2} = [\frac{\beta^2(\beta^2-2\beta\sqrt{n\pi}+2n\pi)}{\beta^4-4\beta^3\sqrt{n\pi}+8\beta^2n\pi-8\beta(n\pi)^{\frac{3}{2}}+4(n\pi)^2}]^{\frac{1}{2}}$$

$$\sqrt{a_n^2 + b_n^2} = [\frac{\beta^2(\beta^2-2\beta\sqrt{n\pi}+2n\pi)}{(\beta^2-2\beta\sqrt{n\pi}+2n\pi)(\beta^2-2\beta\sqrt{n\pi}+2n\pi)}]^{\frac{1}{2}}$$

$$\sqrt{a_n^2 + b_n^2} = [\frac{\beta^2}{\beta^2-2\beta\sqrt{n\pi}+2n\pi}]^{\frac{1}{2}}$$

$$a_n = \frac{\beta(\beta-\sqrt{n\pi})}{(\beta-\sqrt{n\pi})^2+n\pi} \quad ; \qquad b_n = \frac{\beta\sqrt{n\pi}}{(\beta-\sqrt{n\pi})^2+n\pi}$$

$$a_n^2 = \frac{\beta^2(\beta^2-2\beta\sqrt{n\pi}+n\pi)}{[(\beta-\sqrt{n\pi})^2+n\pi]^2} \quad ; \qquad b_n^2 = \frac{\beta^2n\pi}{[(\beta-\sqrt{n\pi})^2+n\pi]^2}$$

$$a_n^2 = \frac{\beta^2(\beta^2-2\beta\sqrt{n\pi}+n\pi)}{[\beta^2-2\beta\sqrt{n\pi}+2n\pi]^2} \quad ; \qquad b_n^2 = \frac{\beta^2n\pi}{[\beta^2-2\beta\sqrt{n\pi}+2n\pi]^2}$$

$$a_n^2 + b_n^2 = \frac{\beta^2(\beta^2-2\beta\sqrt{n\pi}+2n\pi)}{(\beta^2-2\beta\sqrt{n\pi}+2n\pi)^2}$$

$$a_n^2 + b_n^2 = \frac{\beta^2}{\beta^2-2\beta\sqrt{n\pi}+2n\pi}$$

Appendix B: Data from Experimental Work

1. SSPrb - April 07th, 2016: This data has been submitted as a "supplementary file" on this thesis as "G.Villegas-SS-040716".

2. SSPrb - April 27th, 2016: This data has been submitted as a "supplementary file" on this thesis as "G.Villegas-SS-042716".

3. PPrb - September 15th, 2016: This data has been submitted as a "supplementary file" on this thesis as "G.Villegas-PP-091516".

4. H_2SO_4 - March 27th, 2017: This data has been submitted as a "supplementary file" on this thesis as "G.Villegas-H2SO4-032717".

5. WFP - May 11th, 2017: This data has been submitted as a "supplementary file" on this thesis as "G.Villegas-WFP-051117".

6. Burgdorf Data Temperatures- October 21st, 2016: This data has been submitted as a "supplementary file" on this thesis as "G.Villegas-Burgdorf".

7. Burgdorf Data Wind Speed- October 21st, 2016: This data has been submitted as a "supplementary file" on this thesis as "G.Villegas-Burgdorf-wind".